Institute of Experimental Physics
Department of Theoretical Physics
Slovak Academy of Sciences, Košice

Transport of Electrons in Photosynthetic Reaction Centers

Dissertation

2003

RNDr. Richard Pinčák

Venujem
mamke a Evke
za ich nesmiernu podporu.

Acknowledgments

My greatest thanks go to my supervisors RNDr. Michal Pudlák, CSc and Doc.RNDr. Michal Hnatič, CSc, for their encouragement and support, particularly at several turning points when I needed it. I earned a lot of exceptional experience for the future during my PhD study at the Slovak Academy of Sciences in Košice. My equal thanks go to all the collective of Department of Theoretical Physics for their support and advice if I need. I also acknowledge special support from Slovak Academy of Science (VEGA) under the Grants Nos:7043, 3197.

Contents

Introduction

Photosynthetic Reaction Centers (RC's)

The photosynthetic reaction centers is a special pigment-protein complex, that functions as a photochemical trap. The precise details of the charge separations reactions and subsequent dark electron transport (ET) form the central question of the conversion of solar energy into the usable chemical energy of photosynthetic organism. The function of the reaction center is to convert solar energy into biochemical amenable energy.

The concept and physical reality of reaction centers

The capture of solar radiation and the conversion of its free energy into chemical energy involves a sequence of reactions that occur within a physical structure called the photosynthetic RC. Following the initial capture of a photon by antenna pigments, the photon is transferred to the RC pigments, where it gives rise to a separation and stabilization of charge across the photosynthetic membrane. Figure 1 depicts this process and illustrates the time scales typically involved. One feature of the photochemistry is that all photosynthetic RC's undergo charge separation with a quantum yield approaching unity, which makes them marvellous molecular machines.

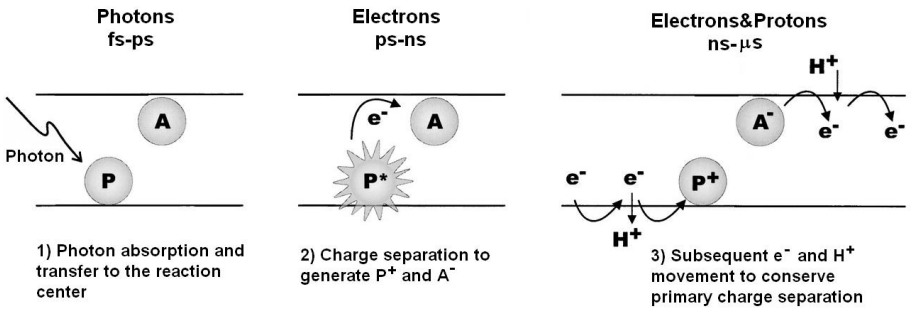

Figure 1: Scheme of the primary processes in the photosynthetic RC. Here, P represents the charge-separating (bacterio) chlorophyll pigments (the *primary electron donor*) and A represents the first *stable* acceptor. Energy transfer from the antenna pigments leads to photoexcitation of P on the fs-ps time scale (left). Charge separation produces oxidized P^+ and A^- on the ps-ns scale (center). The recombination of P^+A^- to produce PA, heat and potentially damaging chemical species is efficiently prevented by further forward electron transfer that is now proton coupled. These more complex chemical processes ultimately produce stable photosynthetic products and occur, initially, on the ns and μs time scales (right).

A photosynthetic unit contains numerous pigments but the photochemically active chromophores are present in much lower concentration. This pioneering concept led to the distinction of two types of pigments: the light-harvesting, but photochemically inactive, an-

tenna chromophores; and the photochemically active RC pigments. The antenna pigments physiologically increase the absorption cross section of the RC dramatically. Moreover, they ensure that the potentially reactive intermediates containing unpaired electron spins (e.g. semiquinones) generated by single photon photochemistry are efficiently converted by a second photochemical event to products (e.g. hydroquinones) that contain only paired spins. For efficient energy transfer between the antenna and the RC, the RC absorbs at longer wavelengths, effectively forming a trap for excitation energy. Despite these conceptual advances, more than 35 years passed before the first physical isolation of a pigment protein RC complex was reported [1]. Since that time, many other RC's have been isolated and characterized biophysically and biochemically.

Light-Harvesting complex in bacterial photosynthesis

Purple photosynthetic bacteria live in polluted water in North America. Under anaerobic conditions they produce photosynthetic apparatus, which is incorporated into an intracytoplasmic membrane. Photochemistry begins at the (bacterial) reaction center where charge is separated across the membrane. The reaction center (RC) molecule requires energy to perform this task, either from direct absorption of a photon, or energy transferred from a light-harvesting complex.

All purple bacteria produce a primary light-harvesting complex (LH1), which is intimately associated with the RC - this composite is termed the Core complex. Most purple bacteria produce a peripheral light-harvesting complex (LH2), and some produce an additional peripheral complex (sometimes called LH3)(Fig. 2). Each light-harvesting complex is

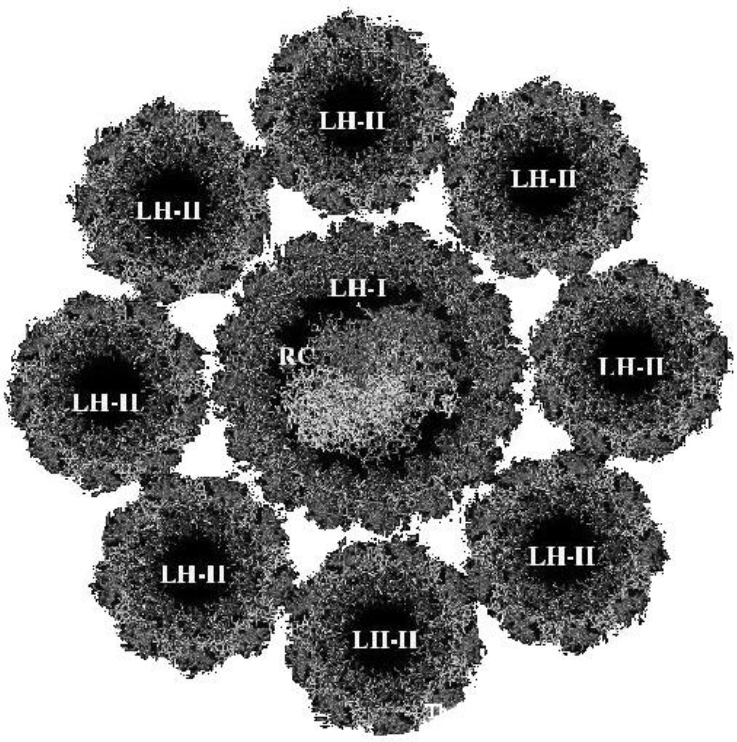

Figure 2: Crystal structure of an integral membrane light-harvesting complex from photosynthetic bacteria (http://www.chem.gla.ac.uk/protein/LH2/core.html).

an oligomer formed from a subunit consisting of two or more polypeptide chains with associated pigment molecules [2]. The pigments used in LH complexes are bacteriochlorophyll a and carotenoid. $BChl_A$ is the primary pigment, carotenoid molecules are primarily used for photoprotection, although they do function as additional light-harvesting pigments. The protein matrix which supports these molecules in each of the distinct LH complexes modulates the absorption of the chromophores. This modulation results in a downward gradient of energy levels from LH3 - LH2 - LH1 (Fig. 3). Energy absorbed by any molecule in this antenna array is funnelled down into LH1 which feeds the RC. In the photosynthetic apparatus, the RC complex is surrounded by the LHI-ring. Transfer from the LH1 ring to the RC is accelerated by bridge BChls. The bacteria synthesize enough LH2 to satisfy the RC, this is directly dependent on the ambient light intensity, the number of $BChl_A$ per RC rises to 250 or more in low light cases. Purple bacteria have been extensively studied as a

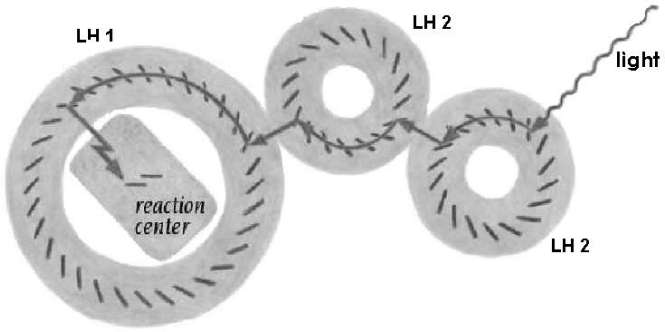

Figure 3: Light harvesting complex and light capturing pathway from LH2 to reaction center (Branden&Tooze, *Introduction to Protein Structure*, 2nd ed, Garland publishing, 1999).

means to understanding the processes involved in photosynthesis. Their light-harvesting systems possess, relatively, many residues per pigment, and the spectra of these bacterial systems are relatively straightforward: they posses only one major chlorin type pigment and the resonant absorption bands arising from this chromophore are generally well resolved. This makes this bacterial system ideal as a model for studying photosynthesis in general.

Structural biology and in particular protein crystallography has been extremely successful in revealing the structures of photosynthetic proteins from purple bacteria [3]. The RC from *Rps. viridis* was the first integral membrane protein to be solved to high resolution by X-ray crystallography. There are also structures of the RC from *Rb. sphaeroides* and the LH2 from *Rs. moliscianum*. Electron microscopy has provided a low resolution projection of the LH1 complex from *Rs. rubrum*, and the LH2 complex from *Rv. sulfidophilum*.

It is through photosynthesis that earth's biosphere derives its energy from sunlight. Photosynthetic organisms, i.e., plants, algae and photosynthetic bacteria, have developed efficient systems to harvest the light of the sun and to use the light energy to drive their metabolic reactions, such as the reduction of carbon dioxide to sugar. The ubiquitous green color of plants is testimony to the key molecular participant in the light harvesting of plants, chlorophylls. More hidden in this respect, but no less widespread, is a second participating molecule, carotenoid. In green leaves the color of the carotenoids is masked by the much more abundant chlorophylls while in red ripe tomatoes or petals of yellow flowers, the carotenoids predominate. Chlorophyll molecules exist in slightly different chemical structures in various photosynthetic organisms, as chlorophyll a or b in plants or algae, and as bacteriochlorophyll a ($BChl_A$) or b in photosynthetic bacteria. Molecules such as chlorophyll and carotenoid that absorb light and impart color to living matter and other

materials are called pigments. In general, biological pigments are non-covalently bound to

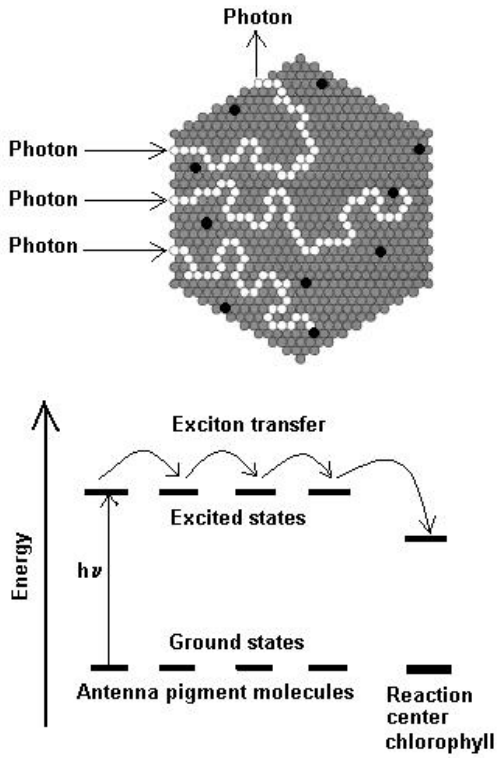

Figure 4: Antenna or light harvesting complex distribution of RC's and LH complex promoting multiple photon absorption (Voet&Voet, *Biochemistry*, 2nd ed, John Wiley&Sons, 1995).

proteins, forming the so-called pigment-protein complexes. The pigment-protein complexes are organized as the photosynthetic unit (PSU). The bacterial PSU consists of two types of pigment-protein complexes: the photosynthetic reaction centers (RCs) and the light-harvesting complexes. The main function of the light-harvesting complexes is to gather light energy and to transfer this energy to the reaction centers for the photo-induced redox processes (Fig. 4). Purple bacteria are great masters of harvesting light. Nearly all the energy gained by the absorption of a photon is transferred on to the reaction center. The purple bacteria exploit elegant quantum physics, the working of which were only fully understood recently after the discovery of the structures of light-harvesting complexes and investigations into their electronic excitations [4].

Photosynthesis in bacteria

Photosynthesis is a reaction in which light energy is converted into chemical energy. The primary process of photosynthesis is carried out by a pigment-protein complex embedded in the membrane, that is, RC. In photosynthetic purple bacteria, the cyclic electron transfer reaction is performed by RC and two other components: the cytochrome (Cyt) bc_1 complex, and the soluble electron carrier protein (Fig. 5 and 6). First, RC accepts light energy from antenna proteins, and promotes a light-induced charge separation across the membrane, which results in the oxidation of the special pair and the reduction of quinone to quinol. The

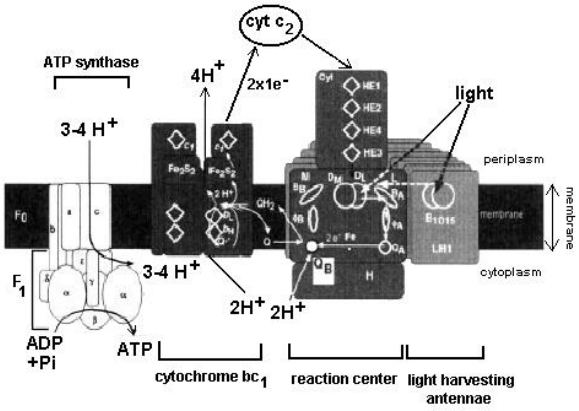

Figure 5: In purple bacteria, the primary reactions of photosynthesis are performed on the inner membrane, referred to as the photosynthetic membrane. First, RC accepts light energy from light harvesting antenna complexes, LH-I and LH-II. The RC complex contains various prosthetic groups that serve as the photosynthetic pigments, such as the bacteriochlrophyll dimer (special-pair), bacteriopheophytin, and quinone; charge separation occurs in this RC complex. As a result of the charge separation, quinone is reduced to quinol. Second, quinol moves to the Cyt bc_1 complex through the membrane. The Cyt bc_1 complex re-oxidizes quinol to quinone, and transfers electrons to the soluble electron carrier proteins. The soluble electron carrier proteins are classified into two groups, Cyt c_2 and the high-potential iron-sulfur protein (HiPIP), depending on the species used physiologically. In each case, the soluble electron carrier protein contains a redox center, such as a heme c group or an Fe-S cluster. Finally, the soluble electron carrier proteins move through the periplasmic space, and transfer electrons to RC. The photo-oxidized special-pair is reduced, and RC returns to the initial state. In the course of this cyclic electron transfer, the oxidation and reduction of quinone bring about a trans-membrane electrochemical gradient of protons, and the resulting energy is utilized for ATP synthesis by ATP synthase. The electron flow, proton transfer, the absorption of light energy and ATP synthesis are represented by arrows (Messerschmidt&Huber, *Handbook of Metalloproteins*, John Wiley&Sons, Ltd, Chichester, 2001).

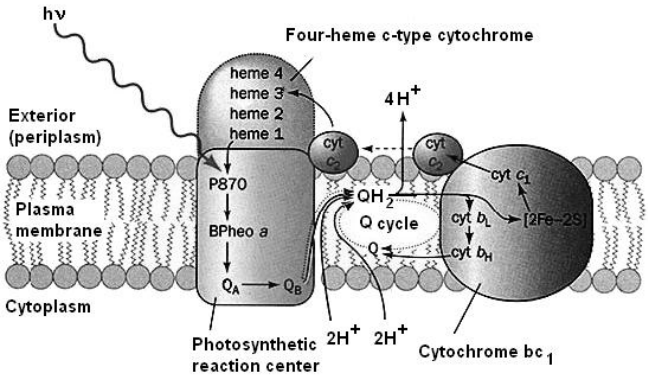

Figure 6: The scheme of primary process of photosynthesis which takes place in a pigment-protein complex embedded in the membrane (Voet&Voet, *Biochemistry*, 2nd ed, John Wiley&Sons, 1995).

quinol molecule then leaves RC and moves to the Cyt bc_1 complex through the quinone-pool in the membrane. Second, the Cyt bc_1 complex re-oxidizes quinol to quinone, and the released electrons are transferred to soluble electron carriers. Third, the soluble electron

carriers transport the electrons to RC through the periplasmic space. Finally, the photo-oxidized special-pair is reduced by the soluble electron carriers, and RC returns to the initial state. In the course of the oxidation and reduction of quinone, a trans-membrane electrochemical gradient of protons is formed, and the energy is utilized for ATP synthesis by ATP synthase [5].

The purple bacterial RC possesses bacteriopheophytin and quinone as the electron acceptor from the exited special-pair, and is, therefore, classified the same as photosystem (PS) II in plants and cyanobacteria. Significant differences are known to exist between purple bacterial RC and PSII in peripheral reactions, such as the light-harvesting mechanism and the presence of the oxygen-evolving system. However, the fundamental reactions are quite similar, for example, the charge separation initiated at the special-pair and the reduction of quinone. To date, many structural studies have been performed on purple bacterial RC complexes in order to elucidate the spatial arrangement of the prosthetic groups and the high quantum yield of the charge separation. Such studies are a help in understanding the structural features of PSII in plants and cyanobacteria [6, 7].

Structural and operational insight

Insight into the molecular organization of the RC has been derived, initially, from spectroscopic studies and, subsequently, from the development and analysis of high-resolution crystal structures of several photosynthetic organisms. The first RC structurally resolved (3 Å) was of the purple bacterial RC from *Rhodopseudomonas viridis* [8], for which the 1988 Nobel Prize was awarded. This was soon followed by the elucidation of several other purple bacterial structures. Good progress is also being made toward achieving two- and three-dimensional structures of photosystem II (PSII) crystals. It is surprising that the structures of all of the different RC's show a dimeric core with a pseudo-C_2 axis of symmetry. This feature is illustrated in Figure 7 in the example of a purple bacterial RC. The holoprotein is shown on the left. The charge-separating RC pigments contained within the structure (Fig. 7, right) are aligned along the C_2 symmetry axis with the two photochemically active (bacterio) chlorophyll pigments positioned in close proximity. Exciton coupling between these two pigments provides a red shift in the optical spectrum that contributes substantially to forming the low-energy trap discussed above. The conversion of photons to chemical potential involves photoexcitation and initial charge separation to produce an oxidized (bacterio) chlorophyll and reduction of one of the other chlorin pigments in the RC. From this chlorin, the electron migrates to reduce a quinone in less than a nanosecond (Fig. 7). It is interesting that the strength of the dimer exciton coupling has changed substantially during the course of oxygenic RC evolution from photosynthetic bacteria. The bacteria usually have strong couplings, approximately $2000\,\mathrm{cm}^{-1}$, whereas the plant and algal RC's have a much weaker coupling, typically approximately $300\,\mathrm{cm}^{-1}$. The weaker coupling in the oxygenic RC's increases the thermodynamic efficiency of photon capture so that a significant improvement in useful free energy capture from the photon is realized. Subsequent proton-coupled electron transfer steps (Fig. 1) stabilize the charge separation effectively and ensure the near-unity quantum efficiency of photosynthesis.

A remarkable aspect of the RC structures is the occurrence of two almost identical electron acceptor pathways arranged along the C_2 axis relative to the primary charge-separating dimer (bacterio) chlorophyll (Fig. 7). This finding posed a key question: Does electron transfer involve both branches? In the purple bacterial RC, only one branch is active although the inactive branch can be forced into operation with modification of amino acid side chains on the active branch [9]. The strong asymmetry imposed on primary charge separation photo-chemistry in the purple bacterial RC results from two homologous

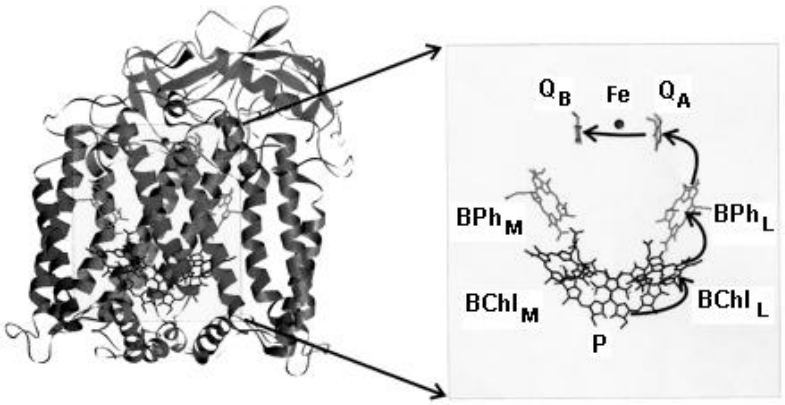

Figure 7: Structure of the purple bacterial RC (*Rhodobacter sphaeroides*). The heterodimeric RC (left) is comprised of a C_2-symmetrical heterodimer of the L, M and subunit H polypeptides. The pseudo-C_2 symmetric cofactor arrangement and the active pathway of electron transfer are indicated on the right. Charge separation from the RC Chl dimer (P) to the BChl monomer to BPh occurs in approximately 3 ps down the active L branch. This is followed by charge stabilization with electron transfer to the quinones.

polypeptides that function as a heterodimer. A heterodimer is also involved in the core of the RC's of PSI and PSII. However, some RC's, such as heliobacteria [10] and green sulfur bacteria [11], contain two identical homodimeric polypeptides, and electron transfer is potentially bifurcated.

Genetic sequence information has greatly improved the understanding of the origin of the RC proteins. From the sequence analysis, it became clear that the purple bacteria RC is remarkably similar to that of PSII, and PSI was also discovered to have similarity with that of the green sulfur bacteria [12]. Recent structural comparisons between PSI and PSII, for example, show a distinct structural homology, which suggests that even these two RC's likely share a common ancestor [13].

Types of RC's

The general details of RC structure and function described above persist among photosynthetic organisms, but differences in detail have become apparent. Today, we recognize six different classes of photosynthetic RC's. The principal variations lie in the RC pigments (chlorophyll versus bacteriochloropyll), the size and nature of the antenna pigment array, the associated longest wavelength maximum and strength of the pigment exciton coupling, and the thermodynamic coupling of the primary donor chlorophyll dimer (P) to its acceptor system (i.e. its midpoint reduction potential). Figure 8 presents a summary of the various RC's, cofactors, and electron transport chains. The six classes of RC divide into two forms: the type I and type II RC's [12, 14]. The type I RC's comprise PSI, the gram-positive heliobacteria, and the green sulfur bacteria, all of which share iron-sulfur clusters as electron acceptors. The type II RC's from PSII, purple bacteria and the green filamentous bacteria, share quinone acceptors that serve as two-electron reductants. Two of these RC's, from heliobacteria and the green filamentous bacteria, have only been recognized quite recently and there may be others that await discovery - the field continues

to progress rapidly.

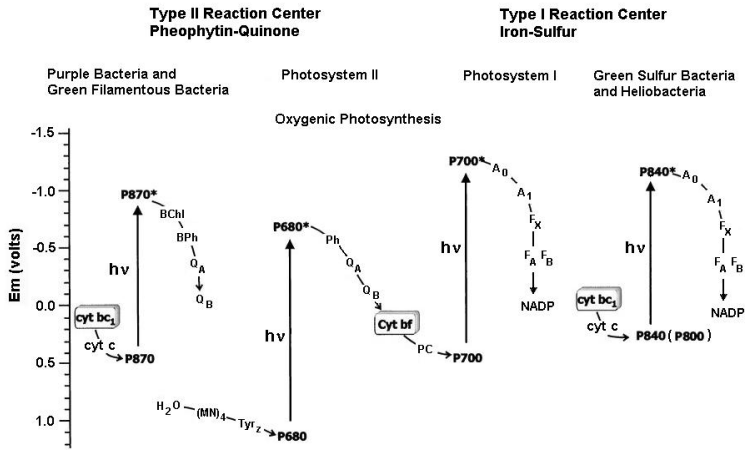

Figure 8: Electron-transfer pathways for the two different types and six classes of RC's shown according to the midpoint potentials of key redox components. In Type I RC's (left), iron-sulfur clusters are used as the electron acceptors. Type I is subdivided into three classes: PSI, green sulfur bacteria, and heliobacteria. In Type II RC's, quinones are used as the first "stable" electron acceptors (left). Type II is also subdivided into three classes: PSII, purple bacteria, and green filamentous bacteria. Intermediates in the scheme have the following designations: the RC primary donor, P; transient initial (bacterio) pheophytin acceptor, (B) Ph; "stable" quinone acceptors, Q_A and Q_B; transient initial chlorophyll (A_0) and quinone (A_1) acceptors; "stable" iron-sulfur cluster acceptors, F_X, F_A, and F_B; and final NADP acceptor (NADP). The electron donors are a Tyr residue, Tyr_Z, and a cluster of 4 manganese ions for PSII, a plastocyanin molecule (PC) for PSI, and cytochrome c for the bacterial RC's. The intermediate electron transfer complexes, cytochrome bc_1 and b_{6f}, are boxed (Allen&Williams, Minireview: *Photosynthetic reaction centers*, FEBS Letters 438 (1998) 5).

Further differentiation in photosynthetic organisms is found in the structure and arrangement of the antenna pigments associated with each RC. The RC from heliobacteria features a very simple organization with a core containing approximately 40 chlorophyll g and no additional auxiliary peripheral antenna proteins [10]. Building on this organizational theme are RC's from PSI and green sulfur bacteria, which contain large numbers ($\sim$100) of pigments attached directly to the polypeptides that bind the RC components [13], as well as an extensive external antenna array with which the RC's communicate in a controlled way. At the other extreme are the RC's from purple bacteria and PSII, which contain only six to eight pigments arranged along the C_2 symmetry axis and are fundamental to the charge separation process. These RC's rely on a substantial antenna system as conduits of excitation energy. This antenna system is bound to polypeptides distinct from the RC polypeptides.

Structural basis of bacterial photosynthetic reaction centers

The photosynthetic reaction center (RC) is the first membrane protein whose three-dimensional structure was revealed at the atomic level by X-ray crystallograph more than fifteen years ago. Structural information about RC made a great contribution to the understanding of the reaction mechanism of the complicated membrane protein complex [15, 16]. High-resolution structures of RC's from three photosynthetic bacteria are now available, namely, those from two mesophilic purple non-sulfur bacteria, *Blastochloris viridis* and *Rhodobacter sphaeroides*, and that from a thermophilic purple sulfur bacterium, *Thermochromatium tepidum*. In addition, a variety of structural studies, mainly by X-ray

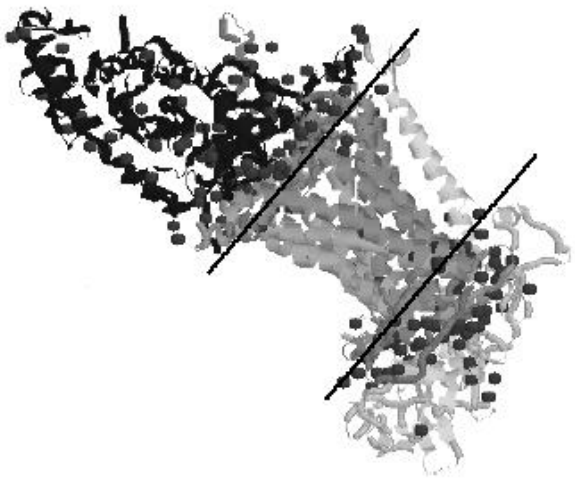

Figure 9: Three-dimensional structure of tetrameric complex of RC penetrate through the membrane. Note that the water and Cytochrome molecules (dark color) do not penetrates the membrane spanning domain (dotted lines) of the reaction center complex. The chains of grey color described M, L and H subunits of RC. (Cox&Lehninger, *Principles of Biochemistry*, Worth Publishing, 3rd ed, 2000).

crystallography, are still being performed to give more detailed insight into the reaction mechanism of this membrane protein. The structural data from three RC's and their electron donors provided reliable models for molecular recognition in the primary step of bacterial photosynthesis. Electron transfer coupled with the uptake of protons across the membrane is a fundamental feature of bioenergetic processes such as oxidative phosphorylation and photosynthesis, and the resulting electrochemical gradient of protons is finally utilized for ATP synthesis. Key players in bioenergetics are integral membrane proteins and co-factors embedded in the membrane protein complexes, where polypeptide chains spanning across the membrane provide a scaffold for the specific arrangement of co-factors in membrane protein complexes. Hence, structural data about membrane protein complexes contribute greatly to obtaining a profound understanding of reaction mechanisms [17].

In fact, a great deal of effort has been made to elucidate the three-dimensional structures of membrane proteins involved in bioenergetics for the sake of functional analyses (Figs. 9 and 10). Of such structural studies, crystallographic studies of the photosynthetic reaction center (RC) provided the first successful description of the three-dimensional structure at an atomic resolution, and the methodology established in this structural work has had a strong influence on subsequent structural studies of membrane proteins. In addition, structure analyses of RC complexes remain one of the most active fields in membrane protein structural biology. This is because it is not yet clear how the RC complex regulates the electrochemical properties of co-factors, especially that of the bacteriochlorophyll dimer (the special pair) that acts as the initiator of photosynthetic electron transfer, how the RC complex takes up protons to reduce quinone, which acts as the final electron acceptor in the complex, and how the RC complex accepts electrons from the electron carrier protein to reduce the photo-oxidized special-pair. Consequently, structure analyses of some modified RC complexes, such as mutants or complexes with substrate analogues, have been carried out extensively so as to relate structural information to physical and chemical properties, in spite of the fact that the three-dimensional structure of the native

Figure 10: X-ray structure arrangement of co-factors of RC embedded in the membrane protein complex (Cox&Lehninger, *Principles of Biochemistry*, Worth Publishing, 3rd ed, 2000).

RC complex has already been determined precisely.

As a result, abundant structural data have been accumulated, which can explain the functional properties of RC to some extent. Since membrane proteins involved in bioenergetics share some functional features as mentioned above, knowledge deduced from structural studies of RC complexes can provide useful information for analyses of the other membrane proteins, for example, with respect to intra- and inter-molecular electron transfer and proton uptake through the membrane.

Crystal structures of bacterial photosynthetic reaction centers

First, the crystal structure of RC from *Rhodopseudomonas(Rp.) viridis* and *Rhodobacter(Rb.) sphaeroides* was done. Based on their subunit compositions, bacterial RC complexes are classified into two groups [18, 19]: Group I is composed of three major subunits (L M, and H), and Group II possesses an additional peripheral subunit, referred to as the Cyt subunit, on the cytoplasmic side. Hence, *Rb. sphaeroides* RC and *Rp. viridis* RC belong to Group I and Group II, respectively (Fig. 11).

In addition to these two RC's, the crystal structure of RC from *Thermochromatium (Tch.) tepidum* has recently been determined is classified into Group II. Since the three-dimensional structure of *Tch. tepidum* RC was the first from a thermophilic organism to be determined, it is of peculiar interest to understand not only the original function of the photosynthetic apparatus, but also the thermostability of its RC molecule.

The RC complex maintains a number of prosthetic groups in the protein subunit scaffold. The prosthetic groups in the trans-membrane region apparently form two branches (A and B) that are related by a pseudo twofold axis perpendicular to the membrane plane (Fig. 11). These two branches run from the special-pair of bacteriochlorophyll (DA and

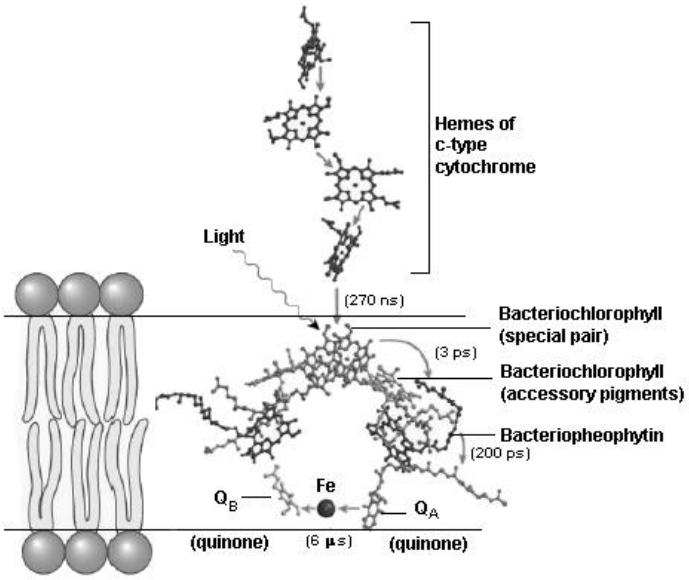

Figure 11: X-ray structural analysis of the reaction center with electron pathway from outer to inner surface of membrane (Cox&Lehninger, *Principles of Biochemistry*, Worth Publishing, 3rd ed, 2000).

DB) to the non-heme iron. Each branch consists of a bacteriochlorophyll monomer ($BChl_A$ or $BChl_B$), bacteriopheophytin (BPh_A or BPh_B), and quinone (Q_A or Q_B). A carotenoid molecule is present in the trans-membrane region near $BChl_B$. For more details on structural arrangement, see [20]. Branch A, mainly associated with the L subunit, is selectively utilized as the pathway of electron transfer, which is induced by charge-separation, in this process, an electron is emitted from the excited special-pair and transferred through BPh_A and Q_A [21, 22]. The involvement of $BChl_A$, which is located between the special-pair and BPh_A, in the electron transfer remains a matter of debate. Branch B, is associated with the M subunit and is inactive in electron transfer. Q_B is the final electron acceptor at this stage, and the reduced Q_B molecule serves as the electron carrier to the Cyt bc_1 complex. The RC structures from photosynthetic bacteria are described schematically in Figs. 10-12.

Topics on RC structure

In addition to the structures of the three native RC complexes, the crystal structures of mutants and complexes with Q_B analogues have also been determined, and the refined models of native RC structures have been re-assessed so as to examine the biophysical and biochemical functions of RC in more detail. Since prosthetic groups play a central role in photosynthetic energy conversion, it is necessary to describe the three-dimensional arrangement of these prosthetic groups and their interactions with protein subunits precisely, this will lead to a better understanding of the functional aspects of RC and probably give answer to the questions why electron transfer through the RC prefers only one branch(L).

Electron transfer through the RC's

A critical aspect of the photochemistry of reaction centers is their ability to perform electron transfer (ET) with a quantum yield of almost unity. This high quantum yield is

achieved by the utilization of a number of intermediate electron acceptors (Fig. 8). Within 30 ps after excitation a stable charge separated state is formed in all photosystems. Although the nature of the spectral changes with time is complex, the role of many factors driving the initial electron transfer process has been established in purple bacteria. For

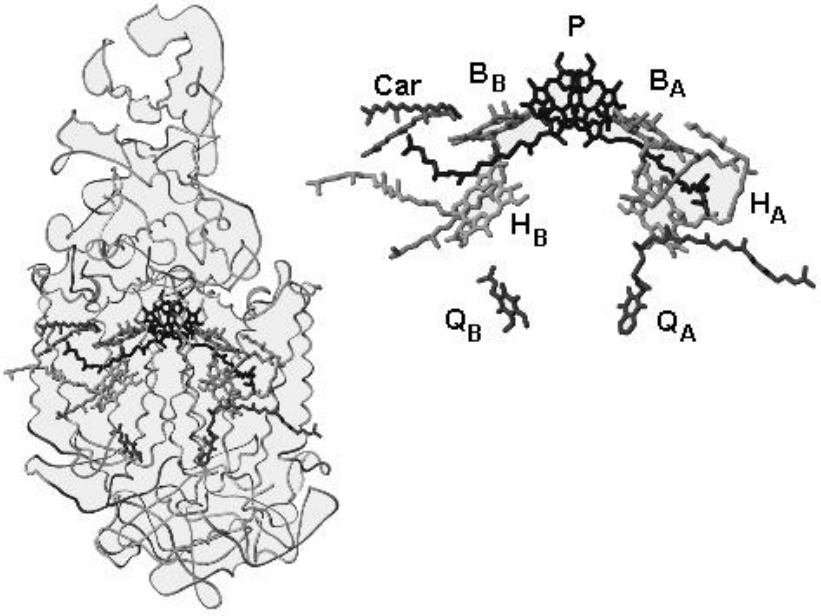

Figure 12: Schematic representation of the X-ray structure of *Rp. viridis* RC showing two symmetrical subunits of the RC (http://www.mpibp-frankfurt.mpg.de/∼michael.hutter/rcenter.html).

other types of reaction centers, the larger number of tetrapyrroles and the highly overlapping nature of the optical bands have hindered interpretation of the optical changes, and research continues to delineate the electron transfer processes. In purple bacteria, the electron rate is sensitive to the free energy difference between the excited state and the charge-separated state but not to the relative distribution of electrons over the two macrocycles of the donor. After extensive studies, the rate is now established to be critically coupled to the properties of the bacteriochlorophyll monomer that lies between the donor and bacteriopheophytin acceptor (Fig. 12). The involvement of the bacteriochlorophyll monomer may give rise to multiple pathways for electron transfer [23] and can partially determine the asymmetry of the electron transfer along one branch [24]. Electron transfer in the reaction center culminates at either quinone acceptors or iron-sulfur centers depending upon the type of reaction center. Although a metal atom, usually iron, is coupled to the quinones in the pheophytin-quinone reaction centers, it is not required for electron transfer. The two quinone acceptors in this type of reaction center have different functional properties, with the primary quinone being a transient one electron acceptor and the secondary quinone being a two electron acceptor coupled to the exogenous quinone pool of the cell membrane. Electron transfer in the iron-sulfur type of reaction center proceeds from the chlorophyll acceptor A_0 to the iron-sulfur center F_X (Fig. 8). A quinone is thought to serve as an intermediate acceptor in photosystem I, but the role of quinones in reaction centers from heliobacteria or green sulfur bacteria is not settled. The electron is then transferred to an external protein, ferredoxin, by way of the two iron-sulfur clusters F_A and F_B that are located in the protein subunit. Despite the striking symmetry of the cofactors into 2 branches (Fig. 12), electron transfer in the pheophytin-quinone reaction centers proceeds only along one branch with at least a 10:1 ratio. Typical distance and electron transfer

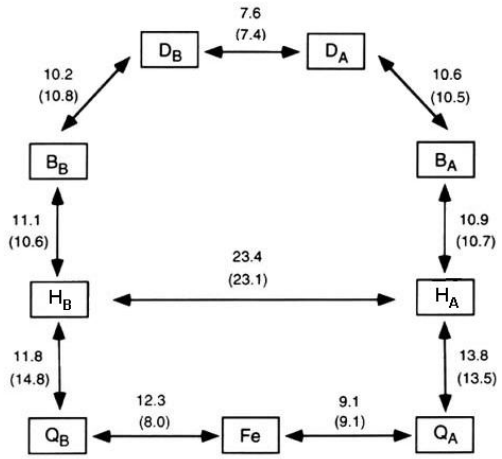

Figure 13: Distances (in Å) between the cofactors in the RC's of *Rb. sphaeroides* and of *Rp. viridis* (in brackets) using only the porphyrin and the quinone rings for the centre of mass calculations.

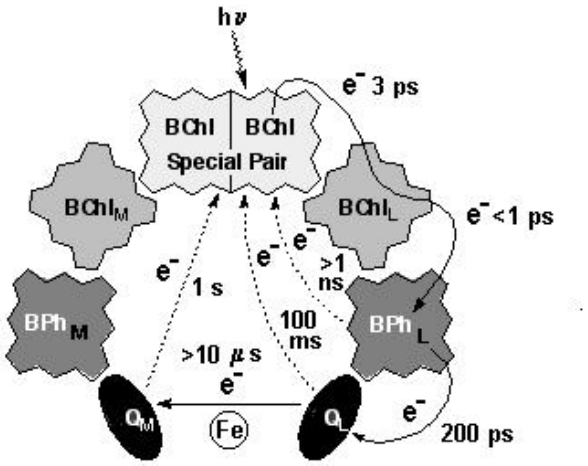

Figure 14: Charge-separated intermediates and their lifetimes in the bacterial photosynthetic reaction center.

rate between cofactors in the RC of Purple Bacteria are shown in Figs. 13, 14.

The functional asymmetry is served by the significantly different properties of the two quinones, which arise from protein-quinone interactions. For example, the primary quinone environment is much more hydrophobic than that of the secondary quinone and the hydrogen bonding is more asymmetric. The protonation states of nearby amino acid residues, in particular carboxylate groups, has been clearly established to be crucial to the function of the secondary quinone, which becomes fully protonated and leaves the reaction center. The quinones of photosystem II are thought to bind in homologous sites although the possible involvement of protonatable residues in the electron transfer process requires

more detailed studies. Open areas of investigation are delineation of the mechanism of electron transfer from the primary to the secondary quinone and the role of quinone movement during electron transfer [25, 26]. Unlike the quinone type of reaction centers, the iron-sulfur reaction centers could ideally be well served by having two functional branches of cofactors. The iron-sulfur clusters are more functionally symmetric than the quinone electron acceptors reflective of their role of single electron carriers to an external protein. Whether electron transfer in the iron-sulfur type of reaction centers is symmetric or asymmetric remains a subject of new investigation.

Our understanding of the primary processes in photosynthesis is not complete without explanation of the strong asymmetry in ET. We believe that the reason for asymmetric ET between prosthetic groups located on different polypeptides is a different molecular dynamics. Dynamics of atoms causes the change of the electrical potential fields and the conformational variations influence the mutual orientations between cofactors. Then the energy gap and overlap of electronic wave functions fluctuates as a result in the system. The net result is a different fluctuation of electronic energy levels on prosthetic groups and also a different fluctuations of the overlaps of the electronic wave functions on L and M branches. On the other hand the chain located on subunit M is inactive in ET and the highly asymmetric functionality, however, can be decreased by amino acid mutations or cofactor modification. This approach can be used to explain the effect of individual amino acid mutation or cofactor modifications on the observed balance between the forward ET reaction on the L-side of the RC, the charge recombination processes, and ET to the M-side chromophores [27, 28, 29, 30].

Structural and functional relevance to the photosystem

All of the above-mentioned bacterial RC's are derived from purple bacteria, and are thought to be the ancestors of PSII in the thylakoid membrane of higher organisms; purple bacterial RC and PSII are classified into the pheophytin-quinone type. On the other hand, RC's belonging to the iron-sulfur type are present in green sulfur bacteria and heliobacteria, and are thought to be the ancestors of PSI. The subunit composition of bacterial RC complexes is simpler than that of PSI and PSII in higher organisms. However, the basic function and assembly of bacterial RC are significantly similar to those of PSI and PSII (Fig. 15).

Three-dimensional structures of PSI and PSII have already been determined by X-ray crystallography, and the spatial arrangement of co-factors and trans-membrane helices have also been described to some extent [31]. These three-dimensional structures have shown, together with those of bacterial RC's, that RC's of any type possess common structural features. For example, a heterodimer of protein subunits forms the central part of the complex. Each monomer possesses five trans-membrane helices and maintains co-factors including the special-pair. These dimeric assemblies, including co-factors as well as protein subunits, are arranged with a pseudo twofold symmetry axis perpendicular to the membrane plane.

In the future, continuous efforts will be made to elucidate the structure-function relationship of PSI and PSII. Until the final goal is reached, however, the high-resolution structures of bacterial RC's will continue to provide important information for understanding the structural features of PSI and PSII. Remarkable progress in the techniques of crystallization and structure determination has made it possible to reveal the three-dimensional structures of super-molecular complexes, including membrane proteins. In particular, progress in the crystallization method of membrane proteins should be emphasized. Further studies in this field will make it possible to determine the structure of the

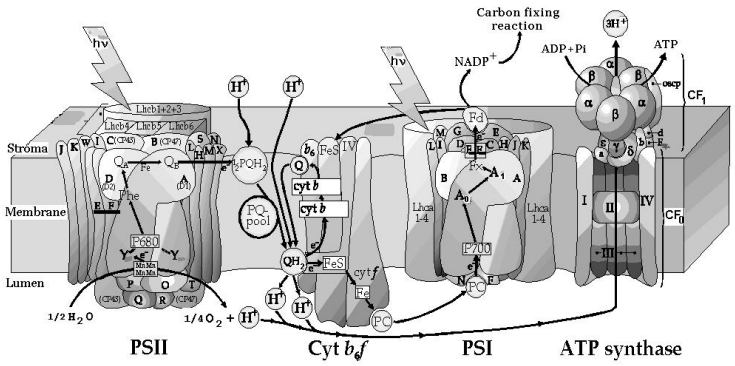

Figure 15: The schematic model of the main photosynthetic complexes situated within the *higher plant* thylakoid membrane, where photosystem II is shown as the second major complex in the electron transport chain, after the light harvesting components. Photosystem II (PSII) is the membrane protein complex found in oxygenic photosynthetic organisms (cyanobacteria and higher plants), which harnesses light energy to split H_2O into O_2, protons and electrons. It drives the most oxidising reaction known to occur in nature and is responsible for the production of atmospheric oxygen, essential for aerobic life on this planet (http://www.life.uiuc.edu/govindjee/photoweb).

super-complex of the photosynthetic apparatus more accurately, which, in turn, will lead to a profound understanding of its molecular mechanisms.

Although the evolutionary pathways cannot be established uniquely, the process giving rise to the two core subunits that are related by an approximate two-fold symmetry axis can be traced by alterations in the structural genes. Comparison of the biosynthetic pathways of the various cofactors found in the reaction centers can also be used to track the evolutionary path. Consideration of both the energetic requirements and the pigment composition needed for photosynthetic capability has led to specific scenarios for the stages in the evolution of photosynthesis. Additional clues should be provided by characterization of newly discovered photosynthetic organisms that contain novel cofactors [32, 33].

Kinetics of reaction centers

In plants and bacteria the energy of light is stored in the energy of the electric potential later used to form chemical bonds. The reaction center complex from the anoxygenic purple photosynthetic bacteria are the best understood of all photosynthetic organisms, from both a structural and a functional point of view. Photosynthesis begins when light is absorbed by an antenna pigment (Fig. 16). Antennas permit an organism to increase

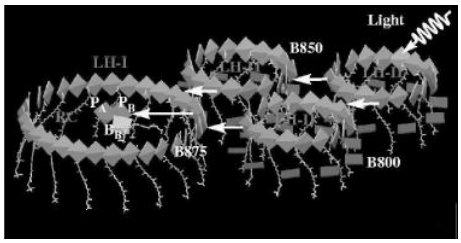

Figure 16: Scheme of the energy transfer from the light-harvesting antenna to the reaction center.

greatly the absorption cross section for light without having to build an entire reaction center and associated electron transfer system for each pigment, which would be very

costly in terms of cellular resources. The excited (bacterio)chlorophyll molecule transfers an electron to a nearby acceptor molecule, thereby creating an ion pair state consisting of the oxidized chlorophyll and reduced acceptor. After the initial electron transfer event, a series of electron transfer reactions takes place that eventually stabilizes the stored energy in forms that can be used by the cell (Fig. 17). Before we start with explanation of our approaches to solve the problem of unidirectionality of ET in reaction center we want to show shortly some historical fundamental steps to understanding of rate of electron transfer in biological systems.

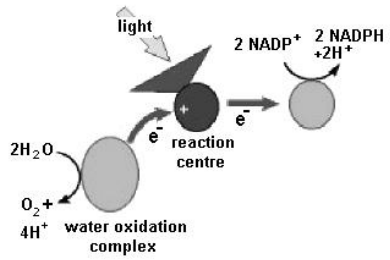

Figure 17: Scheme of the light-induced cyclic electron flow and the generation and utilization of a transmembrane electrochemical potential in the purple bacterium.

Marcus theory

Marcus theory (1992 Nobel Prize in Chemistry) assumes that the energy supplied to the electron by the solvent can be represented by a spring with the spring length representing the reaction coordinate [34]. The variation in energetic state of a biatomic molecule can be described in a simple model in which the bond joining the two atoms vibrates, so that the energy of the bond varies as the length of the bond varies. The change in energy with bond length is given by Hooke's Law.

In Hooke's Law, the relation between energy and bond length gives a parabolic curve, and provides the framework for discussion of the dependence of energy on vibrational state, and hence on temperature. As the temperature increased, the increased vibrational energy allows the molecule to *swing* along the parabola, so that it visits the higher energy levels more frequently. This Hooke's Law description is useful in discussion of the energy levels in more complicated molecules. The distance is replaced by a nuclear coordinate, which lumps together all the distances in all the bonds, and a single representative parabola is used to represent the parabolas of all the bonds. This is obviously a gross simplification, the real picture would require a multidimensional representation, but it provides a handy frame of reference. In the Fig. 18, two different electron transfer reactions are represented, one diabatic, and the other adiabatic. In both cases, the system is represented in two states, that before electron transfer (R the reactant state), and that after electron transfer (P the product state). It is important to realize that these represent two different states of the same system.

(1) Parabolas, because nuclear vibrations are harmonic oscillators, and obey Hooke's Law.

(2) Electron jumping from R to P has to occur at cross-over point (C) because of :

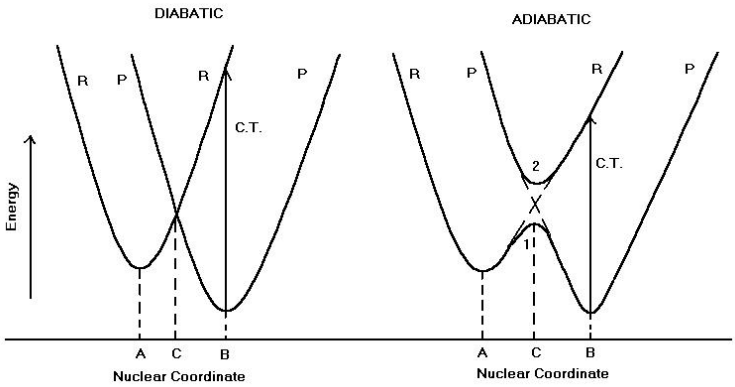

Figure 18: The role of nuclear motion in electron transfer. The ordinates represent potential energy of the nuclei of the whole system: donor + acceptor + surroundings. The curves should be hypersurfaces in a space of as many dimensions as nuclear coordinates (+ 1 for energy). The abscissa represents a combination of the positions of all the nuclei disturbed by the electronic transition and runs along an axis from the initial equilibrium configuration, labelled A, to final equilibrium configuration labelled B. Curve R is the potential energy of the nuclei when the electron donor is reduced and acceptor oxidized. P is the nuclear potential energy when the donor is oxidized and the acceptor reduced. Passage from R to P represents electron transfer and occurs in the vicinity of the crossover, nuclear configuration C. In the non-adiabatic case (diabatic), passage through C does not usually cause transition from R to P. In the adiabatic case it usually does, and interaction between R and P is so strong that appreciable splitting into curves 1 and 2 is seen at C. R rides over to P on the surface, 1 [34].

(a) Frank-Condon principle. Electron transfer occurs so rapidly (in a vibrational frequency) that no change in nuclear configuration can occur during the transfer. This requires that the transfer is a vertical transition in the diagram.

(b) Conservation of energy requires that the transition is a horizontal line on the diagram. The only place where both conditions are fulfilled is where the nuclear energy profiles cross (C). The crossing point represents the energy level to which the reactant state must be raised before progressing to the product state.

(3) Diabatic and adiabatic processes :

(a) Diabatic (the term more often used is non-adiabatic), electron transfer is a quantum jump from one curve to the other (curves cross).

(b) Adiabatic, in thermodynamics, an adiabatic process is one in which no exchange of heat with the environment occurs. In the electron transfer context, an adiabatic process is one in which no quantum jump occurs. Since nuclear motion is generally much slower than electronic motion, one can approximate the electronic part of the wave-function of a molecular system by solving for it with nuclei fixed in position. The electronic energy eigenvalues obtained this way, when plotted as a function of the nuclear positions, form adiabatic surfaces which become potential-energy surfaces for nuclear motion.

(4) Coupling the process to the environment. (See Fig. 19 for terms) λ is the coupling, or the reorganizational energy. It is the energy required to displace the system an amount $Q = X_B - X_A$ without electron transfer. This is the energy required to transfer the electron from the bottom of the energy profile of the acceptor (product)

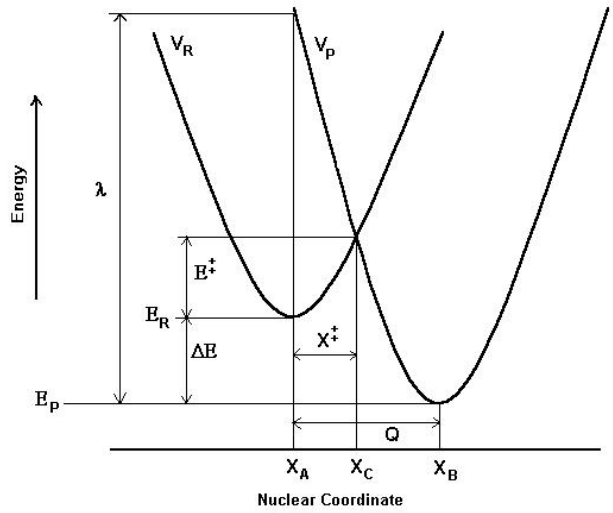

Figure 19: Nuclear motion accompanying electron transfer [34].

state up to the energy profile of the acceptor state in the same nuclear configuration as the energy minimum of the donor state.

Value for λ comes from Hooke's Law

$$\lambda = \frac{k_H Q^2}{2}, \tag{1}$$

where k_H is the Hook's law force constant. Marcus separated λ into two parts, $\lambda_i + \lambda_0$, where λ_i is the reorganizational energy of the inner shell of atoms and λ_0 is that of the surrounding solvent molecules. λ_i is calculated from the parameters of the innershell vibrational modes:

$$\lambda_i = \frac{1}{2} \sum_j k_{Hj} Q_j^2. \tag{2}$$

λ_0 is estimated from the polarizability of the solvent considered to be a continuous polar medium:

$$\lambda_0 = \frac{(\Delta e)^2}{4\pi\varepsilon_0} \left(\frac{1}{2r_1} + \frac{1}{2r_2} - \frac{1}{r_{12}} \right) \left(\frac{1}{D_{op}} - \frac{1}{D_S} \right), \tag{3}$$

where Δe is the charge transferred from donor to acceptor; r_1 and r_2 are the radii of the two reactants when in contact; r_{12} is $r_1 + r_2$; D_{op} is the square of the refractive index of the medium and D_S its static dielectric constant, and ε_0 is the permittivity of space to give S.I. units. In general λ involves moving positively charge polar groups in the vicinity of the electron donor further from the donor and in the vicinity of the acceptor closer to the acceptor. *Vice versa* for negatively charged groups.

From the Fig. 19, it can be seen λ, $E^{\ddagger}$ and $\triangle E$ where $\triangle E = E_R - E_P$ are related, so that :

$$E^{\ddagger} = \frac{(\lambda - \Delta E)^2}{4\lambda}, \tag{4}$$

the reorganizational energy depends on the relative positions of the parabolas in both reaction coordinate and energy dimensions. The main challenge for the Marcus theory is to calculate the *activation Gibbs energy*. An important point is the condition under which the Products parabola intersects the Reactant parabola at the minimum (when activation energy $E^{\ddagger}$ is zero). Under these conditions, since the activation energy is zero,

$$\lambda = -\Delta G^0 \tag{5}$$

($-\Delta G$ is the difference in Gibbs energies corresponding to two equilibrium elongations of the spring and here corresponds to ΔE in the Fig. 19 and equations above) and the reaction proceeds with its maximal rate, with an intrinsic maximal rate constant (k^0_{ET}) normalized to this condition. The dependence of the activation barrier on the standard reaction Gibbs energy is called the *electron transfer energy gap law*. Values for (k^0_{ET}) can be found experimentally by measuring the rate constant for a reaction under different conditions, giving different values for ΔG. The theoretical curve is shown in Fig. 20. An

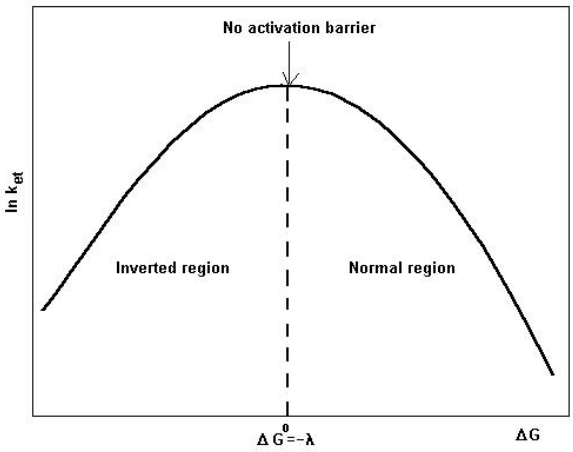

Figure 20: The theoretical curve of the rate constant for different values ΔG. (C. Turro, J. M. Zaleski *et al.*, *Biomolecular Electron Transfer in the Marcus Inverted Region*, J. Am. Chem. Soc. 118 (1996) 6060).

important aspect of this curve is that it goes through a maximum at the value where the above equation holds, and this implies that a value for λ could be determined by experiment. A second important characteristic is the bell-shape, which implies that the rate constant decreases as the driving force ΔG increases beyond the value at which it is equal to $-\lambda$. The conditions under which this dropping-off of rate with increased driving force occurs is known as the Marcus *inverted region* when condition is satisfied:

$$\Delta G < -\lambda. \tag{6}$$

If

$$-\Delta G < \lambda \tag{7}$$

we have the *normal region* of electron transfer. This was an important prediction of the theory subject to experimental test. The Marcus theory predicted the rate constant of

electron transfer in the following form (Fig. 20):

$$\ln k_{et} = \frac{-(\lambda - \Delta E)^2}{4\lambda} + constant. \tag{8}$$

Research on photochemical reaction centers has been a primary arena for advances in understanding of the relation between structure and rates of electron transfer in proteins, because the crystallographically defined structures provided for the first time, in the context of an experimental system in which the rates could be accurately measured by picosecond spectroscopy, the spatial parameters and details of reaction medium (the protein) necessary for understanding these processes. A major advance in these studies came from an extensive set of experiments from Dutton's lab [34], in which several different reactions of the photochemical cycle were measured (and rate constants determined), with a variety of molecular engineering tricks to set up a range of values for ΔG for the reactions. The Fig. 21 summarize the results of this experimental work.

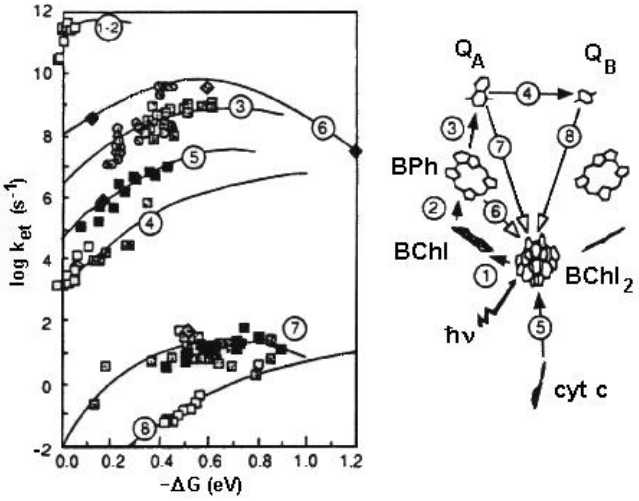

Figure 21: The experimental curve of the rate constants for reaction center of *Rhodopseudomonas viridis* depending on different values ΔG.

We can see excellent coincidence between theory and experiment for solving electron transfer in biological systems as for example in bacterial photosynthetic reaction centers.

Tunnelling in biology

Next way for electron transfer in biological systems is tunnelling of particles between molecules [34, 35]. Electrons occupy states with discrete energy levels in molecules. Tunnelling means that electrons can be located at any of the molecules provided the energy levels for the electrons are equal. Tunnelling is the direct consequence of the Heisenberg uncertainty principle:

$$\Delta x \Delta p \simeq \hbar. \tag{9}$$

As long as one knows the energy of the electron ($\triangle p = 0$), one cannot say where the electron is located. Electrons are transferred by tunnelling through a potential barrier, the

height of which is determined by the ionization energies of the DA and D^+A^- complexes. The energies of electron on the donor and acceptor must be equal. Otherwise no tunnelling is possible. The probability of the particle penetrating the barrier, if small compared to 1,

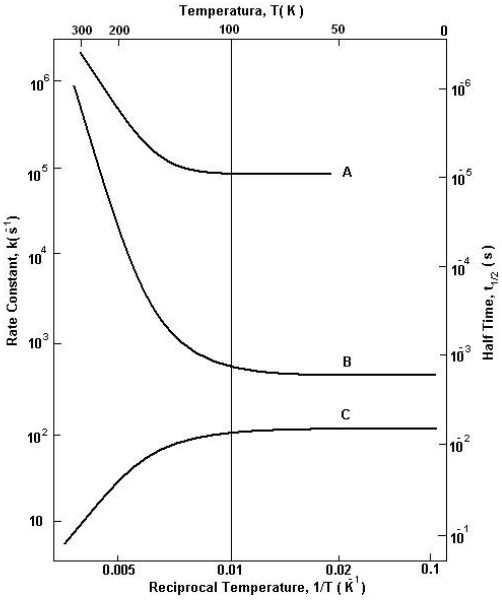

Figure 22: Schematic picture of the temperature-dependence of photosynthetic electron-transfer in bacteria. Curves A and B described: photo-induced cytochrome oxidation. Curves C reversed primary reaction [34].

is:

$$P = 16EV(E+V)^{-2}\exp(-\frac{2b\sqrt{2mV}}{\hbar}), \tag{10}$$

where $\hbar$ is Planck's constant, m is the mass of the particle, E is the kinetic energy of the approaching particle, V is the barrier height and b is the barrier width.

Another way of expressing this probability, used by Oppenheimer (1928), for example, is in terms of an element, H_{ab} of the quantum mechanical Hamiltonian matrix which governs the rate of transition from an initial state, a of the system to a final state b. The rate of transition is proportional to the square of the absolute value of the matrix element $|H_{ab}|^2$. It is often expressed by

$$rate(a \to b) = \frac{2\pi}{\hbar}|H_{ab}|^2\rho, \tag{11}$$

which has been called the *golden rule* of quantum mechanics. ρ is a *density of states* , that is, the number of substates qualifying as b per unit interval of energy. In equation (11) the *transition* may or may not be by tunnelling.

The simplest conceptual framework for modelling the observed rate of the primary charge separation is the Golden Rule expression obtained by Marcus in the high- temperature limit:

$$k_{et} \simeq V^2(\frac{2\pi}{2\lambda k_B T})^{1/2}\exp\{-\frac{(\lambda-\Delta E)^2}{4\lambda k_B T}\}, \tag{12}$$

where $V = H_{ab}$ is the electronic matrix element between the initial (photoexcited) and final (charge-separated) states, ΔE is the free energy gap between these states, λ is the "reorganization energy" of the reaction (the energy to distort the system configuration from reactants to products), k_B is Boltzmann constant, and T is the temperature.

If the electron transfer reaction shows temperature dependence at high temperature and temperature independence at low temperature (Fig. 22), this can be taken as good evidence that the nuclei are tunnelling their activation barrier at the low temperatures.

Objects and organization of the thesis

The charge-separating electron transfer reactions occur with a remarkably high quantum yield of 96%, where from two possible symmetric branches only the branch L is active in the electron transfer. This efficiency relies on the rates of the charge-separating reactions being 2-3 orders of magnitude faster than the rates of the competing reactions. Therefore, we wish to understand which features of the reaction center are responsible for the rate constants of these reactions. Of particular interest are both the primary charge separation from the first excited state P^* to the bacteriochlorophyll BCh_L and consequently to the bacteriopheophytin BPh_L or electron transfer directly to the BPh_L, where BCh_L serves as *virtual* intermediate state for ET. The first type of the electron transfer is referred to as the "sequential", the other one as the "superexchange" mechanism of ET.

The aim of the thesis is to explain the unidirectionality of ET through the RC, where only the branch L is active in the electron transfer. The thesis is divided in two major approaches for solving the electron transfer in photosynthetic organisms: the stochastic and nonstochastic models of electron transfer.

The part Introduction is mainly introductory to the problem of electron transfer from the biological point of view. We discuss systematically all the aspects for making the implementation and understanding of unidirectionality of the electron transfer through bacterial reaction centers. We want to elucidate biological functions of electron transfer in photosynthetic systems. Moreover, we want to reveal some deeper aspects of electron transfer mechanisms for understanding of unidirectionality of electron transfer (ET) in photosynthetic reaction centers. To find general principles for transporting of energy and next utilization by cell we describe the mechanism of ET in bacterial reaction centers as well as in a more complicated PS II, PS I systems in plants.

Part I is devoted to solving the asymmetric electron transfer in bacterial reaction centers and is divided into five chapters. Chapter 1 describes the first theoretical look to the problem of electron transfer, we present the stochastic sequential model to elucidate the unidirectionality of the primary charge separation process in the bacterial reaction centers where two symmetric ways of electron transfer, starting from the common electron donor are possible. We have used a model of three sites/molecules with ET beginning at site 1 with option to proceed to site 2 or site 3. If the direct ET between sites 2 and 3 is not allowed and electron cannot escape from the system then it is shown that the different stochastic fluctuations in the energy of sites and the interaction between sites on these two ways are sufficient to cause the transient asymmetric electron distribution at the sites 2 and 3 during the relaxation to the steady state. It means that the overall asymmetric ET can be caused by the transient asymmetric electron distribution if there is a possibility for electron to escape from the three sites system. To explore this possibility we have introduced a sink into the model at the end of each sites 2 and 3. The dependence of the asymmetry in electron transfer on the value of the sink parameter, introduced through an additional imaginary diagonal matrix element of the Hamiltonian, was investigated. The results show indeed that the unidirectionality of the electron transfer generated in the system of three molecules depends strongly on the sink parameter value. The results from Chapter 1 were published in [36, 37].

In Chapter 2 we also present a model to elucidate the unidirectionality of the primary charge-separation process in the bacterial reaction centers. We have used a model of three

sites/molecules with electron transfer beginning at site 1 with an option to proceed to site 2 or site 3. We used a stochastic sequential model with arbitrary correlation functions. We get the quantum yields of electron escape via the sites 2,3 in two limiting cases that correspond to a spectral density of underdamped and overdamped Brownian oscillator. In the fast modulation limit of an overdamped regime we get the effect, which was named "fear of death," in which for strong enough sink parameters the electron has a tendency to avoid the place with greater sink. The presented model was used to provide a plausible explanation of the temperature dependence of the quantum yields of the *Rhodobacter sphaeroides* photosynthetic reaction center in the high-temperature regime. We finally published results from these models in [38, 39] as well as several new insights and the results are in press [40].

In Chapter 3 the nonstochastic model of electron transfer was employed to elucidate the unidirectionality of the primary charge separation process in the bacterial photosynthetic reaction centers. The model assumes that the vibrational relaxation of the medium modes is sufficiently fast and that the system relaxes to thermal equilibrium after each ET step. ET was investigated for 6-sites (molecules) arranged in two branches. Beginning at molecule 1, ET can proceed in two directions with M branch composed of two molecules and L branch composed of three molecules. The analysis shows that the model can successfully explain the asymmetry in primary electron transfer both in the wild type and several mutants of *Rb. capsulatus* RC. In these cases the dependence of ET asymmetry on temperature was also evaluated. The results are compared with the superexchange mechanism of ET in Chapter 4. This model was published in [41, 42].

In Chapter 4 the superexchange mechanism operating in parallel with the sequential process in both branches was evaluated. Up to now we have assumed that ET has a sequential character in both branches of RC. Chapter 4 describes the contribution from the superexchange mechanism to both M and L side ET. Our analysis reveals only a very small contribution of the superexchange mechanism to ET in bacterial RC. The new results from this approach are being prepared for the submission for publication [43].

In Chapter 5 I summarize the main results from the models of asymmetric electron transfer. Finally, I make some plans to the future.

Part I

MODELS FOR ASYMMETRIC ELECTRON TRANSFER:

Stochastic and nonstochastic models for ET in RC's

Chapter 1

The stochastic model with white noise

1.1 Theory

To describe the first steps of electron transfer processes in the reaction centers we have used the three-site model. The model is basically an extension of the theory of coupled motion of a quantum particle in a fluctuating medium [44-54]. Let us designate the special pair (P) as site 1, the sites 2 and 3 then represent the first molecules on the branches M and L. Because of symmetry we assume that both local energies at 2 (branch M) and 3 (branch L) and the hopping terms between molecule 1 and molecule 2 or 3 on both branches are also the same. We forbid the direct ET between sites 2 to 3 and consider that this three level system is coupled stochastically to a bath with white noise. We assume that the energy levels 2 and 3 have an imaginary part which describes the interaction with the next molecule in the branch. The meaning of the imaginary part is the lifetime of electron localization at the site 2 or 3 in the limit when hopping terms are zero [52] . The imaginary part of the energy level 1 describes the probability of electron deactivation to the ground state. Then the Hamiltonian of our model has the form

$$H = \sum_{k=1}^{3} E_k a_k^\dagger a_k + \sum_{i=2,3} (J + \alpha_i(t))(a_i^\dagger a_1 + \text{H.c.}), \tag{1.1}$$

where J is the electronic coupling parameter (hopping term). The E_i and $a_i^\dagger a_i$ are the site energy and the creation (annihilation) operator of the electron at site i, correspondingly. The terms α_i represent stochastic fluctuations of electronic coupling parameter. We assume that

$$E_1 = \varepsilon_1 - i\Gamma_1\,, \tag{1.2a}$$

$$E_2 = \varepsilon_2 - i\Gamma_2 + \beta_2(t)\,, \tag{1.2b}$$

$$E_3 = \varepsilon_3 - i\Gamma_3 + \beta_3(t)\,. \tag{1.2c}$$

Here β_i represents stochastic fluctuations in the energy at site i. The parameter $\hbar/2\Gamma_i$ has a meaning of the lifetime of the electron localization at the site i in the limit of zero coupling parameter. Our assumption about the stochastic functions is that

$$\langle \beta_k(t) \rangle = \langle \alpha_i(t) \rangle = 0 \tag{1.3}$$

and different from zero are only the following correlation functions

$$\langle \alpha_i(t)\alpha_i(\tau)\rangle = \triangle_i \delta(t-\tau), i=2,3, \tag{1.4a}$$

$$\langle \beta_k(t)\beta_k(\tau)\rangle = \mu_k \delta(t-\tau), k=2,3. \tag{1.4b}$$

Here $\langle\rangle$ denotes the statistical ensemble average. Relations (1.4) imply that the fluctuations at different times are uncorrelated and correspond to the shortest correlation time limit of a Gaussian-Markov process.

The main goal of the present work is to compute the rate of quantum yield Φ_3 and Φ_2 of the electron escape via the branch L (site 3) and M (site 2). We start from the Liouville equation

$$i\hbar\frac{\partial}{\partial t}\rho(t) = [H\rho(t) - \rho(t)H^{\dagger}]. \tag{1.5}$$

In the matrix form we get

$$\begin{aligned}
i\hbar\partial_t\rho_{11}(t) &= (J+\alpha_2(t))(\rho_{21}(t)-\rho_{12}(t)) + (J+\alpha_3(t))(\rho_{31}(t)-\rho_{13}(t)) \\
&\quad -2i\Gamma_1\rho_{11}(t), && (1.6a)\\
i\hbar\partial_t\rho_{12}(t) &= (J+\alpha_2(t))(\rho_{22}(t)-\rho_{11}(t)) + (\varepsilon_1-\varepsilon_2-i\Gamma_1 \\
&\quad -i\Gamma_2-\beta_2(t))\rho_{12}(t) + (J+\alpha_3(t))\rho_{32}(t), && (1.6b)\\
i\hbar\partial_t\rho_{21}(t) &= (J+\alpha_2(t))(\rho_{11}(t)-\rho_{22}(t)) + (\varepsilon_2+\beta_2(t)-i\Gamma_2 \\
&\quad -i\Gamma_1-\varepsilon_1)\rho_{21}(t) - (J+\alpha_3(t))\rho_{23}(t), && (1.6c)\\
i\hbar\partial_t\rho_{22}(t) &= -2i\Gamma_2\rho_{22}(t) + (J+\alpha_2(t))(\rho_{12}(t)-\rho_{21}(t)), && (1.6d)\\
i\hbar\partial_t\rho_{13}(t) &= (J+\alpha_3(t))(\rho_{33}(t)-\rho_{11}(t)) + (\varepsilon_1-\varepsilon_3-i\Gamma_1 \\
&\quad -i\Gamma_3-\beta_3(t))\rho_{13}(t) + (J+\alpha_2(t))\rho_{23}(t), && (1.6e)\\
i\hbar\partial_t\rho_{31}(t) &= -(J+\alpha_3(t))(\rho_{33}(t)-\rho_{11}(t)) - (\varepsilon_1-\varepsilon_3+i\Gamma_3 \\
&\quad +i\Gamma_1-\beta_3(t))\rho_{31}(t) - (J+\alpha_2(t))\rho_{32}(t), && (1.6f)\\
i\hbar\partial_t\rho_{23}(t) &= (\varepsilon_2-\varepsilon_3+\beta_2(t)-\beta_3(t)-i\Gamma_2-i\Gamma_3)\rho_{23}(t) \\
&\quad -(J+\alpha_3(t))\rho_{21}(t) + (J+\alpha_2(t))\rho_{13}(t), && (1.6g)\\
i\hbar\partial_t\rho_{32}(t) &= -(\varepsilon_2-\varepsilon_3+\beta_2(t)-\beta_3(t)+i\Gamma_2+i\Gamma_3)\rho_{32}(t) \\
&\quad +(J+\alpha_3(t))\rho_{12}(t) - (J+\alpha_2(t))\rho_{31}(t), && (1.6h)\\
i\hbar\partial_t\rho_{33}(t) &= -2i\Gamma_3\rho_{33}(t) + (J+\alpha_3(t))(\rho_{13}(t)-\rho_{31}(t)). && (1.6i)
\end{aligned}$$

The averaging (1.6) gives terms $\langle\alpha_k\rho_{ij}\rangle$, $\langle\beta_k\rho_{ij}\rangle$. To split these terms we use Furutsu-Novikov relation [55, 56, 57]

$$\langle \alpha_k(t)\rho_{ij}(t)\rangle = \sum_{\lambda=\alpha}^{\beta}\sum_{l=2}^{3}\int d\tau\langle\alpha_k(t)\lambda_l(\tau)\rangle\left\langle\frac{\delta\rho_{ij}(t)}{\delta\lambda_l(\tau)}\right\rangle, \tag{1.7a}$$

$$\langle \beta_k(t)\rho_{ij}(t)\rangle = \sum_{\lambda=\alpha}^{\beta}\sum_{l=2}^{3}\int d\tau\langle\beta_k(t)\lambda_l(\tau)\rangle\left\langle\frac{\delta\rho_{ij}(t)}{\delta\lambda_l(\tau)}\right\rangle. \tag{1.7b}$$

Then we have

$$\begin{aligned}
\partial_t\langle\rho_{11}(t)\rangle &= -i\frac{J}{\hbar}(\langle\rho_{21}(t)\rangle - \langle\rho_{12}(t)\rangle + \langle\rho_{31}(t)\rangle - \langle\rho_{13}(t)\rangle) \\
&\quad -\frac{2\Delta_2}{\hbar^2}(\langle\rho_{11}(t)\rangle - \langle\rho_{22}(t)\rangle) \\
&\quad -\frac{2\Delta_3}{\hbar^2}(\langle\rho_{11}(t)\rangle - \langle\rho_{33}(t)\rangle) - \frac{2\Gamma_1}{\hbar}\langle\rho_{11}(t)\rangle, \qquad (1.8a)\\
\partial_t\langle\rho_{12}(t)\rangle &= -\frac{\Gamma_1+\Gamma_2}{\hbar}\langle\rho_{12}(t)\rangle - i\frac{\varepsilon_1-\varepsilon_2}{\hbar}\langle\rho_{12}(t)\rangle \\
&\quad -i\frac{J}{\hbar}(\langle\rho_{22}(t)\rangle - \langle\rho_{11}(t)\rangle + \langle\rho_{32}(t)\rangle) \\
&\quad +\frac{2\Delta_2}{\hbar^2}(\langle\rho_{21}(t)\rangle - \langle\rho_{12}(t)\rangle) - \frac{\mu_2+\Delta_3}{\hbar^2}\langle\rho_{12}(t)\rangle, \qquad (1.8b)\\
\partial_t\langle\rho_{21}(t)\rangle &= -\frac{\Gamma_1+\Gamma_2}{\hbar}\langle\rho_{21}(t)\rangle + i\frac{\varepsilon_1-\varepsilon_2}{\hbar}\langle\rho_{21}(t)\rangle \\
&\quad +i\frac{J}{\hbar}(\langle\rho_{22}(t)\rangle - \langle\rho_{11}(t)\rangle + \langle\rho_{23}(t)\rangle) \\
&\quad +\frac{2\Delta_2}{\hbar^2}(\langle\rho_{12}(t)\rangle - \langle\rho_{21}(t)\rangle) - \frac{\mu_2+\Delta_3}{\hbar^2}\langle\rho_{21}(t)\rangle, \qquad (1.8c)\\
\partial_t\langle\rho_{22}(t)\rangle &= -\frac{2\Gamma_2}{\hbar}\langle\rho_{22}(t)\rangle - i\frac{J}{\hbar}(\langle\rho_{12}(t)\rangle - \langle\rho_{21}(t)\rangle) \\
&\quad +\frac{2\Delta_2}{\hbar^2}(\langle\rho_{11}(t)\rangle - \langle\rho_{22}(t)\rangle), \qquad (1.8d)\\
\partial_t\langle\rho_{13}(t)\rangle &= -\frac{\Gamma_1+\Gamma_3}{\hbar}\langle\rho_{13}(t)\rangle - i\frac{\varepsilon_1-\varepsilon_3}{\hbar}\langle\rho_{13}(t)\rangle \\
&\quad -i\frac{J}{\hbar}(\langle\rho_{33}(t)\rangle - \langle\rho_{11}(t)\rangle + \langle\rho_{23}(t)\rangle) \\
&\quad -\frac{\mu_3+\Delta_2}{\hbar^2}\langle\rho_{13}(t)\rangle - \frac{2\Delta_3}{\hbar^2}(\langle\rho_{13}(t)\rangle - \langle\rho_{31}(t)\rangle), \qquad (1.8e)\\
\partial_t\langle\rho_{31}(t)\rangle &= -\frac{\Gamma_1+\Gamma_3}{\hbar}\langle\rho_{31}(t)\rangle + i\frac{\varepsilon_1-\varepsilon_3}{\hbar}\langle\rho_{31}(t)\rangle \\
&\quad +i\frac{J}{\hbar}(\langle\rho_{33}(t)\rangle - \langle\rho_{11}(t)\rangle + \langle\rho_{32}(t)\rangle) \\
&\quad -\frac{\mu_3+\Delta_2}{\hbar^2}\langle\rho_{31}(t)\rangle + \frac{2\Delta_3}{\hbar^2}(\langle\rho_{13}(t)\rangle - \langle\rho_{31}(t)\rangle), \qquad (1.8f)\\
\partial_t\langle\rho_{23}(t)\rangle &= -\frac{\Gamma_2+\Gamma_3}{\hbar}\langle\rho_{23}(t)\rangle + i\frac{\varepsilon_3-\varepsilon_2}{\hbar}\langle\rho_{23}(t)\rangle \\
&\quad -i\frac{J}{\hbar}(\langle\rho_{13}(t)\rangle - \langle\rho_{21}(t)\rangle) \\
&\quad -\frac{\mu_2+\mu_3+\Delta_2+\Delta_3}{\hbar^2}\langle\rho_{23}(t)\rangle, \qquad (1.8g)
\end{aligned}$$

$$\partial_t\langle\rho_{32}(t)\rangle = -\frac{\Gamma_2+\Gamma_3}{\hbar}\langle\rho_{32}(t)\rangle - i\frac{\varepsilon_3-\varepsilon_2}{\hbar}\langle\rho_{32}(t)\rangle + i\frac{J}{\hbar}(\langle\rho_{31}(t)\rangle - \langle\rho_{12}(t)\rangle) - \frac{\mu_2+\mu_3+\Delta_2+\Delta_3}{\hbar^2}\langle\rho_{32}(t)\rangle, \tag{1.8h}$$

$$\partial_t\langle\rho_{33}(t)\rangle = -\frac{2\Gamma_3}{\hbar}\langle\rho_{33}(t)\rangle - i\frac{J}{\hbar}(\langle\rho_{13}(t)\rangle - \langle\rho_{31}(t)\rangle) + \frac{2\Delta_3}{\hbar^2}(\langle\rho_{11}(t)\rangle - \langle\rho_{33}(t)\rangle). \tag{1.8i}$$

We assume that $\Gamma_1 = 0$ and $\Gamma_2 = \Gamma_3 = \Gamma$. In the computations of (1.8) we put $\varepsilon_1 = 0$. The numerical solution of this set of differential equations both for Γ equal to and not equal to zero is presented in Figs. 1.1 and 1.2. In both cases we start with an electron initially localized at the site 1. The behaviour of the system depends strongly on the fluctuation of the parameters. For the case of $\Gamma_2 = \Gamma_3 = \Gamma = 0$ (Fig. 1.1) the probability to find an electron at site 1 is decreasing with the elapsed time. However, the probability to find electron at site 2 and 3 increases asymmetrically. At the site 2 the probability is slowly approaching the value of 1/3 in a long time scale. The different behaviour is observed at the site 3. At this site the probability is rapidly raised and at some specific time it has a value greater than 1/3 and with the elapsing time it relaxes to 1/3. This kind of overall

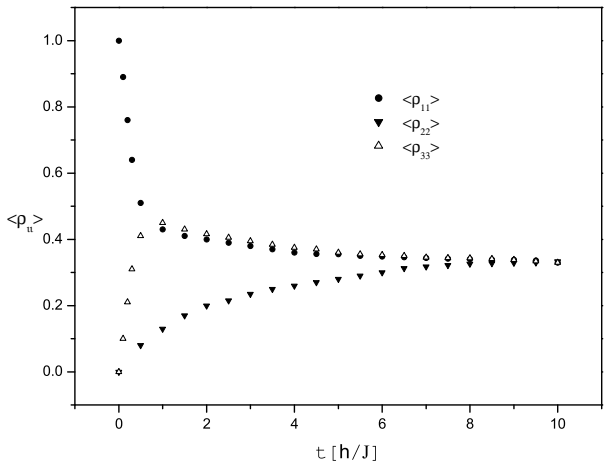

Figure 1.1: The time dependence of the site-occupation probabilities $\langle\rho_{ll}(t)\rangle$ for the sites $l = 1, 2, 3$. The following parameters were used: $J = 1$, $\Gamma = 0$, $\varepsilon_2 = 10$, $\varepsilon_3 = 10$, $\mu_2/\hbar = 2$, $\mu_3/\hbar = 8$, $\Delta_2/\hbar = 0.1$, $\Delta_3/\hbar = 1$. J is a hopping term; ε_i are the site energies; μ_i and Δ_i characterize the energy level fluctuation and the fluctuations of hopping term at site i, respectively. Γ describes the possibility of electronic escape from the system of three molecules. Time is in $\hbar/J$ units and the other parameters are in J units.

transition to the steady state we call the asymmetric relaxation. The final steady state distribution is equal for each site because the noise does not depend on the localization of the electron. The similar results were obtained earlier for the two states model [55, 58]. We can also see that the unidirectionality of the electron transfer generated in the system of three molecules may depend on the next step of electron transport (Fig. 1.1). It means that it depends on the probability of electronic escape from the system. We will assume that this probability is equal for branches L and M. To characterize this probability we have included the parameter Γ to the model. It is *ad hoc* generalization of the Wigner-Weisskopf exponential decay law [59]. The solution of the equations (1.8) with Γ different from zero is presented in Fig. 1.2. The integral below the curve $\langle\rho_{22}(t)\rangle(\langle\rho_{33}(t)\rangle)$ characterizes the

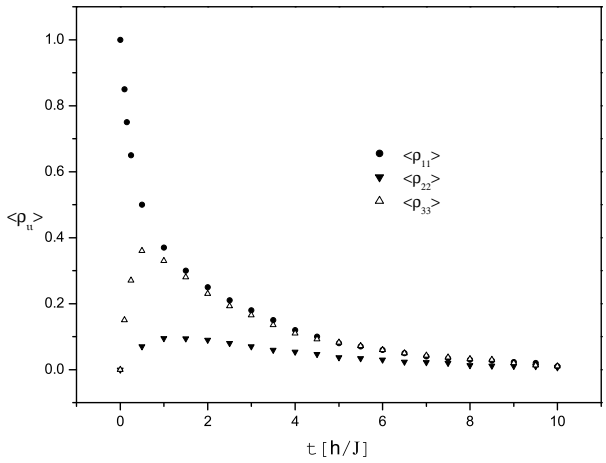

Figure 1.2: The time dependence of the site-occupation probabilities $\langle \rho_{ll}(t) \rangle$ for the sites $l = 1, 2, 3$. The parameters used were: $J = 1$, $\Gamma = 0.3$, $\varepsilon_2 = 10$, $\varepsilon_3 = 10$, $\mu_2/\hbar = 2$, $\mu_3/\hbar = 8$, $\Delta_2/\hbar = 0.1$, $\Delta_3/\hbar = 1$. Units are as described in the legend of Fig. 1.1.

possibility of the electronic escape through the branch $M(L)$. Time is measured in the units $\hbar/J$.

1.2 Calculation of electronic escape through the branches

The quantum yield of the electronic escape via the site i can be characterized by the expression

$$\Phi_i = \frac{2\Gamma_i}{\hbar} \int_0^\infty \langle \rho_{ii}(t) \rangle \, dt = \frac{2\Gamma_i}{\hbar} \lim_{p \to 0^+} \langle \widetilde{\rho_{ii}}(p) \rangle, \qquad i = 1, 2, 3, \tag{1.9}$$

where $\langle \widetilde{\rho_{ii}}(p) \rangle$ is the Laplace transformation of $\langle \rho_{ii}(t) \rangle$. The quantum yields must fulfil the expression

$$\Phi_1 + \Phi_2 + \Phi_3 = 1. \tag{1.10}$$

It means that electron can escape from the system through the branch L or M or the system decay to the ground state which is characterized by the quantity Φ_1. Assuming the initial conditions

$$\langle \rho_{11}(0) \rangle = 1, \quad \langle \rho_{22}(0) \rangle = \langle \rho_{33}(0) \rangle = 0 \tag{1.11}$$

we can solve Eqs. (1.8) in Laplace transformation. For our goal of main importance is the parameter K,

$$K = \frac{\Phi_3}{\Phi_2} = \frac{\langle \widetilde{\rho_{33}}(p \to 0) \rangle}{\langle \widetilde{\rho_{22}}(p \to 0) \rangle}, \tag{1.12}$$

which expresses the asymmetry in probabilities of electronic escape through the branch L (site 3) and M (site 2).

Generally the analytical results are cumbersome. Here we present only some special cases where it is possible to describe the main characteristics of the process. First, we assume the case where $\varepsilon_2 = \varepsilon_3 = \varepsilon$, $\Delta_2 = \Delta_3 = \mu_2 = 0$, and $\mu_3 = \mu$. It means that we

have only the energy level fluctuation on branch L at the site 3. In this case the parameter K has the form

$$K = \frac{J^4 + \Gamma(\Gamma^2+\epsilon^2)\left(\Gamma + \frac{\mu}{\hbar}\right) + J^2\Gamma\left(2\Gamma + \frac{\mu}{\hbar}\right)}{J^4 + 2J^2\Gamma\left(\Gamma + \frac{\mu}{\hbar}\right) + \Gamma^2\left(\Gamma^2 + \epsilon^2 + 2\Gamma\frac{\mu}{\hbar} + \frac{\mu^2}{\hbar^2}\right)}. \tag{1.13}$$

We can see that as $\Gamma \to \infty$, $K \approx 1$. It means that when the electron escapes from the system very quickly the asymmetry of the electron distribution cannot be achieved. For the very slow escape, when $\Gamma \to 0$, the system can achieve the steady state. The steady state is symmetric and so we have the symmetric electron transfer with $K \approx 1$. Now we will analyze the case when all sites in the system have the same energy. If $\epsilon = 0$ we get

$$K = \frac{J^2 + \Gamma^2}{J^2 + \Gamma\left(\Gamma + \frac{\mu}{\hbar}\right)}. \tag{1.14}$$

For $\Gamma \geq 0$ the parameter K has only one extreme. The minimum is achieved when $\Gamma = J$ and K is

$$K = \frac{2J}{2J + \frac{\mu}{\hbar}}. \tag{1.15}$$

If $J \gg \mu/\hbar$ then $K \approx 1$. We get the symmetric electron transfer for any value of Γ. When $J \ll \mu/\hbar$ we have $K \approx 2J\hbar/\mu \ll 1$. In this case we get the asymmetric electron transfer. The electron is transported mainly through the branch M (site 2) where no fluctuations of the energy level exist.

In the second example we consider only the fluctuation of the hopping term between sites 1 and 3 on the branch L. If $\epsilon_2 = \epsilon_3 = \epsilon$, $\Delta_2 = \mu_2 = \mu_3 = 0$, $\Delta_3 = \delta$ we get

$$K = \frac{A}{B}, \tag{1.16}$$

where

$$\begin{aligned} A &= 2J^6\left(\Gamma + \frac{\delta}{\hbar}\right) + \Gamma\frac{\delta}{\hbar}\left(2\Gamma + \frac{\delta}{\hbar}\right)\left(\Gamma^2 + 4\Gamma\frac{\delta}{\hbar} + \varepsilon^2\right) \\ &\quad \times\left[\left(\Gamma + \frac{\delta}{\hbar}\right)^2 + \varepsilon^2\right] \\ &\quad + J^4\left(4\Gamma^3 + 11\Gamma^2\frac{\delta}{\hbar} + 17\Gamma\frac{\delta^2}{\hbar^2} + 4\frac{\delta^3}{\hbar^3} + \varepsilon^2\frac{\delta}{\hbar}\right) \\ &\quad + J^2\Gamma\left(\Gamma + \frac{\delta}{\hbar}\right)\left(2\Gamma^3 + 9\Gamma^2\frac{\delta}{\hbar} + 24\Gamma\frac{\delta^2}{\hbar^2} + 8\frac{\delta^3}{\hbar^3}\right) \\ &\quad + J^2\varepsilon^2\left(2\Gamma^3 + 7\Gamma^2\frac{\delta}{\hbar} + 9\Gamma\frac{\delta^2}{\hbar^2} + \frac{\delta^3}{\hbar^3}\right), \end{aligned} \tag{1.17}$$

$$\begin{aligned} B &= J^2\left(\Gamma + \frac{\delta}{\hbar}\right)\left[J^2 + \Gamma\left(\Gamma + \frac{\delta}{\hbar}\right)\right]\left[2J^2 + \left(2\Gamma + \frac{\delta}{\hbar}\right)\left(\Gamma + 4\frac{\delta}{\hbar}\right)\right] \\ &\quad + J^2\varepsilon^2\left[J^2\frac{\delta}{\hbar} + \left(\Gamma + \frac{\delta}{\hbar}\right)^2\left(2\Gamma + \frac{\delta}{\hbar}\right)\right]. \end{aligned} \tag{1.18}$$

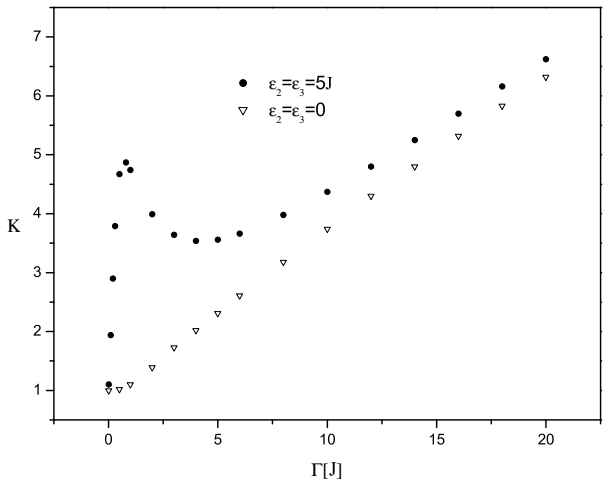

Figure 1.3: The dependence of the ratio of electronic escape probabilities through the branch L and $M(K)$ on Γ with the parameters: $J = 1$, $\mu_2/\hbar = 0.005$, $\mu_3/\hbar = 0.005$, $\triangle_2/\hbar = 0.005$, $\triangle_3/\hbar = 0.3$. Units are as described in the legend of Fig. 1.1.

In the case when $\Gamma \to 0$, $K \cong 1$. At this limit, as in the previous case, the system relaxes to the steady state while the electron is escaping from the system. When $\Gamma \to \infty$ then $K \to (\delta/\hbar J^2)\Gamma$. This limit, in the case when $\Delta_2 \neq 0$, has the form $K \sim \Delta_3/\Delta_2$. With this limit the electron distribution in the system is developing from the time zero highly asymmetrically. We get the asymmetric electron transfer through the system. The electron is transported mainly through the branch where the fluctuation of hopping term is bigger. From Eqs. (1.11)-(1.14) it can be seen that K does not depend on the sign of the energy ε.

In the third example we consider that all fluctuations are equal zero $\Delta_2 = \mu_2 = \Delta_3 = \mu_3 = 0$. In this special case we show the dependence of electron transfer on the value of energy level of the molecules. In this case the parameter K has the form

$$K = \frac{4(J^2+\Gamma^2)^2 + \epsilon_2^2(2J^2+5\Gamma^2+\epsilon_2^2) - 2\epsilon_2\epsilon_3(2J^2+\Gamma^2+\epsilon_2^2) + \epsilon_3^2(2J^2+\Gamma^2+\epsilon_2^2)}{4(J^2+\Gamma^2)^2 + \epsilon_3^2(2J^2+5\Gamma^2+\epsilon_3^2) - 2\epsilon_2\epsilon_3(2J^2+\Gamma^2+\epsilon_3^2) + \epsilon_2^2(2J^2+\Gamma^2+\epsilon_3^2)}. \tag{1.19}$$

If we assume in Eq.(1.19) that $\varepsilon_3 = 0$, we get

$$K = \frac{4(J^2+\Gamma^2)^2 + \epsilon_2^2(2J^2+5\Gamma^2) + \varepsilon_2^4}{4(J^2+\Gamma^2)^2 + \epsilon_2^2(2J^2+\Gamma^2)} \geq 1. \tag{1.20}$$

Likewise, if we assume that $\varepsilon_2 = 0$, we get

$$K = \frac{4(J^2+\Gamma^2)^2 + \epsilon_3^2(2J^2+\Gamma^2)}{4(J^2+\Gamma^2)^2 + \epsilon_3^2(2J^2+5\Gamma^2) + \varepsilon_3^4} \leq 1. \tag{1.21}$$

From Eqs. (1.19)-(1.21) it can be seen that electron transfer in the case of zero fluctuations is strongly dependent on the value of energy level of molecules 2,3. In the case of (1.20) electron transfers mainly via the L side with molecule 3 contrary to the case (1.21) where electron active is the branch M with molecule 2. In this special case the electron is transported mainly through the branch with smaller energy level of the molecule. From expressions above it can be seen that the parameter K does not depend on the sign of the energy level of molecules 2,3.

The dependence of K on Γ for some parameters which characterize our system is illustrated in Figs. 1.3-1.8. Figure 1.3 presents the influence of asymmetry in parameters Δ_i on the electron transport. The electron is transferred mainly through the branch where Δ_i is greater. The influence of asymmetry in parameters μ_i on the ET is illustrated on Fig. 1.4. If $\varepsilon = 0$ we get ET through the branch where the μ_i is smaller. When $\varepsilon_2 = \varepsilon_3 \neq \varepsilon_1$ we can get ET through the branch with bigger μ_i. The increase in the asymmetry of parameters μ_i, Δ_i increases the asymmetry in ET (Fig. 1.5). The same effect increases the energy difference between the sites 2, 3, and 1 (Fig. 1.6).

The influence of energy difference between molecules on the electron transfer asymmetry in the case of small fluctuations is presented in Fig. 1.7. The increase of the fluctuations causes the decrease of ET asymmetry in the case of asymmetric arrangement of energy levels (Fig. 1.7 and 1.8).

1.3 Discussion of the model

From our analysis we can conclude that the fluctuation of the hopping term increases the electron transport in a particular direction. As a consequence is the fact that the branch with a larger Δ_i, characterizing the size of fluctuation in interaction responsible for electron transfer in branch with the ith molecule, has also a larger quantum yield Φ_i.

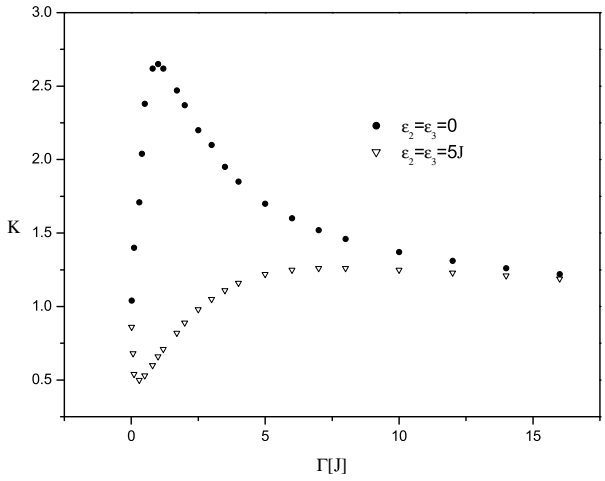

Figure 1.4: The dependence of the ratio of electronic escape probabilities through the branch L and $M(K)$ on Γ with the parameters: $J = 1$, $\mu_2/\hbar = 5$, $\mu_3/\hbar = 0.5$, $\triangle_2/\hbar = 0.01$, $\triangle_3/\hbar = 0.01$. Units are as described in the legend of Fig. 1.1.

The influence of the energy level fluctuation depends on the energy level differences between the molecules. The quantum yield is smaller on the branch where the parameter μ_i, characterizing the size of energy fluctuation at the ith molecule, is greater for the resonance case ($\varepsilon_i = 0$). In the nonresonant case, with a nonzero difference in the energy between sites 2,3 and 1, the situation can be opposite. The quantum yield is higher in the branch with higher energy fluctuation and it is also dependent on the relations between ε_i and μ_i.

The asymmetry is strongly dependent on the parameter Γ. When the value of the parameter Γ is close to J, then the parameter K, describing the asymmetric quantum yield, has a local maximum.

For a large Γ the parameter K achieves the value Δ_3/Δ_2 which can be greater then its local maximum. By changing Γ we can choose the branch where the electron is transported with higher probability. Figure 1.4 illustrates the case where with a small Γ when ET

proceeds mainly trough the branch M and from some specific value of the Γ the electron is transported with higher probability through the branch L.

If we assume that the overall C_2 symmetry is only approximate and there is a difference in energy levels between the branches L and M, we can get highly asymmetric ET. The interesting case is presented in Figs. 1.7 and 1.8 with the small fluctuation of parameters in the asymmetric arrangement of energy levels. The energy asymmetry of a few J (energy is measured in J units) can cause a strong asymmetry in ET through the system for some parameter Γ. The fluctuation of hopping term decreases strongly the asymmetry of ET through the system in the case when C_2 symmetry is only approximate. The effect of the energy level fluctuation depends on the asymmetry arrangement of energy level. Some value of the parameters which characterize the energy level fluctuation can increase the ET asymmetry, however the larger value of the same parameters decreases the ET asymmetry.

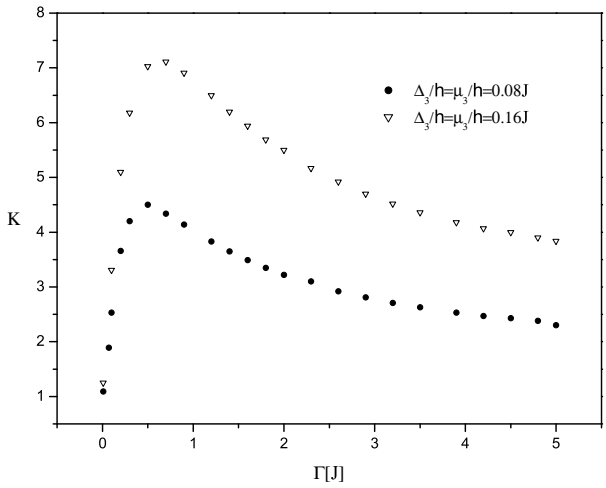

Figure 1.5: The dependence of the ratio of electronic escape probabilities through the branch L and M(K) on Γ with the parameters: $J = 1$, $\varepsilon_2 = 10$, $\varepsilon_3 = 10$, $\mu_2/\hbar = 0.01$, $\triangle_2/\hbar = 0.01$. Units are as described in the legend of Fig. 1.1.

Now we would like to apply our model to the primary charge transfer in bacterial reaction center. Candidates for molecules 2 and 3 are the accessory BChl or some amino acids between P and BChl. Crystallography measurements indicate a higher mobility of the cofactors in the branch M [22]. If we want to elucidate unidirectionality of the primary charge separation through the branch with lower mobility in the case of fully symmetric RC's, we must consider a situation depicted on Fig. 1.4, the resonance case. The asymmetry is caused by fluctuation of energy in the case of zero energy difference between sites 1,2 and 3. In this case electron is transported mainly through the branch with the smaller fluctuation of energy level. The fluctuation of hopping terms must be small. In this case we get the value for $K \sim 2 - 3$. A similar unidirectional asymmetry of electron transfer was measured in modified RC's [24].

To elucidate the higher asymmetry in an electron transfer in the case of exact C_2 symmetry we must assume that there is the larger noise difference between the branch L and M.

However, the overall C_2 symmetry is only approximate in RC's. There are differences in the vicinity of prosthetic groups which can cause the differences in the energy level between molecules in branches L and M. In this case ET can be highly asymmetric (Fig. 1.7 and 1.8). Moreover, the position of atoms in the vicinity of the special pair P must also have a strong stability to get such high asymmetry. In some bacterial reaction center the

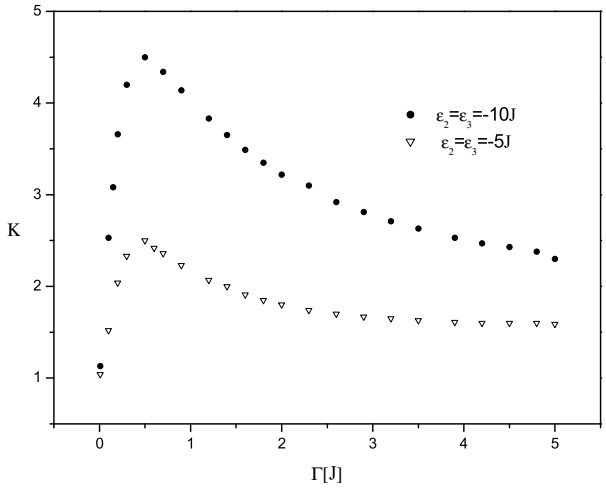

Figure 1.6: The dependence of the ratio of electronic escape probabilities through the branch L and $M(K)$ on Γ with the parameters: $J = 1$, $\mu_2/\hbar = 0.01$, $\mu_3/\hbar = 0.08$, $\triangle_2/\hbar = 0.01$, $\triangle_3/\hbar = 0.08$. Units are as described in the legend of Fig. 1.1.

estimated value of the hopping term to be $J \sim 0.01eV$ [29] for primary charge transfer separation. The difference of a few hundred of eV between energy levels can cause a high asymmetry in the quantum yield of electronic escape through the different branches. This energy difference can be caused by different environments of cofactors on branches L and M.

The model show that the asymmetry of ET can be caused by the difference in the energy levels of molecules whereas the asymmetry in electronic couplings has not to be included in the models. Next possibility is different values of the stochastic fluctuations of interaction between molecules on the branches can be also the reason of a considerable asymmetry of ET and for the description of the quantum yields of some mutants of RC are inevitable. bacteriochlorophylls on the M and L branches of RC's.

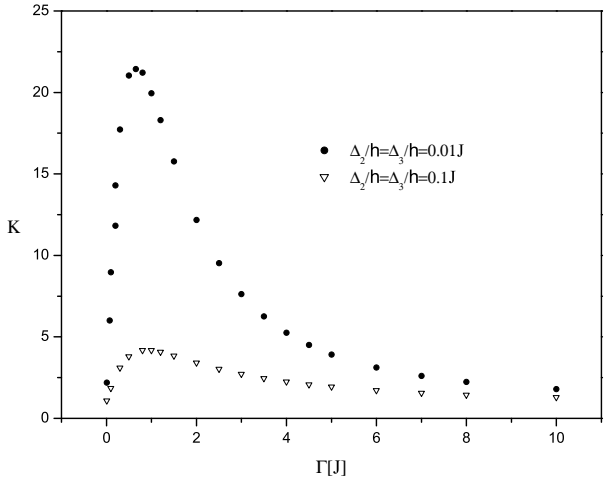

Figure 1.7: The dependence of the ratio of electronic escape probabilities through the branch L and $M(K)$ on Γ for the parameters: $J = 1$, $\varepsilon_2 = 10$, $\varepsilon_3 = 0$, $\mu_2/\hbar = \mu_3/\hbar = 0.01$. Units are as described in the legend of Fig. 1.1.

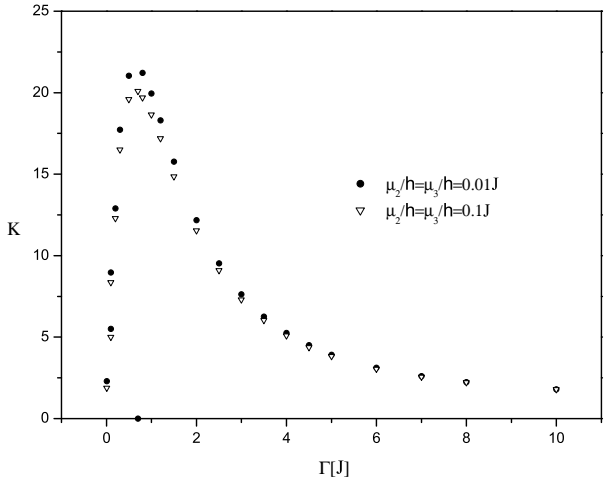

Figure 1.8: The dependence of the ratio of electronic escape probabilities through the branch L and $M(K)$ on Γ with the parameters: $J = 1$, $\varepsilon_2 = 10$, $\varepsilon_3 = 0$, $\Delta_2/\hbar = \triangle_3/\hbar = 0.01$. Units are as described in the legend of Fig. 1.1.

1.4 Application to RC's

The analysis of amino acid mutations or cofactor modifications [24,60-67] that alter the highly asymmetric functionality of RC's can provide the insight into the key factors impacting the directionality and the yield of electron transfer. The cases are described in the literature in which ET to the L versus the M side in the RC was essentially modulated by changing several parameters. The drastically reduced quantum yield (QY) was observed in RC's where substantially different chromophores were in the binding pockets of the electron acceptors [65, 66]. In a series of Rhodobacter capsulatus RC mutants [63] the $G(M201)D/L(M212)H$ (denoted DH) double mutant has 15% electron transfer to M-side bacteriopheophytin, 70% of electron transfer to the L-side cofactors and 15% was deactivated to the ground state. The changes in the ET directionality were explained by the raised free energy of $P^+\mathrm{BChl}_L^-$ in the interaction with Asp $M201$.

With a triple mutant $S(L178)K/G(M201)D/L(M212)H$ (denoted KDH) 62% of electron transfer was observed to the L-side BPh, 23% to the M-side BPh, and 15% was returning to the ground state. In the case of triple mutants, $S(L178)K/G(M201)D/L(M212)H$, the $S(L178)K$ mutation might lower a $P^+\mathrm{BChl}_M^-$ free energy and thus increase the yield of electron transfer to BPh_M in comparison to the $G(M201)D/L(M212)H$ double mutant.

ET to the primary quinone in the normal β-type mutant was $\sim$ 70% and $\sim$ 30% was returning to the ground state [24, 63]. The exact values depend on the specificity of mutation. The $F(L121)D$ mutant exhibits beta type photochemistry [63]. It was proposed that $P^+\mathrm{BChl}_L^-$ lies at higher free energy in the $F(L121)D$ mutant than in the wild-type (WT) RC.

The RC's of Rb. sphaeroides $(M)H202L$ single mutant and $(M)H202L/(L)L131H$ double mutant [64] contain a bacteriochlorophyll/bacteriopheophytin heterodimer as a primary electron donor. These heterodimer mutants display a reduced yield of $P^+Q_L^-$ formation for about 40% (single mutant) and 25% for the double mutants. This perturbation results from an upshift of the heterodimer free energy relative to homodimer primary donor of wild-type RC's. Electron transfer along the M-side was observed in the $H(M182)L$ mutant of Rb. sphaeroides [65]. In this mutant bacteriopheophytin (referred to as Φ_M) is incorporated in place of BChl_M. One would expect that the $P^+\Phi_M^-$ state would be considerably lower in energy than $P^+\mathrm{BChl}_M^-$, thus enhancing the probability of

M-side electron transfers. The yield of the $P^+\Phi_M^-$ state is apparently $30-40\%$.

The RC's of Rhodopseudomonas viridis mutant, where histidine was replaced by glutamate (denoted as $L153HE$), the quantum yield of $P^+Q_L^-$ formation is reduced to 75% [66]. In this mutant rise in the energy level of $P^+\mathrm{BChl}_L^-$ occured because of the presence of glutamate. The exchange of histidine to leucine in RC's of Rh. viridis (the mutant denoted as $L153HL$) causes the incorporation of a bacteriopheophytin b instead of a bacteriochlorophyll b molecule (referred to as B_L). As a consequence of the chromophore exchange the energy level of the electron transfer state $P^+B_L^-$ is lowered in comparison to $P^+\mathrm{BChl}_L^-$ (WT). Consequently the quantum yield of $P^+B_L^-$ is reduced to 50% in this mutant [66]. The presented experimental data show that the free energy of the intermediates $P^+\mathrm{BChl}_L^-$ and $P^+\mathrm{BChl}_M^-$ does have a major importance. If the free energy of $P^+\mathrm{BChl}_L^-$ is raised relative to that of wild type (WT) RC (e.g. by the introduction of a negative charge like in the mutant $L153HE$) the quantum efficiency is considerably lowered.

The implementation of the theory requires information regarding the energetic parameters such as the energy gap of the equilibrium nuclear configuration between P^* and $P^+\mathrm{BChl}_{L(M)}^-$. The energy level of $P^+\mathrm{BChl}_L^-$ in RC's of Rb. sphaeroides is about $450\,\mathrm{cm}^{-1}$ below P^* state [67]. Another calculation shows that this energy level is about $250\,\mathrm{cm}^{-1}$ above the special pair [68]. Theoretical calculation using the Rp. viridis RC crystal structure suggested that the $P^+\mathrm{BChl}_M^-$ state is $2000\,\mathrm{cm}^{-1}$ higher than P^* [69].

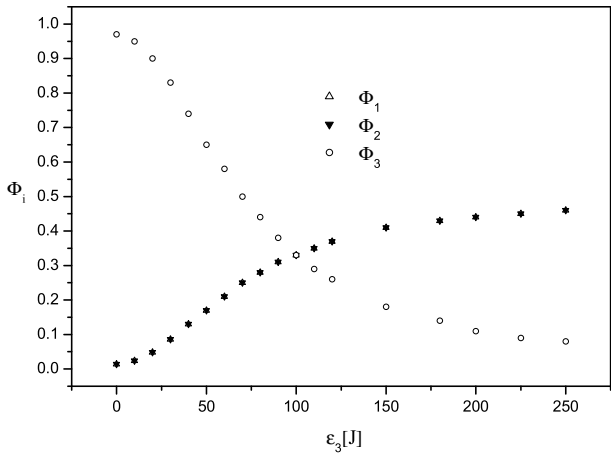

Figure 1.9: The dependence of charge separation quantum yields Φ_i (i=1,2,3) on ε_3 energy. Parameters used for simulation: $J=1$, $\varepsilon_2=100$, $\mu_2/\hbar=\mu_3/\hbar=10$, $\triangle_2/\hbar=\triangle_3/\hbar=0$, $\Gamma_2=\Gamma_3=0.2$ and $\Gamma_1=0.001$. Units are as described in the legend of Fig. 1.1.

The other parameters included in our model are the imaginary parts of the energy levels Γ_1, Γ_2, Γ_3. The value of Γ_1 is calculated from the internal conversion rate of P^*. This rate was estimated to be between $(90\,\mathrm{ps})^{-1}$ and $(350\,\mathrm{ps})^{-1}$ from the measurements on WT RC's [64]. For our theoretical simulations the internal conversion rate of $(130\,\mathrm{ps})^{-1}$ was selected. Then the parameter Γ_1, characterizing the decay of the system to the ground state, is obtained from the expression $2\,\Gamma_1/\hbar \approx (130\,\mathrm{ps})^{-1}$. The values of parameters Γ_2, Γ_3 can be calculated in a similar way from the decay time of $P^+\mathrm{BChl}_L^-$. The decay time of $P^+\mathrm{BChl}_L^-$ in Rhodopseudomonas viridis is 0.65 ps (Ref. [67]) and the transfer integral J is estimated to be about $20\,\mathrm{cm}^{-1}$ [70, 71, 72].

To characterize the wild-type RC in our model the following parameters were chosen: the energy levels ε_2=$2000\,\mathrm{cm}^{-1}$, ε_3=$400\,\mathrm{cm}^{-1}$, hopping term J=$20\,\mathrm{cm}^{-1}$, imaginary part of energy levels $\Gamma_2=\Gamma_3=\Gamma$=$4\,\mathrm{cm}^{-1}$ [$2\Gamma/\hbar \approx (0.65\,\mathrm{ps})^{-1}$]. Similarly to the work [70] it was assumed that Γ_1 is smaller by about two orders of magnitude than the Γ_2 and Γ_3. This assumption has the experimental support [64, 67]. The parameters characterizing

the noise and the decay of the system to the ground state were: $\mu_2/\hbar = \mu_3/\hbar$=200 cm^{-1}, $\Delta_2/\hbar = \triangle_3/\hbar = 0$ and Γ_1=2.10^{-2} cm^{-1} for WT RC's. It has to be noticed that QY in our model does not depend on the sign of the energy levels ε_2, ε_3 and we also assume that the hopping terms do not fluctuate.

Using the above parameters the following quantum yields were obtained for wild-type RC's: $\Phi_1 = 0.05$, $\Phi_2 = 0.05$, $\Phi_3 = 0.9$. If we assume the asymmetry in the noise characterizing parameter and the value of parameter Γ_1 is taken to be equivalent to the internal conversion rate (130 ps)$^{-1}$ then with $\mu_2/\hbar = 0$, $\mu_3/\hbar$=200 cm^{-1} the quantum yields are: $\Phi_1 = 0.05$, $\Phi_2 = 0.001$, $\Phi_3 = 0.949$. Even if the Γ_1 value in calculation is greater than average we will get a relatively high quantum yield to ground state.

Based on our model Figs. 1.9 and 1.10 present the dependence of the quantum yields on the energy gaps between P^* and $P^+\mathrm{BChl}^-_{L(M)}$. These figures describe the mutated RC's, where the mutation changed the relative free energies of the participating states.

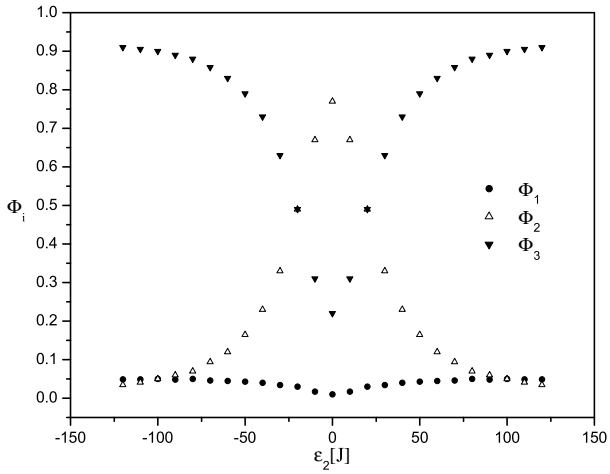

Figure 1.10: The dependence of charge separation quantum yields Φ_i (i=1,2,3) on ε_2 energy. Parameters used for simulation: $J = 1$, $\varepsilon_3 = 20$, $\mu_2/\hbar = \mu_3/\hbar = 10$, $\triangle_2/\hbar = \triangle_3/\hbar = 0$, $\Gamma_2 = \Gamma_3 = 0.2$ and $\Gamma_1 = 0.001$. Units are as described in the legend of Fig. 1.1.

When the energy of ε_3 is increased, as in the $G(M201)D/L(M212)H$ double mutant compared to WT RC's, we have QY: $\Phi_1 = 0.14$, $\Phi_2 = 0.14$, $\Phi_3 = 0.72$ with the parameters: ε_2=2000 cm^{-1}, ε_3=800 cm^{-1}, J=20 cm^{-1}, Γ_2=4 cm^{-1}, Γ_3=0.8 cm^{-1}, $\mu_2/\hbar = \mu_3/\hbar$=200 cm^{-1}, $\Delta_2/\hbar = \triangle_3/\hbar = 0$ and Γ_1=2.10^{-2} cm^{-1}. The smaller value of parameter Γ_3 in comparison to WT is justified by the experimental data [24, 63].

When the energy of ε_2 is decreased, as in $S(L178)K/G(M201)D/L(M212)H$ triple mutant in comparison with the double mutant we have QY: $\Phi_1 = 0.13$, $\Phi_2 = 0.20$, $\Phi_3 = 0.67$ using the parameters: ε_2=1600 cm^{-1}, ε_3=800 cm^{-1}, J=20 cm^{-1}, Γ_2=4 cm^{-1}, Γ_3=0.8 cm^{-1}, $\mu_2/\hbar = \mu_3/\hbar$=200 cm^{-1}, $\Delta_2/\hbar = \triangle_3/\hbar = 0$ and Γ_1=2.10^{-2} cm^{-1}.

When the energy ε_2 is considerably decreased in comparison to WT as in the $H(M182)L$ mutant of Rb. sphaeroides where bacteriopheophytin is incorporated in place of BChl_M we get the following QY: $\Phi_1 = 0.04$, $\Phi_2 = 0.33$, $\Phi_3 = 0.63$ by using the parameters: ε_2=−600 cm^{-1}, ε_3=400 cm^{-1}, J=20 cm^{-1}, Γ_2=4 cm^{-1}, Γ_3=4 cm^{-1}, $\mu_2/\hbar = \mu_3/\hbar$=200 cm^{-1}, $\Delta_2/\hbar = \triangle_3/\hbar = 0$ and Γ_1=2.10^{-2} cm^{-1}.

When the energy ε_3 is sufficiently decreased in comparison to WT as in the $L153HL$ mutant of Rh. viridis where bacteriopheophytin is incorporated in place of BChl_L we have the following QY: $\Phi_1 = 0.12$, $\Phi_2 = 0.44$, $\Phi_3 = 0.44$ with the parameters: ε_2=2000 cm^{-1}, ε_3=−2000 cm^{-1}, J=20 cm^{-1}, Γ_2=4 cm^{-1}, Γ_3=4 cm^{-1}, $\mu_2/\hbar = \mu_3/\hbar$=200 cm^{-1}, $\Delta_2/\hbar = \triangle_3/\hbar = 0$ and Γ_1=6.10^{-3} cm^{-1}. The parameter Γ_1 in comparison with RC's of other

bacteria was lowered. Our value of Γ_1 corresponds to the value of $(390\,\mathrm{ps})^{-1}$ for the P^* internal conversion rate which is relatively small. The higher value of this parameter causes the strong decay to the ground state. It means that the difference between ε_1 and ε_2, ε_3 ought to be smaller.

The normal β-type mutant was not analyzed because of the strong possibility that electron is also delocalized on the BChl(β) which is incorporated in the place of BPh_L. This possibility is not incorporated in our model. And in the case of the heterodimer mutant it is not obvious how the electron levels might be shifted and without this information it is difficult to make the simulations.

1.5 Conclusions

The present study addresses the important problem of the highly asymmetric ET in the photosynthetic reaction centers. Using the stochastic model it was possible to elucidate the unidirectionality of electron transfer. In the model the electron is delocalized to the three molecules (P, BChl_L and BChl_M) with the electron density dependent on the parameters characterizing the system. The electron density in this system can be strongly asymmetric and the energy levels of the BChl_L and BChl_M molecules have been shown to influence profoundly the asymmetry.

We have shown that in mutations of RC's where the difference between energy levels ε_2 and ε_1 are increased in comparison with the wild type, the unidirectionality of electron transfer is also increased. The same effect is observed for the decrease of the energy level difference between ε_3 and ε_1. The results demonstrate that an individual amino acid residue can, through its influence on the free energy of the charge-separated states, effectively dictate the balance between the ET to the L and M-side chromophores of the RC's.

In the present model the temperature dependence of ET was not analyzed. Nevertheless, we would like to say a few words about the temperature effect. A noise which influences the asymmetric ET in the present analysis is dependent on the temperature. It would be interesting to know whether the unidirectionality of the primary charge separation process in RC's is temperature dependent. The primary processes in photosynthetic reaction centers have the anomal temperature dependence. This dependence can be explained by the inclusion of the relative motion of exchanging groups into the electron-transport theory [73]. The main effect will be the temperature dependence of J [73, 74]. Because the parameter Γ can also be dependent on the temperature there is a possibility to change the asymmetry of ET in RC's with the temperature.

However, the primary electron transfer reactions in RC's have the slight temperature dependence. The charge separation time constant decreases only two to three times on cooling from 300 to 10 K [22]. If consequently the parameter Γ is changed two times in the vicinity of maximum asymmetry ($\Gamma \sim J$) there is no sufficient change in asymmetry of ET. As a result we have a weak temperature dependence of asymmetry in electron transfer in the RC's. Also in the case of small fluctuations the asymmetry of ET through the system is temperature independent. When $\Gamma \ll \varepsilon_L$ and ε_M then the several times increase or decrease of the parameter Γ does not affect strongly the asymmetry of ET and its temperature dependence.

It was shown that the different hopping terms (electron-transfer integrals) in the branches can result in the asymmetry of charge separation across the L and M branches of the RC [75, 76]. However, the present work demonstrates that for the asymmetric ET it is not sufficient to consider only the asymmetry in electron-transfer integrals. For example, in the case of small Γ, the system approaches the quasi steady state, where asymmetry is determined by the equilibrium electron density distribution and does not depend on

electron-transfer integrals.

For example, there is a mutant of RC's where hopping integrals are not changed significantly and yet the unidirectionality is suppressed considerably [63]. It is in contradiction to the work [77] where the unidirectionality was explained only on the basis of the asymmetry of transfer integrals in the L and M regions. It was suggested also that the dimmer of RC's plays the decisive role for the vectorial charge separation [78]. However, this explanation is in contrast to the experimental data. The profound changes in the unidirectionality of ET were observed for some mutants of RC's without the changes in the aggregation state [24, 63, 66].

Chapter 2

The stochastic model with color noise

2.1 Theory

In this model we assume that the electron transfer has a hot character because of the very fast primary charge-separation process. This means that ET is so fast that the bath does not have sufficient time to relax to the new thermal equilibrium before the particle moves away. The result of this assumption is that we used the stochastic model where the fluctuations do not depend on the localization of electron in the branch. We begin with the Liouville equation for the density matrix ρ of the total electron-bath system

$$i\hbar\frac{\partial\rho(t)}{\partial t} = [H\rho(t) - \rho(t)H^{\dagger}], \tag{2.1}$$

where the Hamiltonian H consist of two parts

$$H = H_0 + V, \tag{2.2}$$

with

$$H_0 = \sum_{i=1}^{n}[h_i(\vec{R}) + \varepsilon_i - \Gamma_i]a_i^{\dagger}a_i, \tag{2.3}$$

$$V = \sum_{i,j=1}^{n} V_{ij}(a_i^{\dagger}a_j + \text{H.c.}), \quad i \neq j. \tag{2.4}$$

We assume that the total statistical system described by the density matrix ρ consists of a system of interest (electrons) and a bath (molecules of the environment). V is a perturbation causing a transition between the eigenstates of H_0. The ε_i and $a_i^{\dagger}(a_i\ )$ are the site energy and the creation (annihilation) operator of the electron at site i. The parameter $\hbar/2\Gamma_i$ has a meaning of the lifetime of the electron localization at the site i in the limit of the zero coupling parameter. We denote the solvent Hamiltonian when the electron is at site i by $h_i(\vec{R})$. $\vec{R}$ denotes the coordinates of the position and orientation of the solvent molecules. We assume that

$$h_i(\vec{R}) - h_j(\vec{R}) = \Delta_{ij} + W_{ij}(t). \tag{2.5}$$

$W_{ij}(t)$ is taken to be a Gaussian-Markovian process with zero mean and the correlation function

$$\langle W_{ij}(t)W_{ij}(\tau)\rangle = K_{ij}(t-\tau), \tag{2.6}$$

where the functions K_{ij} will be defined below. We start from the Liouville equation and designate

$$\rho_I(t) = \left[\overrightarrow{T}\exp\left(\frac{i}{\hbar}\int_0^t H_0(\tau)d\tau\right)\right]\rho(t)\left[\overleftarrow{T}\exp\left(-\frac{i}{\hbar}\int_0^t H_0^\dagger(\tau)d\tau\right)\right], \tag{2.7}$$

$$V_I(t) = \left[\overrightarrow{T}\exp\left(\frac{i}{\hbar}\int_0^t H_0(\tau)d\tau\right)\right]V(t)\left[\overleftarrow{T}\exp\left(-\frac{i}{\hbar}\int_0^t H_0(\tau)d\tau\right)\right]. \tag{2.8}$$

$\overrightarrow{T}(\overleftarrow{T})$ is a time ordering operator ordering the later times to the right (left). The Liouville equation for the density matrix in the interaction picture reads

$$i\frac{\partial\rho_I(t)}{\partial t} = \frac{1}{\hbar}[V_I(t)\rho_I(t) - \rho_I(t)V_I^\dagger(t)] = L(t)\rho_I(t), \tag{2.9}$$

where $L(t)$ is the Liouville operator in the interaction picture. Now using standard projection techniques [49, 79, 80] we get

$$\partial_t D\rho_I(t) = -iDL(t)D\rho_I(t) - iDL(t)(1-D)\rho_I(t), \tag{2.10a}$$

$$\partial_t (1-D)\rho_I(t) = -i(1-D)L(t)(1-D)\rho_I(t) - i(1-D)L(t)D\rho_I(t). \tag{2.10b}$$

Here D is a projection operator. Solving the last equation and introducing the result into (2.10a) yields

$$\begin{aligned}\partial_t D\rho_I(t) &= -iDL(t)D\rho_I(t) \\ &\quad -DL(t)\int_0^t\left[\overleftarrow{T}\exp\left(-i(1-D)\int_\tau^t L(\tau_1)d\tau_1\right)\right](1-D)L(\tau)D\rho_I(\tau)d\tau,\end{aligned} \tag{2.11}$$

where it is assumed that the initial condition is

$$(1-D)\rho_I(0) = 0. \tag{2.12}$$

We will work to second order of perturbation theory. In this approximation we have (Appendix A)

$$\partial_t D\rho_I(t) = -iDL(t)D\rho_I(t) - DL(t)\int_0^t (1-D)L(\tau)D\rho_I(\tau)d\tau. \tag{2.13}$$

We use the identity (Appendix E)

$$DL(t)D = 0 \tag{2.14}$$

and from (2.13)we get

$$\partial_t D\rho_I(t) = -DL(t)\int_0^t L(\tau)D\rho_I(\tau)d\tau. \tag{2.15}$$

Now we are using the projector in the form

$$(DA)_{mn} = \delta_{mn}\langle A_{mm}\rangle. \tag{2.16}$$

The bracket $\langle\rangle$ is the ensemble average over the solvent motion. For eq. (2.15) we take the matrix elements $\langle i|...|i\rangle$, $|i = 1, 2, ...n\rangle$ are the eigenstates of H_0. We get the generalized master equations (GME) [39] for the population probabilities (Appendix B)

$$\begin{aligned}\frac{\partial P_i(t)}{\partial t} &= -\frac{2\Gamma_i}{\hbar}P_i(t) - \sum_{j=1}^{n}\frac{2 \mid V_{ij} \mid^2}{\hbar^2}\int_0^t \cos\left(\frac{\varepsilon_i - \varepsilon_j + \Delta_{ij}}{\hbar}(t-\tau)\right) \\ &\times\Theta_{ij}(t-\tau)\exp\left(-\frac{\Gamma_i + \Gamma_j}{\hbar}(t-\tau)\right)\{P_i(\tau) - P_j(\tau)\}d\tau, \\ &i = 1...n \quad , \quad i \neq j \end{aligned} \tag{2.17}$$

where $P_i(t)$ is the population probability $P_i(t) = \langle\rho_{ii}(t)\rangle$ and $\Theta_{ij}(t)$ has the form

$$\Theta_{ij}(t) = \exp\left(-\frac{1}{2\hbar^2}\int_0^t\int_0^t K_{ij}(\tau_2 - \tau_1)d\tau_1 d\tau_2\right). \tag{2.18}$$

2.2 Model of Reaction Center

To describe the first steps of electron transfer processes in the reaction centers we have used the three-sites model. Let us designate the special pair (P) as sites 1, the sites 2 and 3 then represent the molecules of accessory bacteriochlorophyll on the branches M and L. We assume that the hopping terms between molecule 1 and molecule 2 or 3 on both branches are not the same. We forbid the direct ET between sites 2 to 3. We assume that the energy levels 2 and 3 have imaginary part which describes the interaction with the next molecule in the branch. The imaginary part of the energy level 1 describes the probability of electron deactivation to the ground state. In this three sites model Eqs.(2.17) has the form

$$\begin{aligned}\frac{\partial P_1(t)}{\partial t} &= -\frac{2\Gamma_1}{\hbar}P_1(t) \\ &-\frac{2J_M^2}{\hbar^2}\int_0^t \cos\left(\frac{\varepsilon_M}{\hbar}(t-\tau)\right)\exp\left(-\frac{\Gamma_1 + \Gamma_2}{\hbar}(t-\tau)\right)\Theta_M(t-\tau)\{P_1(\tau) - P_2(\tau)\}d\tau \\ &-\frac{2J_L^2}{\hbar^2}\int_0^t \cos\left(\frac{\varepsilon_L}{\hbar}(t-\tau)\right)\exp\left(-\frac{\Gamma_1 + \Gamma_3}{\hbar}(t-\tau)\right)\Theta_L(t-\tau)\{P_1(\tau) - P_3(\tau)\}d\tau, \end{aligned} \tag{2.19a}$$

$$\begin{aligned}\frac{\partial P_2(t)}{\partial t} &= -\frac{2\Gamma_2}{\hbar}P_2(t) \\ &-\frac{2J_M^2}{\hbar^2}\int_0^t \cos\left(\frac{\varepsilon_M}{\hbar}(t-\tau)\right)\exp\left(-\frac{\Gamma_1 + \Gamma_2}{\hbar}(t-\tau)\right)\Theta_M(t-\tau)\{P_2(\tau) - P_1(\tau)\}d\tau, \end{aligned} \tag{2.19b}$$

$$\begin{aligned}\frac{\partial P_3(t)}{\partial t} &= -\frac{2\Gamma_3}{\hbar}P_3(t) \\ &-\frac{2J_L^2}{\hbar^2}\int_0^t \cos\left(\frac{\varepsilon_L}{\hbar}(t-\tau)\right)\exp\left(-\frac{\Gamma_1 + \Gamma_3}{\hbar}(t-\tau)\right)\Theta_L(t-\tau)\{P_3(\tau) - P_1(\tau)\}d\tau, \end{aligned} \tag{2.19c}$$

where we denote $\varepsilon_L = \varepsilon_1 - \varepsilon_3 + \Delta_{13}$, $\varepsilon_M = \varepsilon_1 - \varepsilon_2 + \Delta_{12}$, $\Theta_{12} = \Theta_M$, $\Theta_{13} = \Theta_L$, $V_{12} = J_M$, and $V_{13} = J_L$. The quantum yield (QY) Φ_i of the electronic escape via the site i can be characterized by the expression [52]

$$\Phi_i = \frac{2\Gamma_i}{\hbar}\int_0^\infty P_i(t)dt = \frac{2\Gamma_i}{\hbar}\lim_{p\to 0^+}\widetilde{P}_i(p), \quad i = 1,2,3, \tag{2.20}$$

where $\tilde{P}_i(p)$ is the Laplace transformation of $P_i(t)$. The Laplace transform to Eqs. (2.19), with the initial conditions $P_1(0) = 1$, $P_2(0) = P_3(0) = 0$, reads

$$\begin{aligned} p\tilde{P}_1(p) - 1 &= -\frac{2\Gamma_1}{\hbar}\tilde{P}_1(p) - w_M(p)[\tilde{P}_1(p) - \tilde{P}_2(p)] \\ &\quad -w_L(p)[\tilde{P}_1(p) - \tilde{P}_3(p)], \qquad (2.21a) \\ p\tilde{P}_2(p) &= -\frac{2\Gamma_2}{\hbar}\tilde{P}_2(p) - w_M(p)[\tilde{P}_2(p) - \tilde{P}_1(p)], \qquad (2.21b) \\ p\tilde{P}_3(p) &= -\frac{2\Gamma_3}{\hbar}\tilde{P}_3(p) - w_L(p)[\tilde{P}_3(p) - \tilde{P}_1(p)], \qquad (2.21c) \end{aligned}$$

where

$$\begin{aligned} w_M(p) &= \frac{2J_M^2}{\hbar^2}\int_0^\infty \cos[\frac{\varepsilon_M}{\hbar}t]\exp[-\frac{\Gamma_1+\Gamma_2+\hbar p}{\hbar}t]\Theta_M(t)dt, \qquad (2.22a) \\ w_L(p) &= \frac{2J_L^2}{\hbar^2}\int_0^\infty \cos[\frac{\varepsilon_L}{\hbar}t]\exp[-\frac{\Gamma_1+\Gamma_3+\hbar p}{\hbar}t]\Theta_L(t)dt. \qquad (2.22b) \end{aligned}$$

These integrals can be expressed as [81]

$$\begin{aligned} w_M(p) &= \frac{2J_M^2}{\hbar^2}\tau_M \mathrm{Re}\frac{M(1,d_M+1,z_M)}{d_M}, \qquad (2.23a) \\ w_L(p) &= \frac{2J_L^2}{\hbar^2}\tau_L \mathrm{Re}\frac{M(1,d_L+1,z_L)}{d_L}, \qquad (2.23b) \end{aligned}$$

where $M(1,d+1,z)$ is the confluent hypergeometric function and

$$\begin{aligned} d_M &= \frac{\Gamma_1+\Gamma_2+\Gamma_M+\hbar p - i\varepsilon_M}{\hbar}\tau_M, \quad z_M = \frac{\Gamma_M\tau_M}{\hbar}, \qquad (2.24a) \\ d_L &= \frac{\Gamma_1+\Gamma_3+\Gamma_L+\hbar p - i\varepsilon_L}{\hbar}\tau_L, \quad z_L = \frac{\Gamma_L\tau_L}{\hbar}, \qquad (2.24b) \end{aligned}$$

where we denote $\Gamma_L = \Gamma_{13}^e$, $\Gamma_M = \Gamma_{12}^e$, $\tau_L = \tau_{13}^e$ and $\tau_M = \tau_{12}^e$.

2.3 Overdamped regime

In this section, we assume that the correlation function corresponds to a spectral density of the strongly overdamped Brownian oscillator. In this regime we have [39, 82, 83]

$$\begin{aligned} K_{ij}(t) &= \langle\xi_{ij}^2\rangle_{slv}\exp(-\frac{\mid t \mid}{\tau_{ij}^e}), \qquad (2.25a) \\ \Theta_{ij}(t) &= \exp\left(-\frac{\Gamma_{ij}^e}{\hbar}\left\{t - \tau_{ij}^e\left[1-\exp\left(-\frac{t}{\tau_{ij}^e}\right)\right]\right\}\right), \quad i,j = 1,...,n. \qquad (2.25b) \end{aligned}$$

2.3.1 Fast modulation limit

We start with the fast modulation limit, where we will work in the limit of short correlation time of the solvent where we assume that $\Gamma^e_{ij}\tau^e_{ij}/\hbar \ll 1$. Here $\Gamma^e_{ij} = \langle\xi^2_{ij}\rangle\tau^e_{ij}/\hbar$. In this limit we have

$$w_M(p) = \frac{2J_M^2}{\hbar^2}\frac{p+(\Gamma_1+\Gamma_2+\Gamma_M)/\hbar}{[p+(\Gamma_1+\Gamma_2+\Gamma_M)/\hbar]^2+[\varepsilon_M/\hbar]^2}, \tag{2.26a}$$

$$w_L(p) = \frac{2J_L^2}{\hbar^2}\frac{p+(\Gamma_1+\Gamma_3+\Gamma_L)/\hbar}{[p+(\Gamma_1+\Gamma_3+\Gamma_L)/\hbar]^2+[\varepsilon_L/\hbar]^2}. \tag{2.26b}$$

Here we denote $\Gamma_L = \Gamma^e_{13}$, $\Gamma_M = \Gamma^e_{12}$, $\tau_L = \tau^e_{13}$, and $\tau_M = \tau^e_{12}$. Using the solution of Eqs.(2.21), we can compute the quantum yields. Here we present the ratio $K_{32} = \Phi_3/\Phi_2$ which characterizes the asymmetry of electron transfer through the L and M branches and the ratio $K_{13} = \Phi_1/\Phi_3$ which characterizes the decay of the system to the ground state:

$$K_{32} = \frac{J_L^2\Gamma_3(\Gamma_1+\Gamma_3+\Gamma_L)\{J_M^2(\Gamma_1+\Gamma_2+\Gamma_M)+\Gamma_2[(\Gamma_1+\Gamma_2+\Gamma_M)^2+\varepsilon_M^2]\}}{J_M^2\Gamma_2(\Gamma_1+\Gamma_2+\Gamma_M)\{J_L^2(\Gamma_1+\Gamma_3+\Gamma_L)+\Gamma_3[(\Gamma_1+\Gamma_3+\Gamma_L)^2+\varepsilon_L^2]\}}, \tag{2.27a}$$

$$K_{13} = \frac{\Gamma_1\{J_L^2(\Gamma_1+\Gamma_3+\Gamma_L)+\Gamma_3[(\Gamma_1+\Gamma_3+\Gamma_L)^2+\varepsilon_L^2]\}}{J_L^2\Gamma_3(\Gamma_1+\Gamma_3+\Gamma_L)}. \tag{2.27b}$$

Now we want to present optimal relations between the model parameters for the maximal asymmetry of ET through the system. The parameter Γ_1 ought to be small in comparison to other parameters to get relatively small electronic decay to the ground state. In this case we have

$$K_{32} = \frac{J_L^2\Gamma_3(\Gamma_3+\Gamma_L)\{J_M^2(\Gamma_2+\Gamma_M)+\Gamma_2[(\Gamma_2+\Gamma_M)^2+\varepsilon_M^2]\}}{J_M^2\Gamma_2(\Gamma_2+\Gamma_M)\{J_L^2(\Gamma_3+\Gamma_L)+\Gamma_3[(\Gamma_3+\Gamma_L)^2+\varepsilon_L^2]\}} \tag{2.28}$$

and $K_{13} \sim 0$. When $\varepsilon_L, \varepsilon_M \gg \Gamma_L, \Gamma_M, J_L, J_M$ and $\Gamma_L \gg \Gamma_3$, $\Gamma_M \gg \Gamma_2$ we have

$$K_{32} = \frac{J_L^2\Gamma_L\varepsilon_M^2}{J_M^2\Gamma_M\varepsilon_L^2}. \tag{2.29}$$

When Γ_M , Γ_L are large in comparison to other model parameters from Eq.(2.28), we get

$$K_{32} = \frac{J_L^2\Gamma_M}{J_M^2\Gamma_L}. \tag{2.30}$$

In this limiting case Γ_L and Γ_M are in inverse relation as in the previous case. The electron is transported mainly through the branch where the fluctuation of energy level is smaller. In the next cases we assume that the values of parameters Γ_L and Γ_M are small. From Eq.(2.28), we get

$$K_{32} = \frac{J_L^2\Gamma_3(J_M^2+\Gamma_2^2+\varepsilon_M^2)}{J_M^2\Gamma_2(J_L^2+\Gamma_3^2+\varepsilon_L^2)}. \tag{2.31}$$

If we assume that the parameters J_M, J_L are very large in comparison to parameters ε_L, ε_M, Γ_2 and Γ_3, we get

$$K_{32} = \frac{\Gamma_3}{\Gamma_2}. \tag{2.32}$$

Here we get electron transfer through the branch with greater sink. It means that the first step of ET is so fast that the next step of ET is limiting for unidirectionality. When we assume that the parameters ε_L, ε_M are very large in comparison to parameters Γ_2, Γ_3, J_M and J_L from Eq.(2.31), we get

$$K_{32} = \frac{J_L^2 \Gamma_3 \varepsilon_M^2}{J_M^2 \Gamma_2 \varepsilon_L^2}. \tag{2.33}$$

As similar result was obtained in the works [76, 84], for the superexchange mechanism of electron transfer. Now we assume the case which is interesting from a theoretical point of view. If the parameters Γ_2, Γ_3 are very large in comparison to the parameters ε_L, ε_M, J_L, J_M, Γ_L, Γ_M and $\Gamma_1 \approx 0$ we get

$$K_{32} = \frac{J_L^2 \Gamma_2}{J_M^2 \Gamma_3}, \quad K_{13} \approx 0. \tag{2.34}$$

In this limit of strong sink at place 2 (branch M) and 3 (branch L) we have inverted the regime of electron transfer in comparison with the previous cases. When we assume that $J_L \sim J_M$, an electron is transported mainly through the branch with a smaller value of the sink parameter. In this case, the electron has a tendency to avoid the place with greater sink parameter. A similar result was obtained in [85] where the energy transport in a semi-infinite chain with one sink was described. This effect was named *fear of death*. It is caused because of memory functions in the equations which describe the dynamics of the system depending on the value of the sink parameters. On the other hand, if the parameter Γ_1 is large, the electron escapes from the system through site 1. Because of small sink parameters in comparison to energy differences between molecules, these cases can be hardly realized in RC.

The implementation of the theory requires information regarding some parameters, such as the energy gaps, hopping terms, imaginary parts of energy levels and parameters characterizing the noise. The energy level of $P^+\mathrm{BChl}_L^-$in RC's of Rb. Sphaeroides is about $450\,\mathrm{cm}^{-1}$ below P^* [67]. Another calculations show that this energy level is about $250\,\mathrm{cm}^{-1}$ above special pair [68]. Theoretical calculations, using the Rp. viridis RC crystal structure suggested that the $P^+\mathrm{BChl}_M^-$ state is $2000\,\mathrm{cm}^{-1}$ higher than P^* [69]. The value of Γ_1 is calculated from the internal conversion rate of P^*. This rate was estimated to be between $(90\,\mathrm{ps})^{-1}$ and $(350\,\mathrm{ps})^{-1}$ from the measurements on wild-type RC's [67]. For our theoretical simulations the internal conversion rate $2\,\Gamma_1/\hbar$=$(170\,\mathrm{ps})^{-1}$ was selected. The values of the parameters Γ_2, Γ_3 can be calculated from the decay time $P^+\mathrm{BCh}_L^-$. The decay time of $P^+\mathrm{BCh}_L^-$ in Rhodopseudomonas viridis is 0.9 ps [67]. The transfer integral J_L is estimated to be about $20\,\mathrm{cm}^{-1}$ [70, 71, 72]. We have chosen the next parameters which characterize the wild-type of RC in our model. The energy levels are ε_M=$2000\,\mathrm{cm}^{-1}$ and ε_L=$430\,\mathrm{cm}^{-1}$, the hopping terms are $J_L = J_M$=$26\,\mathrm{cm}^{-1}$ and the rate constants are $2\,\Gamma_2/\hbar = 2\,\Gamma_3/\hbar$=$(0.9\,\mathrm{ps})^{-1}$. We assume, as in the works [64, 70], that Γ_1 is smaller than Γ_2, Γ_3 by about two orders of magnitude.

We used in the computations the following values of the parameters which characterized the noise: $\Gamma_L = \Gamma_M$=$800\,\mathrm{cm}^{-1}$ for wild-type of RC. With these parameters we get the following quantum yields and the constants k_L, k_M for WT of RC in our simulation: $\Phi_1 = 0.023$, $\Phi_2 = 0.170$, $\Phi_3 = 0.807$, k_L=$(4\,\mathrm{ps})^{-1}$, k_M=$(23\,\mathrm{ps})^{-1}$. Here we denote $w_L(p \to 0) = k_L$ and $w_M(p \to 0) = k_M$. In the computations it was assumed that $J_L = J_M$. Possible contributions to unidirectionality of ET from asymmetry of hopping terms J_M, J_L and sink parameters Γ_2, Γ_3 were derived in the works [75, 76, 77, 84].

When we assume similarly as in the work [75] that there exists the asymmetry $J_L/J_M = 2.8$ and $\Gamma_3/\Gamma_2 = (2.1)^2$, we get the following QY and constants k_L, k_M: $\Phi_1 = 0.027$, $\Phi_2 =$

0.026, $\Phi_3 = 0.947$, k_L=$(4\,\mathrm{ps})^{-1}$, k_M=$(178\,\mathrm{ps})^{-1}$. We used the parameters: ε_M=2000 cm^{-1}, ε_L=430 cm^{-1}, J_L=26 cm^{-1}, $2\,\Gamma_3/\hbar \approx (0.9\,\mathrm{ps})^{-1}$, $2\,\Gamma_1/\hbar$=$(170\,\mathrm{ps})^{-1}$, $\Gamma_L = \Gamma_M$=800 cm^{-1}.

When we assume that the only one asymmetry is the above mentioned asymmetry in the hopping terms and in the imaginary parts of energy levels, we have QY: $\Phi_1 = 0.025$, $\Phi_1 = 0.119$, $\Phi_1 = 0.856$, k_L=$(4\,\mathrm{ps})^{-1}$, k_M=$(32\,\mathrm{ps})^{-1}$ with parameters: $\varepsilon_M = \varepsilon_L$=430 cm^{-1}, J_L=26 cm^{-1}, $2\,\Gamma_3/\hbar \approx (0.9\,\mathrm{ps})^{-1}$, $2\,\Gamma_1/\hbar$=$(170\,\mathrm{ps})^{-1}$, Γ_L=800 cm^{-1}, Γ_M=800 cm^{-1}.

Special cases

Now we present some special cases where we describe the main characteristics of the process. We assume that $J_M = J_L = J$ and $\Gamma_1 = 0$, $\Gamma_2 = \Gamma_3 = \Gamma$. In this case we compute the parameter $K_{32} = \Phi_3/\Phi_2$ that characterizes the ratio between the probability of electronic escape through the L and M branch of RC. From (2.27a) we have

$$K_{32} = \frac{(\Gamma + \Gamma_L)[J^2(\Gamma + \Gamma_M) + \Gamma(\Gamma^2 + 2\Gamma\Gamma_M + \Gamma_M^2 + \varepsilon_M^2)]}{(\Gamma + \Gamma_M)[J^2(\Gamma + \Gamma_L) + \Gamma(\Gamma^2 + 2\Gamma\Gamma_L + \Gamma_L^2 + \varepsilon_L^2)]}. \tag{2.35}$$

We can see that at $\Gamma \to \infty$, $K \approx 1$. It means that when the electron escapes from the system very quickly, the asymmetry of the electron distribution cannot be achieve. For the very slow escape, when $\Gamma \to 0$ and $\Gamma_L = \Gamma_M = 0$, we get

$$K_{32} = \frac{J^2 + \varepsilon_M^2}{J^2 + \varepsilon_L^2}. \tag{2.36}$$

At this limit the steady state does not exist. The asymmetry in the electron distribution is caused by the asymmetry arrangement of the energy levels. If they are not zero the system can achieve the steady state. The probability to find electron at site 2 and 3 is raising asymmetrically. From Eq.(2.20) we can see that the probability of electronic escape depends on the history of the system. Because of the steady state is fully symmetric in this case the asymmetry in the quantum yields depends on the parameters which caused the asymmetry in the relaxation and does not depend on the steady state. For large ε_L, ε_M from Eq.(2.35), we get

$$K_{32} = \frac{(\Gamma + \Gamma_L)\varepsilon_M^2}{(\Gamma + \Gamma_M)\varepsilon_L^2}. \tag{2.37}$$

At this limit the asymmetry in the relaxation is caused by the asymmetry in parameters which characterize the energy level fluctuations. For large Γ_L, Γ_M we have

$$K_{32} = \frac{\Gamma_M}{\Gamma_L}. \tag{2.38}$$

In this case the electron is transported mainly through the branch with smaller fluctuation of the energy level. For small Γ and large Γ_L, Γ_M, when the conditions $J^2\Gamma_L \gg \Gamma(\Gamma_L^2 + \varepsilon_L^2)$ and $J^2\Gamma_M \gg \Gamma(\Gamma_M^2 + \varepsilon_M^2)$ are fulfilled, we have electron transfer with $K \approx 1$. At this limit the system reaches the steady state very fast. The quantum yields are determined by the steady state. We have the same probability of the electronic escape through the branch L and M. From equations (2.35-2.38) we can see that the main effect on the unidirectionality of ET has asymmetry of the energy levels. The quantum yields do not depend on the sign of the energy level. The implementation of the theory requires information regarding energetic parameters, such as the energy gap between the equilibrium nuclear configuration between P^* and $P^+\mathrm{BChl}^-_{L(M)}$ which, in spite of the recent progress, cannot be reliably calculated. The energy level of $P^+\mathrm{BChl}^-_L$ in RCs of *Rb. Sphaeroides* is about

50 meV below P^* [67]. Another calculations show that this energy level is about 30 meV above special pair [68]. Theoretical calculation, using the *Rp.viridis* RC crystal structure suggested that the $P^+\mathrm{BChl}_M^-$ state is 240 meV higher than P^* [69]. The $(200\,\mathrm{ps})^{-1}$ P^* internal conversion rate is the average of the values of $(90-350\,\mathrm{ps})^{-1}$ that have been estimated from measurements in wild-type RC's [67]. The decay time of $P^+\mathrm{BChl}_L^-$ in *Rp. viridis* is 0.65 ps [67]. The transfer integral J is estimated to be about 2.5 meV [70, 71, 72]. We have chosen the next parameters which characterized the wild type of RC in our model. The energy levels are ε_M=250 meV, ε_L=50 meV, the hopping term is J=2.5 meV, the rate constants are $2\,\Gamma_2/\hbar = 2\,\Gamma_3/\hbar = 2\,\Gamma/\hbar \approx (0.65\,\mathrm{ps})^{-1}$. We assume, as in the work [70], that Γ_1 is smaller than Γ_2, Γ_3 by about 2 orders of magnitude. This also follows from experimental date [64, 67]. We used in computations the next values of parameters which characterized the noise and the decay of the system to the ground state: $\Gamma_L = \Gamma_M$=25 meV and $2\,\Gamma_1/\hbar = (200\,\mathrm{ps})^{-1}$ for wild-type (WT) of RC. We get the following quantum yields for WT of RC in our simulation: $\Phi_1 = 0.03$, $\Phi_2 = 0.05$, $\Phi_3 = 0.92$.

Electron transfer reactions in modified RC

The highly asymmetric functionality can be changed by amino acid mutations or cofactor modifications [24, 29]. These mutants have provided insights into key factors impacting the directionality and yields of electron transfer in the RC by changing the relative free energies of the participating states [60-67]. Electron transfer to the L-versus the M-sides in the RC may be substantially modulated by the relative free energies of $P^+\mathrm{BChl}_L^-$ and $P^+\mathrm{BChl}_M^-$.

A drastically reduced quantum yield is observed in RC's where substantially different chromophores were in different binding pockets of the electron acceptors. In the work [63] electron transfer in a series of *Rhodobacter capsulatus* RC mutants is reported. In the $G(M201)D/L(M212)H$ (denoted DH) double mutant 15% electron transfer to M-side bacteriopheophytin, 70% electron transfer to the L-side cofactors and 15% deactivate to the ground state. It is proposed that the Asp at $M201$ raised the free energy of $P^+\mathrm{BChl}_L^-$. In the $S(L178)K/G(M201)D/L(M212)H$ (denoted KDH) triple mutants 62% electron transfer to the L-side BPh, 23% electron transfer to the M-side bacteriopheophytin and 15% return to the ground state. In the $S(L178)K/G(M201)D/L(M212)H$ triple mutants the $S(L178)K$ mutation might lower $P^+\mathrm{BChl}_M^-$ in free energy and increase the yield of electron transfer to BPh_M in comparison to the $G(M201)D/L(M212)H$ double mutant. Electron transfer along the M-side was observed in the $H(M182)L$ mutant of *Rb.sphaeroides* [65]. In this mutant bacteriopheophytin (referred to as Φ_M) is incorporated in place of BChl_M. One would expect that the $P^+\Phi_M^-$ state would be considerably lower in energy than $P^+\mathrm{BChl}_M^-$, thus enhancing the probability of M-side electron transfers. The yield of the $P^+\Phi_M^-$ state is apparently $30-40\%$.

The exchange of histidine to leucin in RC's of *Rhodopseudomonas viridis* (mutant denotes as $L153HL$) caused the incorporation of a bacteriopheophytin b instead of a bacteriochlorophyll b molecule (referred to as B_L). As a consequence of this chromophore exchange, the energy level of the electron transfer state $P^+\mathrm{B}_L^-$ is lowered in comparison to $P^+\mathrm{BChl}_L^-$ in WT. The quantum yield of $P^+\mathrm{B}_L^-$ in this mutant is reduced to 50%.

When we increase the energy ε_L in the theoretical simulations, as in the $G(M201)D/L(M212)H$ *Rhodobacter capsulatus* RC double mutants, we get the following QY: $\Phi_1 = 0.14$, $\Phi_2 = 0.14$, $\Phi_3 = 0.72$. We use the parameters: ε_M=250 meV, ε_L=100 meV, J=2.5 meV, $2\,\Gamma_2/\hbar = (0.65\,\mathrm{ps})^{-1}$, $2\,\Gamma_3/\hbar = (3.25\,\mathrm{ps})^{-1}$, $\Gamma_L = \Gamma_M$=25 meV, $2\,\Gamma_1/\hbar = (130\,\mathrm{ps})^{-1}$.

If we decrease the energy ε_M as in $S(L178)K/G(M201)D/L(M212)H$ triple mutant in comparison to double mutant we get the following QY: $\Phi_1 = 0.13$, $\Phi_2 = 0.20$, $\Phi_3 =$

0.67. We use the parameters: ε_M=200 meV, ε_L=100 meV, J=2.5 meV, $2\,\Gamma_2/\hbar=(0.65\,\mathrm{ps})^{-1}$, $2\,\Gamma_3/\hbar=(3.25\,\mathrm{ps})^{-1}$, $\Gamma_L=\Gamma_M$=25 meV, $2\,\Gamma_1/\hbar=(130\,\mathrm{ps})^{-1}$. We lowered here the rate from molecules 3 which agrees with experimental results [24, 63].

When we considerably decrease the energy ε_M in comparison to WT as in the $H(M182)L$ mutant of Rb.sphaeroides where bacteriopheophytin is incorporated in place of BChl_M, we get the following QY: $\Phi_1 = 0.04$, $\Phi_2 = 0.33$, $\Phi_3 = 0.63$. We use the parameters: ε_M=−75 meV, ε_L=50 meV, J=2.5 meV, $2\,\Gamma_2/\hbar=2\,\Gamma_3/\hbar=(0.65\,\mathrm{ps})^{-1}$, $\Gamma_L=\Gamma_M$=25 meV, $2\,\Gamma_1/\hbar=(130\,\mathrm{ps})^{-1}$.

When we considerably decrease the energy ε_L in comparison to WT as in the $L153HL$ mutant of *Rh. viridis* where bacteriopheophytin is incorporated in place of BChl_L, we get the following QY: $\Phi_1 = 0.16$, $\Phi_2 = 0.42$, $\Phi_3 = 0.42$. We use the parameters: ε_M=225 meV, ε_L=−225 meV, J=2.5 meV, $2\,\Gamma_2/\hbar=2\,\Gamma_3/\hbar=(0.65\,\mathrm{ps})^{-1}$, $\Gamma_L=\Gamma_M$=25 meV, $2\,\Gamma_1/\hbar=(260\,\mathrm{ps})^{-1}$.

Discussion of the model

The special case solves specific problem of the highly asymmetric ET in the photosynthetic reaction centers. Because of the very fast primary charge separation process we use the stochastic model with the memory functions equal for the forward and backward electron transfer. When the conditions $\Gamma_2=\Gamma_3=\Gamma_1=0$, $\Gamma_M\neq 0$ and $\Gamma_L\neq 0$ are fulfilled we get the fully symmetric steady state. It means that the electron occupation $P_i(\infty)$ probabilities relax to the equilibrium distribution $P_i(\infty)=1/3$. When one of the parameters Γ_M, Γ_L is also zero, for instance Γ_M, we have asymmetric steady state with equilibrium occupation probabilities and $P_1(\infty)=P_3(\infty)=(\varepsilon_M^2+2J^2)/2(\varepsilon_M^2+3J^2)$ and $P_2(\infty)=J^2/(\varepsilon_M^2+3J^2)$. At this limit when $\varepsilon_M=0$, the fully symmetric steady state is restored. On the other hand, when $\varepsilon_M^2\gg J^2$ we get $P_1(\infty)=P_3(\infty)\to 1/2$ and $P_2(\infty)\to 0$. In this case M-branch is practically inactive and we get the steady state as in the stochastic two-sites models [51, 54, 55, 58].

Extensive experimental efforts have been devoted to elucidation of the role of accessory bacteriochlorophyll molecules. We considered that the electron is delocalized to the molecules P, BChl_M and BChl_L. The electron density depends on the parameters which characterize the three molecules system. The data show that the free energy of the intermediates $P^+\mathrm{BChl}_L^-$, $P^+\mathrm{BChl}_M^-$ is of major importance. For instance, if the free energy of $P^+\mathrm{BChl}_L^-$ is raised relative to that of wild type RC (as, likely, if negative charge is introduced in the mutant $L153HE$), the quantum efficiency is lowered considerably. In this special case we have shown that there is a correlation between the shift of energy levels of accessory bacteriochlorophyll molecules and the quantum yields. Theoretical simulations are in correspondence with experimental results. The influence of energy fluctuations must not be neglected. When we assume asymmetry in the parameters which characterize the fluctuations ($\Gamma_M=0$, Γ_L=25 meV), we get the following quantum yields in WT of RC: $\Phi_1 = 0.034$, $\Phi_2 = 0.001$, $\Phi_3 = 0.965$. To elucidate the unidirectionality the Markovian approximation was used in the previous model. It must not be proper for describing the primary charge transfer processes in the RC. In [75, 76] it was shown that different hopping terms (electron-transfer integrals) in the branches can result in the asymmetry of charge separation across the L and M branches of the RC. In the present model we have demonstrated that for the asymmetric ET it is not sufficient to consider only an asymmetry in electron-transfer integrals. For example, in the case of small Γ the system approaches the quasi steady state, where asymmetry is determined by equilibrium electron density distribution and does not depend on the electron-transfer integral.

We have mutant, where hopping integrals are not changed significantly, and unidirec-

tionality is lowered considerably [60]. It is in contradiction with the work [77], where the unidirectionality is explained only through the asymmetry of the transfer integrals in the L and M regions. The results of the work [78] suggest that the dimmer is playing the decisive role for the vectorial charge separation. There are mutations where dimmer is not changed and we have strong changes in unidirectionality [24, 63, 66]. The asymmetry of the hopping terms can also contribute to unidirectionality. It was not assume in this special case.

2.3.2 Slow modulation limit

Now we analyze the slow modulation limit. We will work in the limit of long correlation time of the solvent. This limit is obtained when the condition $\Gamma^e_{ab}\tau^e_{ab}/\hbar \gg 1$ is fulfilled. In this limit we have

$$w_M(p) = \frac{2J_M^2}{\hbar^2}\int_0^\infty \cos[\frac{\varepsilon_M}{\hbar}t]\exp[-\frac{\Gamma_1+\Gamma_2+\hbar p}{\hbar}t-\frac{\langle\xi_M^2\rangle}{2\hbar^2}t^2]dt, \tag{2.39a}$$

$$w_L(p) = \frac{2J_L^2}{\hbar^2}\int_0^\infty \cos[\frac{\varepsilon_L}{\hbar}t]\exp[-\frac{\Gamma_1+\Gamma_3+\hbar p}{\hbar}t-\frac{\langle\xi_L^2\rangle}{2\hbar^2}t^2]dt. \tag{2.39b}$$

Similarly as in the previous limit using the solution of Eqs.(2.21), we can compute the quantum yields. The ratio $K_{32} = \Phi_3/\Phi_2$ has the form

$$K_{32} = \frac{k_L(k_M+\frac{2\Gamma_2}{\hbar})\Gamma_3}{k_M(k_L+\frac{2\Gamma_3}{\hbar})\Gamma_2}, \tag{2.40}$$

and the ratio $K_{13} = \Phi_1/\Phi_3$ has the following form:

$$K_{13} = \frac{(k_L+\frac{2\Gamma_3}{\hbar})\Gamma_1}{k_L\Gamma_3}, \tag{2.41}$$

where we denote $k_L = w_L(p\to 0^+)$ and $k_M = w_M(p\to 0^+)$. Now we analyze some special cases of ET in the RC. In the case when $k_M \gg 2\Gamma_2/\hbar$ and $k_L \gg 2\Gamma_3/\hbar$ we get $K_{32} = \Gamma_3/\Gamma_2$ and $K_{13} = \Gamma_1/\Gamma_3$. In the opposite case we have

$$K_{32} = \frac{k_L}{k_M}, \tag{2.42}$$

and

$$K_{13} = \frac{2\Gamma_1}{\hbar k_L}. \tag{2.43}$$

In the static limit, when the conditions $(2\xi_L^2)^{1/2} \gg \Gamma_1+\Gamma_3$ and $(2\xi_M^2)^{1/2} \gg \Gamma_1+\Gamma_2$ are fulfilled,

$$k_L = \frac{2\pi}{\hbar}J_L^2\sqrt{\frac{1}{2\pi\langle\xi_L^2\rangle}}\exp[-\frac{\varepsilon_L^2}{2\langle\xi_L^2\rangle}], \tag{2.44a}$$

$$k_M = \frac{2\pi}{\hbar}J_M^2\sqrt{\frac{1}{2\pi\langle\xi_M^2\rangle}}\exp[-\frac{\varepsilon_M^2}{2\langle\xi_M^2\rangle}]. \tag{2.44b}$$

In this case we can see that the sink parameters have similar values as the constants k_L, k_M so that this limit predicts that the balance between the ET to the L and M branch

can be effectively regulated also with the change of the sink parameters, in contrast to the fast modulation limit.

Now we compute the QY's and rate constants in the slow modulation limit. When we assume the only asymmetry in the energy levels we have: $\Phi_1 = 0.019$, $\Phi_2 = 0.003$, $\Phi_3 = 0.978$, k_L=$(2.4\,\mathrm{ps})^{-1}$, k_M=$(918\,\mathrm{ps})^{-1}$ with the parameters: ε_M=$2000\,\mathrm{cm}^{-1}$, ε_L=$430\,\mathrm{cm}^{-1}$, $J_L = J_M = 26\,\mathrm{cm}^{-1}$, $2\,\Gamma_2/\hbar = 2\,\Gamma_3/\hbar \approx (0.9\,\mathrm{ps})^{-1}$, $2\,\Gamma_1/\hbar$=$(170\,\mathrm{ps})^{-1}$ and $\sqrt{2\langle\xi_L^2\rangle} = \sqrt{2\langle\xi_M^2\rangle}$= $800\,\mathrm{cm}^{-1}$ for wild-type of RC.

When we assume as in the fast modulation limit that there exist the asymmetry $J_L/J_M = 2.8$ and $\Gamma_3/\Gamma_2 = (2.1)^2$ we have: $\Phi_1 = 0.0189$, $\Phi_2 = 0.0004$, $\Phi_3 = 0.9807$, k_L=$(2.4\,\mathrm{ps})^{-1}$, k_M=$(7200\,\mathrm{ps})^{-1}$ with the parameters: $\varepsilon_M = 2000\,\mathrm{cm}^{-1}$, $\varepsilon_L = 430\,\mathrm{cm}^{-1}$, $J_L = 26\,\mathrm{cm}^{-1}$, $2\,\Gamma_3/\hbar \approx (0.9\,\mathrm{ps})^{-1}$, $2\,\Gamma_1/\hbar$=$(170\,\mathrm{ps})^{-1}$ and $\sqrt{2\langle\xi_L^2\rangle} = \sqrt{2\langle\xi_M^2\rangle}$= $800\,\mathrm{cm}^{-1}$.

When we assume that the only one asymmetry is the above mentioned asymmetry in the hopping terms and the asymmetry in the imaginary parts of energy levels we have : $\Phi_1 = 0.016$, $\Phi_2 = 0.125$, $\Phi_3 = 0.859$, k_L=$(2.4\,\mathrm{ps})^{-1}$, k_M=$(18\,\mathrm{ps})^{-1}$ with the parameters: $\varepsilon_M = \varepsilon_L$=$430\,\mathrm{cm}^{-1}$, J_L=$26\,\mathrm{cm}^{-1}$, $2\,\Gamma_3/\hbar \approx (0.9\,\mathrm{ps})^{-1}$, $2\,\Gamma_1/\hbar$=$(170\,\mathrm{ps})^{-1}$ and $\sqrt{2\langle\xi_L^2\rangle} = \sqrt{2\langle\xi_M^2\rangle}$= $800\,\mathrm{cm}^{-1}$.

2.4 Underdamped regime

In the present section, we assume the regime where the correlation function corresponds to a strongly underdamped Brownian oscillator. It means that we assume the correlation function $K_{ij}(t)$ in the form [82, 83]

$$K_{ij}(t) = \langle\xi_{ij}^2\rangle_{slv} \exp\Big(- |t|/\tau_{ij}^e\Big)\Big\{ \cos[\omega_{ij}t] + \frac{1}{\omega_{ij}\tau_{ij}^e}\sin[\omega_{ij}|t|]\Big\}. \tag{2.45}$$

We will work in the strongly underdamped limit where the condition $\omega_{ij}\tau_{ij}^e \gg 1$ is fulfilled. In this regime, we proceed in the same way as in the previous sections

$$\begin{aligned} w_L(p) &= \frac{2J_L^2}{\hbar^2}\int_0^\infty \cos[\frac{\varepsilon_L}{\hbar}t]\exp[-\frac{\Gamma_1+\Gamma_3+\hbar p}{\hbar}t] \\ &\quad \exp\Big\{ - \frac{\langle\xi_L^2\rangle}{\hbar^2\omega_L^2}\Big[\frac{2t}{\tau_L} + 1 - \exp(-\frac{t}{\tau_L})\Big(\cos(\omega_L t) + \frac{3}{\omega_L\tau_L}\sin(\omega_L t)\Big)\Big]\Big\}dt, \end{aligned} \tag{2.46a}$$

$$\begin{aligned} w_M(p) &= \frac{2J_M^2}{\hbar^2}\int_0^\infty \cos[\frac{\varepsilon_M}{\hbar}t]\exp[-\frac{\Gamma_1+\Gamma_2+\hbar p}{\hbar}t] \\ &\quad \exp\Big\{ - \frac{\langle\xi_M^2\rangle}{\hbar^2\omega_M^2}\Big[\frac{2t}{\tau_M} + 1 - \exp(-\frac{t}{\tau_M})\Big(\cos(\omega_M t) + \frac{3}{\omega_M\tau_M}\sin(\omega_M t)\Big)\Big]\Big\}dt, \end{aligned} \tag{2.46b}$$

and the constant k_L can be expressed in the form (Appendix B)

$$\begin{aligned} k_L &= \frac{2J_L^2}{\hbar^2\omega_L}e^{-S_L}\Big\{\sum_{k=0}^{\infty}\frac{1}{k!k!}(S_L/2)^{2k}\frac{\Omega_L+2k/\alpha_L}{(\Omega_L+2k/\alpha_L)^2+p_L^2} \\ &+\sum_{k=0}^{\infty}\sum_{q=1}^{\infty}\frac{1}{k!(k+q)!}(S_L/2)^{2k+q}\Big[\frac{\Omega_L+(2k+q)/\alpha_L+\frac{3q}{\alpha_L}(q-p_L)}{[\Omega_L+(2k+q)/\alpha_L]^2+[q-p_L]^2} \\ &+\frac{\Omega_L+(2k+q)/\alpha_L+\frac{3q}{\alpha_L}(q+p_L)}{[\Omega_L+(2k+q)/\alpha_L]^2+[q+p_L]^2}\Big]\Big\}, \end{aligned} \tag{2.47}$$

where $S_L=\frac{\langle\xi_L^2\rangle}{\hbar^2\omega_L^2}$, $\alpha_L=\omega_L\tau_L$, $\Omega_L=\frac{\Gamma_1+\Gamma_3}{\hbar\omega_L}+\frac{2S_L}{\alpha_L}$ and $p_L=\frac{\varepsilon_L}{\hbar\omega_L}$. Changing $L\to M$ and $\Gamma_3\to\Gamma_2$, we get the expression for the constant k_M.

Now we compute QY's in this regime. When we assume the only asymmetry in the energy levels we have: $\Phi_1=0.019$, $\Phi_2=0.034$, $\Phi_3=0.947$, k_L=$(2.6\,\mathrm{ps})^{-1}$, k_M=$(96.5\,\mathrm{ps})^{-1}$ with the parameters: $\varepsilon_M=2000\,\mathrm{cm}^{-1}$, $\varepsilon_L=430\,\mathrm{cm}^{-1}$, $\hbar\omega_L=\hbar\omega_M$=$100\,\mathrm{cm}^{-1}$, $J_L=J_M$=$26\,\mathrm{cm}^{-1}$, $2\,\Gamma_2/\hbar=2\,\Gamma_3/\hbar\approx(0.9\,\mathrm{ps})^{-1}$, $2\,\Gamma_1/\hbar$=$(170\,\mathrm{ps})^{-1}$, $\sqrt{2\langle\xi_L^2\rangle}=\sqrt{2\langle\xi_M^2\rangle}$= $800\,\mathrm{cm}^{-1}$ and $\alpha_L=\alpha_M=20$ for wild-type of RC.

When we assume as in the previous cases that there exist the asymmetry $J_L/J_M=2.8$ and $\Gamma_3/\Gamma_2=(2.1)^2$ we have: $\Phi_1=0.02$, $\Phi_2=0.005$, $\Phi_3=0.975$, k_L=$(2.6\,\mathrm{ps})^{-1}$, k_M=$(754\,\mathrm{ps})^{-1}$ with the parameters: ε_M=$2000\,\mathrm{cm}^{-1}$, ε_L=$430\,\mathrm{cm}^{-1}$, $\hbar\omega_L=\hbar\omega_M$=$100\,\mathrm{cm}^{-1}$, $J_L=26\,\mathrm{cm}^{-1}$, $2\,\Gamma_3/\hbar\approx$$(0.9\,\mathrm{ps})^{-1}$, $2\,\Gamma_1/\hbar$=$(170\,\mathrm{ps})^{-1}$, $\sqrt{2\langle\xi_L^2\rangle}=\sqrt{2\langle\xi_M^2\rangle}$= $800\,\mathrm{cm}^{-1}$ and $\alpha_L=\alpha_M=20$.

When we assume that the only asymmetry is the above mentioned asymmetry in the hopping terms and the asymmetry in the imaginary parts of energy levels we have: $\Phi_1=0.017$, $\Phi_2=0.139$, $\Phi_3=0.844$, $k_L=(2.6\,\mathrm{ps})^{-1}$, k_M=$(21\,\mathrm{ps})^{-1}$ with the parameters: $\varepsilon_M=\varepsilon_L$=$430\,\mathrm{cm}^{-1}$, $\hbar\omega_L=\hbar\omega_M=100\,\mathrm{cm}^{-1}$, J_L=$26\,\mathrm{cm}^{-1}$, $2\,\Gamma_3/\hbar\approx$$(0.9\,\mathrm{ps})^{-1}$, $2\,\Gamma_1/\hbar$=$(170\,\mathrm{ps})^{-1}$, $\sqrt{2\langle\xi_L^2\rangle}=\sqrt{2\langle\xi_M^2\rangle}$= $800\,\mathrm{cm}^{-1}$ and $\alpha_L=\alpha_M=20$.

Now we will use the presented model to elucidate the observed ET in the $YM210W$ mutant of the *Rhodobacter spheroides* photosynthetic reaction center. We assume that the underdamped regime can correctly describe the ET in this reaction center. In the mutant tyrosine, $M210$ residue is replaced by tryptophan [23, 62, 86, 87]. The general view is that the free energy of the state $P^+\mathrm{BChl}_L^-$ has been raised in this mutant. As a result of this mutation, the observed time constant associated with the charge separation from P^* is about 70 ps at room temperature and $320-400$ ps at cryogenic temperature. The decrease in the primary electron transfer rate in a diminishing of the efficiency of $P^+Q_L^-$ formation to 80% at room temperature and 60-70% at cryogenic temperature [23, 86].

To get the observed results we will examine three low frequency modes. The numerical results are collected in Table 2.1. In the computation, it was assumed that the expression $\langle\xi_{ij}^2\rangle=2E_{ijr}k_BT$ is valid in the classical limit [82, 83], where E_{ijr} is the "reorganization" energy. In $YM210W$ mutant the parameter $2\Gamma_3/\hbar$ was decreased, similar to the work [86], to the value $(2\,\mathrm{ps})^{-1}$ in comparison to WT. To imitate the possible temperature dependence of the parameter $2\Gamma_1/\hbar$, we used the value $(300\,\mathrm{ps})^{-1}$ of this parameter at temperature 200 K in the computations. The numerical computations show that the $\hbar\omega$=$80\,\mathrm{cm}^{-1}$ mode gives the results that are in the best correspondence with observed data. The mode $\hbar\omega$=$100\,\mathrm{cm}^{-1}$ gives a small increase of QY to the L-branch with a decrease in the temperature in the $YM210W$ mutant. The mode $\hbar\omega$=$50\,\mathrm{cm}^{-1}$ can indicate that the lifetime of P^* in WT increases with a decrease in the temperature, which is not in accordance with experimental results. In the numerical computation, it was assumed

Sample	T (K)	$\hbar\omega^b$ (cm^{-1})	S^c	$\hbar/2\Gamma_1$ (ps)	$\hbar/2\Gamma_3$ (ps)	ε_L (cm^{-1})	$1/k_L$ (ps)	$1/k_M$ (ps)	Φ_1	Φ_2	Φ_3
WT	300	100	30	170	0.9	430	2.57	119	0.019	0.028	0.953
	200	100	20	300	0.9	430	2.31	469	0.01	0.007	0.983
YM210W	300	100	30	170	2	1300	15	119	0.08	0.115	0.805
	200	100	20	300	2	1300	35.8	469	0.104	0.067	0.829
WT	300	80	30	170	0.9	430	2.34	329	0.019	0.01	0.971
	200	80	20	300	0.9	430	2.29	1109	0.01	0.003	0.987
YM210W	300	80	30	170	2	1280	29	329	0.143	0.073	0.784
	200	80	20	300	2	1280	97.6	1109	0.234	0.063	0.703
WT	300	50	30	170	0.9	430	2.53	1517	0.02	0.002	0.978
	200	50	20	300	0.9	430	3.4	3056	0.014	0.001	0.985
YM210W	300	50	30	170	2	900	33	1517	0.167	0.019	0.814
	200	50	20	300	2	900	125	3056	0.29	0.029	0.681

Table 2.1: Computed constants $1/k_L$, $1/k_M$ and quantum yields for wild type and $YM210W$ mutant of the Rhodobacter sphaeroides RC's. The value $\hbar/2\Gamma_2$=0.9 ps, ε_M=2000 cm^{-1}, $\alpha_M = \alpha_L = 20$, $J_L = J_M$=26 cm^{-1} were taken in the computations. We have assumed that $\omega = \omega_L = \omega_M$ and $S = S_L = S_M$.

that the changes of parameter $\tau_L(\tau_M)$ are small in the considered temperature range. To characterize the effect of electron-vibration coupling on the ET, we present the dependence of the effective time constant $A_L/k_L(A_M/k_M)$ where $A_{L(M)} = 2J^2_{L(M)}/\hbar^2\omega_{L(M)}$ on the parameter $S_L(S_M)$ and $\alpha_L(\alpha_M)$ in the Figs. 2.1, 2.2.

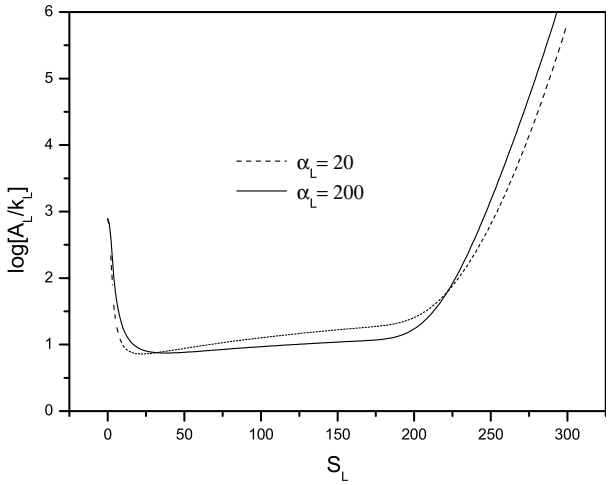

Figure 2.1: Plot of $\log_{10}(A_L/k_L)$ vs S_L with $\hbar/2\Gamma_1$=170 ps, $\hbar/2\Gamma_3$=0.9 ps, ε_L=430 cm^{-1} and $\hbar\omega_L$=80 cm^{-1} for various values of α_L. k_L is the effective rate constant and $A_L = 2J^2_L/\hbar^2\omega_L$.

In the slow mutant where the lifetime of P^* is very long, there is a possibility that the ET has an incoherent character. It means that there exist vibrational modes that relax sufficiently fast after each step of electron/energy transfer. In this case, the same projector operator as in the works [81, 88, 89, 90, 91] and in the next incoherent model has to be used.

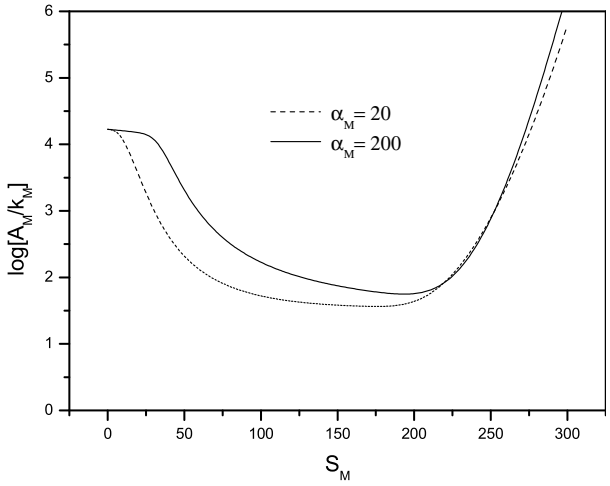

Figure 2.2: Plot of $\log_{10}(A_M/k_M)$ vs S_M with $\hbar/2\Gamma_1$=170 ps, $\hbar/2\Gamma_2$=0.9 ps, ε_M=2000 cm^{-1} and $\hbar\omega_M$=80 cm^{-1} for various values of α_M. k_M is the effective rate constant and $A_M = 2J_M^2/\hbar^2\omega_M$.

2.5 Discussion

In the previous theories with more than one sink parameter, these parameters were added in the GME ad hoc, neglecting the effect of the sink parameters on the memory kernels in the GME [52]. As a result, the requirement of non-negativity of population probabilities $P_i(t)$ was not always fulfilled. The theory presented in this model allows computation of quantum yields of electronic escape via the branches L, M, and of direct ground-state recombination. Computed quantum yields give subsidiary information, and together with transient state lifetimes they can help to determine the free parameters of the system. The lifetimes ought to be defined from *GME*. The temperature dependence of quantum yields are very important experimental data, which can be theoretically described by effective rate constants also in the case where the dynamics of electrons must be described by GME. However, it is not the case of lifetimes.

In this present model, we describe the system by a relatively simple model with one vibrational mode and symmetry in all parameters excluding energies. The obtained results are in agreement with the published experimental data [86]. Since the experiments do not give full information about the temperature dependence of quantum yields, we can compare with experimentally measured data only the temperature dependence of the computed quantum yields Φ_3 of electronic escape via the L branch. To better characterize the free parameters of the system, full information about the temperature dependence of the quantum yields is needed. This information can then show whether the presented model is realistic or not.

To describe the effective rate constant, the two-vibration modes approximation is used with high- and low-frequency modes [70, 91, 92]. The high-frequency mode is important mainly for very fast second ET step, where there is a great free-energy gap. Using only the low-frequency mode, the second ET step is slower than the first ET step, which is not in accordance with experimental data. In contrast, in the first ET step, the high-frequency mode does not seem to be so important, thus we expect that the one-mode approximation could be realistic. The high-frequency mode can play an important role in the M-branch ET in the case of large free-energy gap. This case can be described also in the one-mode approximation assuming asymmetry in the frequencies ω_L, ω_M. Figs 2.1, 2.2 shows the lack of the unidirectionality of electron transfer even when large asymmetry in the energies is present when very small or great values of the parameters $S_{L(M)}$ are used. In

this study, the value of $S_{L(M)}$ corresponds to the "reorganization" energy $E_r \approx 460\,\mathrm{cm}^{-1}$ when the vibrational mode $\hbar\omega$=80 cm^{-1} is used. The similar value of the reorganization energy was used in the paper [92] where the L branch ET was elucidated. With this value of $S_{L(M)}$ the difference between the calculated values k_L and k_M is sufficient to obtain the observed unidirectionality as seen in Table 2.1. The unidirectionality was previously explained by the effective rate constants describing the first electron transfer step in bacterial RC [76]. It was shown that assuming only the first ET step is not enough to elucidate the unidirectionality [91].

2.6 Conclusions

This model addresses a specific problem of the highly asymmetric ET in the photosynthetic reaction centers. Extensive experimental efforts have been devoted to the elucidation of the role of accessory bacteriochlorophyll molecules [96]. At least two alternative models have been proposed for the role of these molecules [72]. In this model, we considered that the electron is delocalized to the molecules P, BChl_M and BChl_L. In the present model we also assumed that the stochastic fluctuation does not depend on the localization of the electron in the branch, it means we assumed that the ET has a hot character [97]. On the studied time scale, the model excludes the repopulation processes of some electron-accepting sites. This exclusion requires the introduction of an imaginary part of the energy level.

In the present model, the generalized master equation (*GME*) was derived to describe the primary charge transfer in the photosynthetic reaction centers. This integro-differential equation (*GME*) can be changed to a differential equation (master equation). To justify this change, it has to be shown that the memory kernels $w_{ij}(t)$ in Eqs. (2.17) fulfill certain conditions. Specifically, it has to be shown that the memory kernels damp very quickly in comparison to the relaxation of the system to the steady state. However, a verification of this condition is questionable if for the description of surrounding medium only two vibrational modes are used, which is the most common case. This means roughly that in the fast modulation limit the conditions, $\Gamma_1+\Gamma_3+\Gamma_L, \Gamma_1+\Gamma_2+\Gamma_M \gg J_L, J_M$, must be fulfilled [98]. Here $(\Gamma_1+\Gamma_3+\Gamma_L)/\hbar$, $(\Gamma_1+\Gamma_2+\Gamma_M)/\hbar$ characterize the loss of memory and $J_L/\hbar, J_M/\hbar$, characterize the "coherent propagation." In the slow modulation limit, the conditions $\sqrt{2\langle\xi_L^2\rangle}, \sqrt{2\langle\xi_M^2\rangle} \gg J_L, J_M$ must be satisfied. When these conditions are not fulfilled, ET has coherent or partially coherent (damped with oscillations) character and the *GME* must be used to describe the relaxation of the system to the steady state. On the other hand we have shown in the present model that the quantum yields can be described by the parameters k_L, k_M usually used as rate constants.

At the fast modulation limit the maximal asymmetry of primary charge transfer is in the case of great energy difference between molecules. In this case all asymmetries of the system contribute to the unidirectionality of the ET. It means that the asymmetry of the hopping terms, asymmetry of parameters Γ_2, Γ_3 and asymmetry of parameters Γ_M, Γ_L contribute to unidirectionality. At slow modulation limit the energy parameters can more effectively dictate the balance between the ET to the L and M side chromophores of the RC's than the hopping terms.

Of course the observed QY can be reproduced also by the selection of another parameters. Still a little is known to give the definite answer what is the dominated factor in regulations of ET to L and M branch, the energy or hopping terms asymmetry. The data show [30, 60-66, 93-95] that the free energy of the intermediates $P^+\mathrm{BChl}_L^-$, $P^+\mathrm{BChl}_M^-$ is of major importance. This can be testified in the temperature dependence of QY. And

thus we think that the experiments which measured the temperature dependence of QY in the mutants can shed more light into this problem.

We used the stochastic model where the interaction of electron with medium was described with the correlation functions (2.6). Similar results can be obtained when we describe the medium as the vibronic manifolds with the spectral density $J(\omega) = 2\lambda\omega/(1+\omega^2\tau_e^2)$ [99] or when we use the frequency dependence of the dielectric function in the form $\mathrm{Im}\varepsilon(\omega)/|\varepsilon(\omega)|^2 = c\omega\tau_e/(1+\omega^2\tau_e^2)$ for the polar medium [81, 100]. When the dielectric function in the resonance approximation is used, we can get the correlation function, which was used in the underdamped regime of the single-mode approximation [101]. The parameter $\varepsilon_L(\varepsilon_M)$ is obviously split up into the free-energy difference and the reorganization energy. This splitting in hot electron transfer strongly depends on the medium state frozen during the ET and hardly can be verified with experiments. Thus the energy $\varepsilon_L(\varepsilon_M)$ was used as one free model parameter.

The observed L-branch electron transfer is slower in the $YM210W$ mutant than in the wild-type bacterial RC, suggesting that the character of electron transfer reaction in the mutant and wild-type RC can be different.

Chapter 3

The nonstochastic model of electron transfer

3.1 Theory

In this Chapter we attempt to analyze the possibility that ET asymmetry can be described by model which assumes, contrary to the previous models, that there exists the vibrational modes of the medium which has a sufficient time for relax to the thermal equilibrium after each ET step. We start by considering an electron transfer system in which the electron has N accessible sites, embedded in a medium. We denote by $|j\rangle$ the state with electron localized at the jth site and $j = 1, 2, ..., N$. The j and k sites are coupled by V_{jk}. The interaction of the solvent with the system depends on the electronic states $|j\rangle$ by H_j. The total model Hamiltonian for the system and medium is

$$H = H_0 + V, \tag{3.1}$$

where

$$H_0 = \sum_{j=1}^{N} |j\rangle[\varepsilon_j - i\Gamma_j + H_j]\langle j|, \tag{3.2}$$

$$V = \sum_{j,k=1}^{N} V_{jk}|j\rangle\langle k|, \quad j \neq k, \tag{3.3}$$

where ε_j is the site energy. The parameter $\hbar/2\Gamma_j$ has a meaning of the lifetime of the electron at site j in the limit of the zero coupling parameter. It can characterize the possibility of the electron escape from the system by another channel, for instance a nonradiative internal conversion or recombination process.

The Hamiltonian describing the reservoir consisting of harmonic oscillators is

$$H_j = \sum_a \left\{ \frac{p_\alpha^2}{2m_\alpha} + \frac{1}{2} m_\alpha \omega_\alpha^2 (x_\alpha - d_{j\alpha})^2 \right\}. \tag{3.4}$$

Here, m_α and ω_α are frequency and the mass of the αth oscillator, and $d_{j\alpha}$ is the equilibrium configuration of the αth oscillator when the system is in the electronic state $|j\rangle$. The total density matrix $\rho(t)$ of the ET system and the medium satisfies the Liouville equation,

$$\partial_t \rho(t) = -\frac{i}{\hbar}[H\rho(t) - \rho(t)H^\dagger] = -iL\rho(t). \tag{3.5}$$

In the interacting picture,

$$\rho_I(t) = \exp\left(\frac{i}{\hbar}H_0 t\right)\rho(t)\exp\left(-\frac{i}{\hbar}H_0^\dagger t\right). \tag{3.6}$$

The Liouville equation in the interacting picture has the following form:

$$\partial_t\rho(t) = -\frac{i}{\hbar}[V_I(t)\rho_I(t) - \rho_I(t)V_I^\dagger(t)] = -iL(t)\rho_I(t), \tag{3.7}$$

where

$$V_I(t) = \exp\left(\frac{i}{\hbar}H_0 t\right)V\exp\left(-\frac{i}{\hbar}H_0 t\right). \tag{3.8}$$

Here we denote the total trace, and the partial traces over the ET system and over the medium by Tr, Tr^e, Tr^Q, respectively. By definition $Tr \equiv Tr^Q Tr^e$. The population on state $|j\rangle$ at time t is given by

$$P_j(t) = Tr(|j\rangle\langle j|\rho(t)). \tag{3.9}$$

We assume that the vibrational relaxation is sufficiently rapid so that the system can relax to thermal equilibrium after each ET step. This assumption determines a choice of projector operator. The projector operator D acting on an arbitrary operator B in the Hilbert space of the total ET system and medium is defined by [81]

$$DB = \sum_{j=1}^{N} Tr(|j\rangle\langle j|B)\rho_j|j\rangle\langle j|, \tag{3.10}$$

where ρ_j is the equilibrium medium density matrix in the state $|j\rangle$, i.e.,

$$\rho_j = \frac{\exp(-H_j/k_BT)}{Tr^Q\exp(-H_j/k_BT)}. \tag{3.11}$$

One can show, using Eqs.(3.9)-(3.10) that (Appendix E)

$$DL(t)D = 0. \tag{3.12}$$

Using the standard projection operator techniques [79, 80] we can derive a generalized master equation for the populations (Appendix D),

$$\begin{aligned}\partial_t P_j(t) &= -\frac{2\Gamma_j}{\hbar}P_j(t) - \sum_{k=1}^{N}\int_0^t W_{jk}(t-\tau)P_j(\tau)d\tau \\ &\quad + \sum_{k=1}^{N}\int_0^t W_{kj}(t-\tau)P_k(\tau)d\tau, \quad j = 1,...,N, \quad j \neq k,\end{aligned} \tag{3.13}$$

where

$$\begin{aligned}W_{jk}(t) &= 2\frac{|V_{jk}|^2}{\hbar^2}\mathrm{Re}\Bigg\{\exp\left[-\frac{\Gamma_j+\Gamma_k}{\hbar}t\right]\exp\left[\frac{i(\varepsilon_j-\varepsilon_k)}{\hbar}t\right] \\ &\quad \times\exp\left\{\sum_\alpha\frac{E_{jk}^\alpha}{\hbar\omega_\alpha}[(\bar n_\alpha+1)e^{-i\omega_\alpha t} + \bar n_\alpha e^{i\omega_\alpha t} - (2\bar n_\alpha+1)]\right\}\Bigg\}.\end{aligned} \tag{3.14}$$

Here, $\bar{n}_\alpha = [\exp(\hbar\omega_\alpha/k_BT) - 1]^{-1}$ is a thermal population of the αth mode and

$$E_{jk}^{\alpha} = \frac{1}{2} m_\alpha \omega_\alpha^2 (d_{j\alpha} - d_{k\alpha})^2 \tag{3.15}$$

is the reorganization energy of the αth mode when system transfer from state $|j\rangle$ to state $|k\rangle$.

3.2 Model of Reaction Center

To describe the first step of electron transfer processes in the reaction centers we have used the 6-sites kinetic model of RC Fig(3.1).

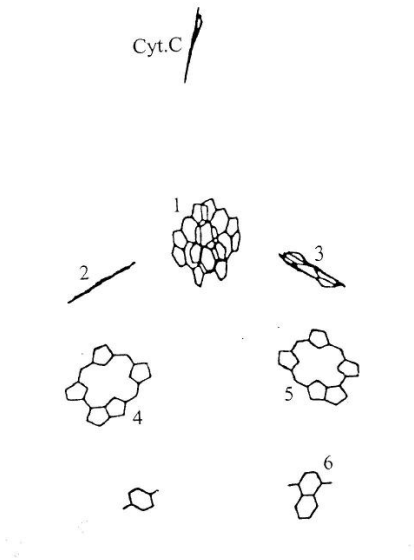

Figure 3.1: The RC of purple bacteria are composed of three protein subunits called L, M and H. Dimer P is describing by molecule 1. Cofactors in the subunits L are: 3 represent ($BChl_L$) molecule 5 (BPh_L) and 6 is (Q_L) and identically in the subunits M ($BChl_M$) is describing by molecule 2 and molecule 4 represent (BPh_M). Cytochrom C serve as a source of electrons for reaction center.

3.2.1 6-sites kinetic model

We have established 6-sites kinetic model for solving electron transfer in some mutations of RC. A similar 5-sites kinetic model was developed in the work [91]. We designate the special pair P as site 1, the sites 2 and 3 represent the molecules $BChl_M$ and $BChl_L$, and the sites 4 and 5 then represent the molecules BPh_M and BPh_L. The site 6 represents the quinone molecule Q_L (Fig. 3.2). We assume that this system is coupled to a bath (medium). Based on experimental observations of ET in RC, it is expected that bacteriochlorophyll play a crucial role in ET. In this 6-sites model we have assumed that ET in RC is sequential where P^+BChl^- is a real chemical intermediate, and also that the repopulation of accessory bacteriochlorophyll ($BChl_L$) from the molecule of bacteriopheophytin (BPh_L) is possible because of the small energy difference between the states $P^+BChl_L^-$ and $P^+BPh_L^-$ in several of mutations especially in the $F(L121)D$, $L(M212)H$ [93]. The repopulation of accessory bacteriochlorophyll ($BChl_M$) from the molecule of bacteriopheophytin (BPh_M) is neglected because of the large energy difference between the molecules. The imaginary part of energy level 1 describes the probability of electron deactivation to the ground state. Other imaginary parts of the energy levels are neglected. In this model we

denote the molecules BChl as B and molecules BPh as H on the corresponding branches L, M of RC. We describe the ET in RC by the following kinetic model

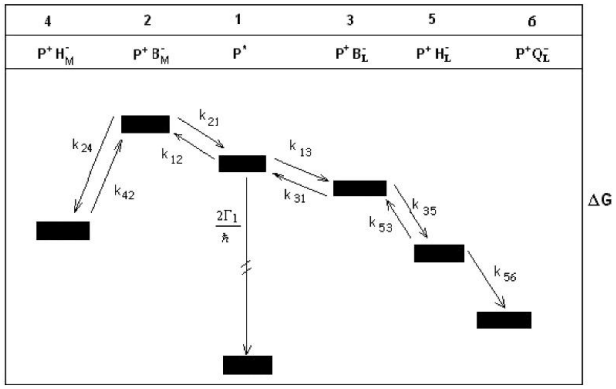

Figure 3.2: Kinetic scheme for the primary electron transfer in bacterial photosynthetic reaction centers.

$$\partial_t P_1(t) = -\frac{2\Gamma_1}{\hbar}P_1(t) - \int_0^t W_{12}(t-\tau)P_1(\tau)d\tau - \int_0^t W_{13}(t-\tau)P_1(\tau)d\tau + \int_0^t W_{21}(t-\tau)P_2(\tau)d\tau + \int_0^t W_{31}(t-\tau)P_3(\tau)d\tau, \tag{3.16a}$$

$$\partial_t P_2(t) = -\int_0^t W_{24}(t-\tau)P_2(\tau)d\tau - \int_0^t W_{21}(t-\tau)P_2(\tau)d\tau + \int_0^t W_{12}(t-\tau)P_1(\tau)d\tau, \tag{3.16b}$$

$$\partial_t P_3(t) = -\int_0^t W_{35}(t-\tau)P_3(\tau)d\tau - \int_0^t W_{31}(t-\tau)P_3(\tau)d\tau + \int_0^t W_{13}(t-\tau)P_1(\tau)d\tau + \int_0^t W_{53}(t-\tau)P_5(\tau)d\tau, \tag{3.16c}$$

$$\partial_t P_5(t) = -\int_0^t W_{53}(t-\tau)P_5(\tau)d\tau - \int_0^t W_{56}(t-\tau)P_5(\tau)d\tau + \int_0^t W_{35}(t-\tau)P_3(\tau)d\tau. \tag{3.16d}$$

Here $\mathrm{P}_i(t)$ is the occupation probability of the site i and $\mathrm{W}_{ij}(t)$ is a memory function.

3.3 Electronic escape through the branches

The quantum yields (QY's) ϕ_{L}, ϕ_{M} of the electronic escape via the branches L and M, and the quantum yields ϕ_{G} of the direct ground state recombination for 6-sites model can

be characterized by the expressions

$$\phi_G = \frac{2\Gamma_1}{\hbar}\int_0^\infty P_1(t)dt = \frac{2\Gamma_1}{\hbar}P_1(s\to 0^+), \tag{3.17a}$$

$$\phi_M = \int_0^\infty\int_0^t W_{24}(t-\tau)P_2(\tau)d\tau dt = k_{24}(s\to 0^+)P_2(s\to 0^+), \tag{3.17b}$$

$$\phi_L = \int_0^\infty\int_0^t W_{56}(t-\tau)P_5(\tau)d\tau dt = k_{56}(s\to 0^+)P_5(s\to 0^+), \tag{3.17c}$$

where $\mathrm{P}_i(s)$, $\mathrm{k}_{ij}(s)$ are the Laplace transformations of $\mathrm{P}_i(t)$ and $\mathrm{W}_{ij}(t)$. The quantum yields must fulfill the expression $\phi_G + \phi_M + \phi_L = 1$.

For our goals these two parameters are of principal importance,

$$K = \frac{\Phi_L}{\Phi_M} \quad , \quad R = \frac{\Phi_L}{\Phi_G}, \tag{3.18}$$

which express the asymmetry in the probabilities of electronic escape through the branches L and M. We can solve equation (3.16) in the Laplace transformation. Using this solution, we have

$$K = \frac{k_{13}(\exp(\frac{-G_{12}}{k_BT})k_{12} + k_{24})k_{35}k_{56}}{k_{12}k_{24}[k_{35}k_{56} + \exp(\frac{-G_{13}}{k_BT})k_{13}(\exp(\frac{-G_{35}}{k_BT})k_{35} + k_{56})]}, \tag{3.19a}$$

$$R = \frac{k_{13}k_{35}k_{56}}{\frac{2\Gamma_1}{\hbar}[k_{35}k_{56} + \exp(\frac{-G_{13}}{k_BT})k_{13}(\exp(\frac{-G_{35}}{k_BT})k_{35} + k_{56})]}. \tag{3.19b}$$

Here we denote $k_{ij}(s\to 0^+)$ as k_{ij}. Where $k_{ji} = k_{ij}\exp(-G_{ij}/k_BT)$ is the back electron transfer reaction rate constant which is calculated by using the detailed balance relation. It was assumed that at the initial time the electron is localized on the first molecule.

Now we analyze some special cases of ET in the RC. In the case when backward ET from sites 2, 3 and 5 are much greater than k_{24}, k_{35} and k_{56}, we get

$$K = \exp\left(\frac{G_{25}}{k_BT}\right)\frac{k_{56}}{k_{24}} \quad , \quad R = \frac{\hbar k_{56}}{2\Gamma_1}\exp\left(\frac{G_{15}}{k_BT}\right). \tag{3.20}$$

In the case when backward ET from sites 2 and 3 are much greater than k_{24}, k_{35} and constant k_{56} is greater then backward rate constant k_{53}, we get identical expressions as in [91] for 5-sites kinetic model

$$K = \exp\left(\frac{G_{23}}{k_BT}\right)\frac{k_{35}}{k_{24}} \quad , \quad R = \frac{\hbar k_{35}}{2\Gamma_1}\exp\left(\frac{G_{13}}{k_BT}\right). \tag{3.21}$$

It means that with small constants k_{24} and k_{35} the system can reach a quasiequilibrium and a the unidirectionality is modified mainly by the Boltzmann factors. It does not depend on the electron couplings V_{12} and V_{13}.

In the opposite case when backward reactions are slow in comparison to constants k_{24} and k_{35}, we have

$$K = \frac{k_{13}}{k_{12}} \quad , \quad R = \frac{\hbar k_{13}}{2\Gamma_1}. \tag{3.22}$$

The form of parameter K is the same as the one used to characterize the unidirectionality in an earlier study [84]. Using in equation (3.14) multinominal expansion of

$$\exp\{\frac{E_{jk}}{\hbar\omega}[(\bar{n}+1)e^{-i\omega t}+\bar{n}e^{i\omega t}-(2\bar{n}+1)]\}=$$
$$\exp\{-\frac{E_{jk}}{\hbar\omega}(2\bar{n}+1)\sum_{\alpha=0}^{\infty}\sum_{\beta=0}^{\infty}\frac{[S(\bar{n}+1)]^{\alpha}[S\bar{n}]^{\beta}}{\alpha!\beta!}\exp[i\omega(\alpha-\beta)\tau]\}=$$
$$\exp\{-\frac{E_{jk}}{\hbar\omega}(2\bar{n}+1)\sum_{q=-\infty}^{\infty}\left(\frac{\bar{n}+1}{\bar{n}}\right)^{q/2}I_q(2S[\bar{n}(\bar{n}+1)]^{1/2})e^{i\omega q\tau}\}, \tag{3.23}$$

when we have assumed that $\hbar\omega_{jk}\gg\Gamma_j+\Gamma_k$ and that our system is characterized by two vibrational modes $\alpha=2$, we get the expression for the rate constant in the form $\hbar\omega_{cij}\gg k_BT\gg\hbar\omega_{mij}$ for intermediate temperature range

$$k_{ij}(s\to 0^+)=\int_0^{\infty}W_{ij}(t)dt=\frac{2\pi V_{ij}^2}{\hbar^2\omega_{mij}}\exp[-S_{mij}(2\bar{n}_m+1)]\exp(-S_{cij})$$
$$\times\sum_{n=0}^{\infty}\frac{S_{cij}^n}{n!}\left(\frac{\bar{n}_m+1}{\bar{n}_m}\right)^{p(n)/2}I_{|p(n)|}(2S_{mij}[\bar{n}_m(\bar{n}_m+1)]^{1/2}), \tag{3.24}$$

where $p(n)=(-G_{ij}-n\hbar\omega_{cij})/\hbar\omega_{mij}$, $G_{ij}=\varepsilon_i-\varepsilon_j$ and $I_{|p(n)|}$ is the modified Bessel function.

We assume that the memory function which characterizes ET can be described by both a low frequency medium vibrational mode and a high frequency intramolecular vibrational mode. At a high temperature regime the constant $k_{ij}(s\to 0^+)$ is in the form [102]:

$$k_{ij}=\int_0^{\infty}W_{ij}(t)dt=\frac{2\pi}{\hbar}V_{ij}^2(\frac{1}{4\pi\lambda_{mij}k_BT})^{1/2}\exp(-S_{cij})$$
$$\times\sum_{n=0}^{\infty}\frac{S_{cij}^n}{n!}\exp[-\frac{(G_{ji}+\lambda_{mij}+n\hbar\omega_{cij})^2}{4\lambda_{mij}k_BT}]. \tag{3.25}$$

Here, $G_{ij}=\epsilon_i-\epsilon_j$ and $S_{cij}=\frac{1}{2\hbar}m_{cij}\omega_{cij}(d_{ci}-d_{cj})^2$ is the scaled reorganization constant for the high frequency ij-th mode, which is nonzero when electron is transferring from the state $|i\rangle$ to the state $|j\rangle$, and $\lambda_{mij}=\frac{1}{2}m_{mij}\omega_{mij}^2(d_{mi}-d_{mj})^2$ is the reorganization energy of the low-frequency mode when the electron is transferring from the state $|i\rangle$ to the state $|j\rangle$. In the derivation of the constants k_{12} and k_{13} it was also assumed that $\Gamma_1<<\hbar\omega_{12},\hbar\omega_{13}$.

To solve Eq.(3.13) the inverse Laplace transformation of $P_i(s)$ has to be applied and for this purpose a complete frequency dependence of $k_{ij}(s)$ is needed. Changing Eq.(3.13)to the ordinary rate constants, where the constants k_{ij} are employed as rate constants, gives the solutions for the population probabilities $P_i(t)$ which are different from the exact solutions of Eq.(3.13). The solution of $P_i(t)$ from the ordinary rate equations which employ constant k_{ij} as a rate constant may even yield a negative population in the short time scales [103]. In the longer time scales it is assumed that these equations approach the exact solutions. However, it was shown that it is not generally true [98]. Assuming in Eq. 3.14 that reorganization energies E_{13}^{α}, and E_{12}^{α} are zero we get the coherent sequential electron transfer in both branches. This case was already described in our previous models [37, 39, 40].

The presented 6-sites kinetic model excludes on the studied time scale the repopulation processes of electron accepting sites. Similarly as in the previous model this exclusion requires the introduction of imaginary part of energy levels both to explain the observed asymmetry and to have physically meaningful occupational probabilities. Without the imaginary part the solution of equations for the occupational probability can lead to the negative values.

Chapter 4

Superexchange vs. sequential model of electron transfer

The implementation of the theory of the incoherent model of electron transfer requires an information regarding the energetic parameters, the medium reorganization energies, the high frequency modes, and electronic coupling terms. Several sets of parameters were used to describe a charge transfer in the RC. A set of parameters based on molecular dynamics simulations [95] corresponds to a dominance of superexchange mechanisms for the primary ET reaction in RC's. Another set of parameters [70, 92] was used to fit experimental data. This second set of parameters derives a dominant contribution from the sequential mechanism. The first set of parameters has the larger reorganization energies and the greater coupling factors. This set of parameters makes the ET rate much larger than it is found in the wild-type proteins.

4.1 Sequential model

First, we assume that ET has sequential character in both branches of RC. Because ET kinetic in *Rb.capsulatus* is similar to kinetic of *Rb.sphaeroides*, we adapt in this model the set of parameters that characterizes the observed L-side experimental kinetics of *Rb.sphaeroides* RC very well [70, 92]. The following parameters were used to describe the electron transfer in the L-branch of the wild type (WT) and mutants of reaction centers: the high frequency modes have the same value $\hbar\omega_{cij}$=1500 cm^{-1} besides one which is $\hbar\omega_{c56}$=1600 cm^{-1}, the values $V_{12} = V_{13}$=32 cm^{-1}, $V_{24} = V_{35}$=59 cm^{-1} and V_{56}=4.8 cm^{-1} for the electronic coupling constants, and $S_{cij} = 0.5$ for the scaled reorganization constants for the high frequency ijth mode with only one distinguished value which is $S_{c56} = 1$. The energetic parameters for WT of RC at room temperature are: $\epsilon_1 = 0$, ϵ_3=−450 cm^{-1}, ϵ_2=800 cm^{-1}, ϵ_4=−1000 cm^{-1}, ϵ_5=−2000 cm^{-1}, ϵ_6=−7200 cm^{-1}, and the medium's low frequency vibrational modes have the same value for each step of electron transfer, λ_{mij}=800 cm^{-1} except one, λ_{m56}=4800 cm^{-1}. The P* internal conversion rate is $\frac{2\Gamma_1}{\hbar}$=(170 ps)$^{-1}$. We assume similarly as in the work [94] for WT of RC that the free energy of $P^+BPh^-_M$ is about 1000 cm^{-1} above $P^+BPh^-_L$. In this case the M-branch is practically inactive. In a series of Rhodobacter capsulatus RC mutants [93] the $F(L121)D$ mutant shows 78% of the electron transfer to L-side cofactors and 22% recombination to the ground state at room temperatures. The suggested model for the $F(L121)D$ mutant assumes that $P^+H^-_L$ has higher free energy than in the wild-type of RC, thus we had to increase the energy ϵ_5 from the value ϵ_5=−2000 cm^{-1} to the value ϵ_5=−450 cm^{-1}.

To characterize the structural changes on the L branch in the $F(L121)D$ mutant we

also slightly changed the free energy of the $P^+BChl_L^-$ state and in the computation we used the value ϵ_3=$-350\,cm^{-1}$. Other parameters stay the same as in the WT of RC. Experimental observations in the $F(L121)D$ mutant at low temperature ($77K$) show 88% quantum yield via the L-side in comparison with 78% at room temperature. The results of our numerical computations for WT and mutant RCs are collected in Table 4.1.

Sample	T (K)	ϵ_3 (cm^{-1})	ϵ_5 (cm^{-1})	$1/k_{12}$ (ps)	$1/k_{24}$ (ps)	$1/k_{13}$ (ps)	$1/k_{35}$ (ps)	$1/k_{56}$ (ps)	Φ_L	Φ_M	Φ_G
WT	295	-450	-2000	96.7	1.02	2.35	0.9	200	0.97	0.016	0.014
	200			508	1.2	2.11	1.1	186	0.985	0.002	0.013
F(L121)D	295	-350	-450	96.7	1.02	2.65	1.2	205	0.763	0.123	0.114
	200			508	1.2	2.53	1.42	195	0.934	0.011	0.055
L(M212)H	295	-520	-440	96.7	1.02	2.2	1.9	205	0.746	0.136	0.118
	200			508	1.2	1.9	2.7	194	0.929	0.013	0.058

Table 4.1: Computed constants $1/k_{ij}$ and quantum yields for wild type and $F(L121)D$, $L(M212)H$ mutants of RC's. The site energy $\varepsilon_1 = 0$. Sequential mechanism on both branches was assumed.

Charge separation in the $L(M212)H$ mutant of *Rp. Capsulatus* [93] is very similar to that reported previously in other RC's where BPh is replaced with a BChl (denoted β) or with a pheophytin and mutation raised the free energy of $P^+BPh_L^-$ roughly to the free energy level of $P^+BPh_M^-$. To characterize this change of energy level we have used the value of energy ε_5=$-440\,cm^{-1}$ which are above the energy level ε_3 in this mutant. Observed quantum yields $P^+Q_A^-$ of this mutation is 76% near room temperature and slightly decrease or stay about the same at low temperature. The measured quantum yields can be reproduced by the following parameters: $\hbar\omega_{cij}$=$1500\,cm^{-1}$, $\hbar\omega_{c56}$=$1600\,cm^{-1}$, $V_{12} = V_{13}$=$32\,cm^{-1}$, $V_{24} = V_{35}$=$59\,cm^{-1}$, V_{56}=$4.8\,cm^{-1}$, $S_{cij} = 0.5$, $S_{c56} = 1$ and λ_{mij}=$800\,cm^{-1}$, λ_{m56}=$4800\,cm^{-1}$, $2\,\Gamma_1/\hbar$=$(170\,ps)^{-1}$ and energetic parameters are ϵ_3=$-520\,cm^{-1}$, ϵ_5=$-440\,cm^{-1}$, other energy levels stay the same as in the WT of RC. The results of our numerical computations for WT and mutant RCs are collected in Table 4.1. In both branches only the sequential mechanism of ET was assumed.

4.2 Parallel superexchange/sequential model

Up to now we have assumed that ET has sequential character in both branches of reaction centers. Now we would like to analyze the contribution from a superexchange mechanism to both branches M and L where sequential mechanism of electron transfer will be still assumed. We would like to show the contribution of superexchange mechanism of ET to unidirectionality of electron transfer through RC. Kinetic scheme of ET with the contribution of superexchange mechanism in RC is described in Fig. 4.1. If we assume also superexchange mechanism of ET, we can write for 6-sites kinetic model of RC the following

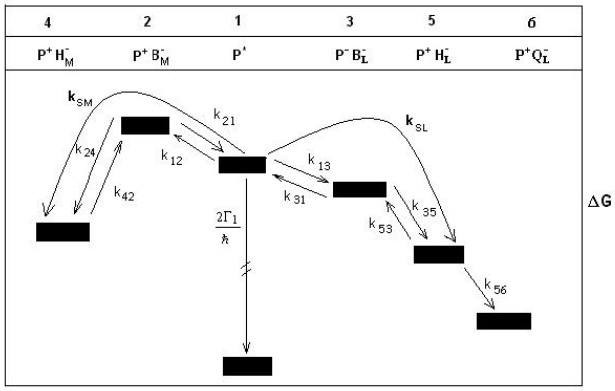

Figure 4.1: Kinetic scheme for the primary electron transfer in RC with contribution of superexchange mechanism of ET.

equations:

$$\begin{aligned}
\partial_t P_1(t) &= -(\frac{2\Gamma_1}{\hbar} + k_{12} + k_{13} + k_{SM} + k_{SL})P_1(t) \\
&\quad + k_{21}P_2(t) + k_{31}P_3(t) + k_{SL}\exp[-\frac{\Delta G_{15}}{k_B T}]P_5(t), && (4.1a)\\
\partial_t P_2(t) &= -(k_{21} + k_{24})P_2(t) + k_{12}P_1(t), && (4.1b)\\
\partial_t P_3(t) &= -(k_{35} + k_{31})P_3(t) + k_{13}P_1(t) + k_{53}P_5(t), && (4.1c)\\
\partial_t P_5(t) &= -(k_{53} + k_{56} + k_{SL}\exp[-\frac{\Delta G_{15}}{k_B T}])P_5(t) + k_{35}P_3(t) + k_{SL}P_1(t). && (4.1d)
\end{aligned}$$

Here we denote $k_{ij}(s \to 0^+) = k_{ij}$. The formula for superexchange rate based on different approximations was derived in the earlier works [103-110]. Using the formula derived in the work [104], which is proper for the bath used in the presented model, we get the rate constant which characterizes the superexchange mechanism at the M branch in the following form:

$$\begin{aligned}
k_{SM} &= \frac{2\pi}{\hbar}\frac{V_{12}^2 V_{24}^2}{E^2}\left(\frac{1}{4\pi\lambda_{14}k_B T}\right)^{1/2}\exp(-S_{14}) \\
&\quad \times \sum_{n=0}^{\infty}\frac{S_{14}^n}{n!}\exp\left[-\frac{(G_{41} + \lambda_{14} + n\hbar\omega_{14})^2}{4\lambda_{14}k_B T}\right], && (4.2)
\end{aligned}$$

where

$$E = \varepsilon_1 - \varepsilon_2 - \tilde{\lambda}_{12} - A(\varepsilon_1 - \varepsilon_4 - \tilde{\lambda}_{14}), \tag{4.3}$$

$$\tilde{\lambda}_{12} = S_{12}\hbar\omega_{12} + \lambda_{12}, \tag{4.4}$$

$$\tilde{\lambda}_{14} = S_{14}\hbar\omega_{14} + \lambda_{14}, \tag{4.5}$$

$$A = \frac{\sqrt{S_{12}S_{14}}\hbar^2\omega_{14}^2 + 2\sqrt{\lambda_{12}\lambda_{14}}k_B T}{S_{14}\hbar^2\omega_{14}^2 + 2k_B T\lambda_{14}}. \tag{4.6}$$

Similar to the work [92], for the computations the values, $S_{15} = S_{14} = 1$, $\hbar\omega_{15} = \hbar\omega_{14}$=1500 cm^{-1}, and $\lambda_{15} = \lambda_{14}$=1600 cm^{-1} were taken. All other parameters were as defined in the Sequential Model. With these parameters we get $A = \sqrt{0.5}$. Changing $2 \to 3$ and $4 \to 5$ in Eqs. (4.2)-(4.6) we get the expression for k_{SL} which characterizes the superexchange mechanism in the L branch of RC. The quantum yields Φ_L, Φ_M of electronic escape via branch L, M and the quantum yields Φ_G of direct ground state recombination can be characterized for 6-sites parallel superexchange/sequential kinetic model by the expressions

$$\phi_G = \frac{2\Gamma_1}{\hbar} P_1(s \to 0^+), \tag{4.7a}$$

$$\phi_M = k_{24}(s \to 0^+) P_2(s \to 0^+) + k_{SM} P_1(s \to 0^+), \tag{4.7b}$$

$$\phi_L = k_{56}(s \to 0^+) P_5(s \to 0^+). \tag{4.7c}$$

In the special case when we assume that in the M branch the ET have superexchange character and in the L branch the ET have sequential character, the parameters R and K have the form,

$$K = \frac{k_{13}k_{35}k_{56}}{k_{SM}[k_{35}k_{56} + \exp(\frac{-G_{13}}{k_B T})k_{13}(\exp(\frac{-G_{35}}{k_B T})k_{35} + k_{56})]}, \tag{4.8a}$$

$$R = \frac{k_{13}k_{35}k_{56}}{\frac{2\Gamma_1}{\hbar}[k_{35}k_{56} + \exp(\frac{-G_{13}}{k_B T})k_{13}(\exp(\frac{-G_{35}}{k_B T})k_{35} + k_{56})]}. \tag{4.8b}$$

Moreover, if we assume that $k_{56} \gg k_{53}$ we get the expressions as in the work [91] for 5-sites superexchange/sequential kinetic model

$$K = \frac{k_{13}k_{35}}{k_{SM}(k_{35} + k_{31})}, \tag{4.9a}$$

$$R = \frac{k_{13}k_{35}}{\frac{2\Gamma_1}{\hbar}(k_{35} + k_{31})}. \tag{4.9b}$$

The results of numerical calculations of QY's and superexchange rate constants for the parallel sequential and the superexchange mechanism in both branches of RC for different samples of RC are collected in Table 4.2.

Sample	T (K)	$1/k_{SL}$ (ps)	$1/k_{SM}$ (ps)	Φ_L	Φ_M	Φ_G
WT	295	105	1232	0.968	0.018	0.014
	200	102	1195	0.984	0.003	0.013
F(L121)D	295	1607	1232	0.751	0.136	0.113
	200	2160	1195	0.925	0.019	0.056
L(M212)H	295	2609	1232	0.734	0.15	0.116
	200	3535	1195	0.927	0.018	0.055

Table 4.2: Computed constants $1/k_{SL}$, $1/k_{SM}$ and quantum yields for wild type and mutant RC's. Parallel sequential and superexchange mechanism in both branches was assumed.

4.3 Asymmetry in electronic couplings

There is also a possibility that the the asymmetry of the electronic factors can contribute to the unidirectionality [75, 77, 84, 111, 112]. When we assume, similarly as in the work [75], that there is an asymmetry in the electronic couplings, $V_{13}/V_{12} \approx 2.8$ and $V_{35}/V_{24} \approx 2.1$, and also using the parameters for computations: $\hbar\omega_{ij}$=1500 cm^{-1}, $\hbar\omega_{56}$=1600 cm^{-1}, V_{12}=11.4 cm^{-1}, V_{13}=32 cm^{-1}, V_{24}=28 cm^{-1}, V_{35}=59 cm^{-1}, V_{56}=4.8 cm^{-1}, $S_{ij} = 0.5$, $S_{15} = S_{14} = S_{56} = 1$, $\varepsilon_1 = 0$, ϵ_3=−450 cm^{-1}, ϵ_2=800 cm^{-1}, ϵ_4=−1000 cm^{-1}, ϵ_5=−2000 cm^{-1}, ϵ_6=−7200 cm^{-1}, λ_{ij}=800 cm^{-1}, $\lambda_{15} = \lambda_{14}$=1600 cm^{-1}, λ_{56} = 4800 cm^{-1}, and $2\Gamma_1/\hbar = (170\,\text{ps})^{-1}$, we get the corresponding quantum yields and constants k_{ij} for the wild type of RC in the case if only sequential mechanism of ET via both branches L, M at T=295 K was assumed: $\Phi_G \approx 0.015$, $\Phi_M \approx 0.002$, $\Phi_L \approx 0.983$, $k_{13}=(2.35\,\text{ps})^{-1}$, $k_{35}=(0.9\,\text{ps})^{-1}$, $k_{12}=(762\,\text{ps})^{-1}$, $k_{24}=(4.5\,\text{ps})^{-1}$, $k_{56}=(200\,\text{ps})^{-1}$. At a temperature T=200 K: $\Phi_G \approx 0.0125$, $\Phi_M \approx 0.0004$, $\Phi_L \approx 0.9871$, $k_{13}=(2.1\,\text{ps})^{-1}$, $k_{35}=(1.1\,\text{ps})^{-1}$, $k_{12}=(4\,\text{ns})^{-1}$, $k_{24}=(5.4\,\text{ps})^{-1}$, $k_{56}=(186\,\text{ps})^{-1}$. If we assume also superexchange mechanism of ET we get the values of corresponding quantum yields and rate constant k_{ij} for the wild type of RC as is shown in Table 4.3.

Sample	T (K)	ε_2 (cm^{-1})	ε_3 (cm^{-1})	ε_4 (cm^{-1})	ε_5 (cm^{-1})	$1/k_{SL}$ (ps)	$1/k_{SM}$ (ps)	Φ_L	Φ_M	Φ_G
WT	295	800	-450	-1000	-2000	105	43092	0.984	0.002	0.014
	200					102	41827	0.9873	0.0004	0.0123
WT	295	-450	-450	-2000	-2000	105	3694	0.873	0.115	0.012
	200					102	3581	0.881	0.108	0.011

Table 4.3: Computed constants and quantum yields for wild type of RC in the case of asymmetry in the electronic couplings $V_{13}/V_{12} \approx 2.8$ and $V_{35}/V_{24} \approx 2.1$. Parallel sequential and superexchange mechanism in both branches was assumed. Rate constants k_{ij} has the same values as in the case of sequential mechanism of ET.

However, if there is only one asymmetry in the electronic couplings, we have the following QY and k_{ij} for wild type of RC in the case if only sequential mechanism of ET in both branches at T=295 K was assumed : $\Phi_G \approx 0.013$, $\Phi_M \approx 0.116$, $\Phi_L \approx 0.871$, $k_{13}=(2.35\,\text{ps})^{-1}$, $k_{35}=(0.9\,\text{ps})^{-1}$, $k_{12}=(18\,\text{ps})^{-1}$, $k_{24}=(4\,\text{ps})^{-1}$, $k_{56}=(200\,\text{ps})^{-1}$. At temperature T=200 K we have : $\Phi_G \approx 0.011$, $\Phi_M \approx 0.110$, $\Phi_L \approx 0.879$, $k_{13}=(2.1\,\text{ps})^{-1}$, $k_{35}=(1.1\,\text{ps})^{-1}$, $k_{12}=(17\,\text{ps})^{-1}$, $k_{24}=(5\,\text{ps})^{-1}$, $k_{56}=(186\,\text{ps})^{-1}$. In the computations the following parameters were utilized: $\hbar\omega_{ij}$=1500 cm^{-1}, V_{12}=11.4 cm^{-1}, V_{13}=32 cm^{-1}, V_{24} = 28 cm^{-1}, V_{35}=59 cm^{-1}, S_{ij} = 0.5, $S_{15} = S_{14}$ = 1, $\varepsilon_1 = 0$, ϵ_3=−450 cm^{-1}, ϵ_2 = −450 cm^{-1}, ϵ_4 = −2000 cm^{-1}, ϵ_5 = −2000 cm^{-1}, ϵ_6 = −7200 cm^{-1}, λ_{ij} = 800 cm^{-1}, $\lambda_{15} = \lambda_{14}$=1600 cm^{-1}, and $2\Gamma_1/\hbar=(170\,\text{ps})^{-1}$. Similarly as in the previous case if we assume the contribution of superexchange mechanism to ET we get the values of corresponding quantum yields and rate constant $k_{SL(M)}$ for the wild type of RC as is shown in Table 4.3.

Now we would like to get observed QY of the D, DH, KDH mutants of RC. Based on *Rb.capsulatus* RC mutants [63, 94] it was suggested that the $L(M212)H$ mutation (denoted β) raises a free energy of $P^+H_L^-$ roughly to the free energy level of $P^+H_M^-$. We expect that the value ε_5=−1000 cm^{-1} should correctly characterize these mutants. $G(M201)D/L(M212)H$ of *Rb.capsulatus* RC double mutant (denoted DH) shows 15% of ET to M-side bacteriopheophytin, 70% to the L-side cofactors, and 15% was deactivated to the ground state. The suggested model for the DH mutant assumes that the $G(M201)D$ mutation increases a free energy of $P^+B_L^-$ above P^* (ref. [69]) and so we

had to increase the energy ε_3 from the value ε_3=$-450\,\mathrm{cm}^{-1}$ to the value ε_3=$-200\,\mathrm{cm}^{-1}$. With this energy change, comparing to wild type of RC, we can reproduce the observed quantum yields in the DH mutants. With a triple mutant of *Rb.capsulatus* [63], $S(L178)K/G(M201)D/L(M212)H$ (denoted KDH), 62% of ET was observed to the L-side bacteriopheophytin, 23% to the M-side, and 15% was returning to the ground state. It is expected that in this mutation, it is the $S(L178)K$ mutation which lowers the free energy of the $P^+B_M^-$ state. To characterize this change of energy level we have used the value ε_2=$700\,\mathrm{cm}^{-1}$. This is the only change in parameters comparing to the previous mutant to elucidate the quantum yields.

If we want to elucidate the observed quantum yields also in D, DH, and KDH mutants of RC, we have to assume, similarly as in the works [111, 112] that there is an asymmetry in the electronic couplings $(V_{13}^{mut}/V_{13}^{WT})^2 \approx 0.42$ on the branch L for this kind of mutants. Moreover, that DH, KDH mutants of RC change also value of the electronic coupling V_{35} from the value V_{35}=$59\,\mathrm{cm}^{-1}$ to the value V_{35}=$6\,\mathrm{cm}^{-1}$ because of the mutation near bacteriopheopytin BPh_L.

Sample	T (K)	ε_3 (cm^{-1})	ε_5 (cm^{-1})	ε_2 (cm^{-1})	$1/k_{12}$ (ps)	$1/k_{24}$ (ps)	$1/k_{13}$ (ps)	$1/k_{35}$ (ps)	$1/k_{56}$ (ps)	$1/k_{SL}$ (ps)	$1/k_{SM}$ (ps)	Φ_L	Φ_M	Φ_G
WT	295	-450	-2000	800	96.7	1.02	2.35	0.9	200	105	1232	0.97	0.02	0.01
	200				508	1.2	2.1	1.1	186	102	1195	0.984	0.003	0.013
D	295	-200	-2000	800	96.7	1.02	13.5	1.03	200	1332	1231	0.85	0.08	0.07
	200				508	1.2	14.5	1.21	186	1291	1195	0.91	0.01	0.08
DH	295	-200	-1000	800	96.7	1.02	13.5	55	192	11589	1231	0.69	0.17	0.14
	200				508	1.2	14.5	46	179	11249	1195	0.85	0.02	0.13
KDH	295	-200	-1000	700	60	0.99	13.5	55	192	11589	963	0.62	0.25	0.13
	200				253	1.23	14.5	46	179	11249	935	0.83	0.05	0.12

Table 4.4: Computed constants and quantum yields for D, DH, KDH mutants compare with WT of RC in the case of the asymmetry in the electronic couplings $(V_{13}^{mut}/V_{13}^{WT})^2 \approx 0.42$ and in addition for DH, KDH mutants V_{35}=$6\,\mathrm{cm}^{-1}$. Parallel sequential and superexchange mechanism in both branches was assumed.

The following parameters which are not included in Table (4.4) for WT and D, DH, KDH mutants of RC were used to described the electron transfer in the both branches of RC: ε_1=0, ε_4=$-1000\,\mathrm{cm}^{-1}$, ε_6=$-7200\,\mathrm{cm}^{-1}$, V_{12}=$32\,\mathrm{cm}^{-1}$, V_{24}=$59\,\mathrm{cm}^{-1}$, V_{56}=$4.8\,\mathrm{cm}^{-1}$, all next parameters which we need for calculations are the same as in the previous case for computations of WT of RC in case of the asymmetry in electronic couplings. Only the following parameters were different for calculations: for computations of WT of RC we use value of the electronic couplings V_{13}=$32\,\mathrm{cm}^{-1}$, V_{35}=$59\,\mathrm{cm}^{-1}$, in the case of D mutant we chose (because of the mutation near bacteriochlorophyll) V_{13}=$16\,\mathrm{cm}^{-1}$, V_{35}=$59\,\mathrm{cm}^{-1}$, and finally for DH, KDH mutant of RC we chose the following values (because of the mutation also near bacteriopheophytin) V_{13}=$16\,\mathrm{cm}^{-1}$, V_{35}=$6\,\mathrm{cm}^{-1}$ for computations of quantum yields and the rate constants for the mutants of RC. The results of our numerical calculations for D, DH, KDH mutants of RC compare with WT of RC for 6-sites parallel superexchange/sequential kinetic model of ET are collected in Table (4.4). All the results from the parallel superexchange/sequential model of electron transfer are being prepared for the submission for publication. [43].

4.4 Conclusions

Of course, the observed QY can be also reproduced by the selection of another parameter. However, at the present there is not very much known about the change of electronic coupling in the mutants to proceed in the discussion about these parameters. In case that there is a strong asymmetry in the electronic couplings for the wild type of RC, the QY of the mutants must be elucidated with other energetic parameters than the ones used in this thesis. We believe that to discriminate between these options the determination of the temperature dependence of QY can be most valuable.

The assignment of free-energy arrangement can be verified by similar temperature measurements. For this purpose temperature effects on ET were calculated. We have predicted the quantum yield for *Rb.capsulatus* mutant at $200K$. Moreover, the calculated temperature dependence of ET with the selected energy arrangement shows that the asymmetry of primary charge transfer is increasing with decreasing the temperature in the case of wild type of RC. We have not demonstrated a strong increase of the ground state recombination with a decrease of temperature in the case of $F(L121)D$, $L(M212)H$ mutants compared with double and triple mutants of *Rb.capsulatus* or $YM210W$ mutant from our previous models, because the free energy ε_3 for $F(L121)D$, $L(M212)H$ mutants is below P^*(not as in the case D, DH, KDH, YFH, $YM210W$ where the free energy ε_3 is above P^*).

Moreover, there is a possibility to elucidate the observed QY in the D mutant which can be in accordance with the observed P^* lifetime temperature dependence. Experimental data indicate a small temperature dependence of the lifetime of P^* state in a temperature range $77 - 295\,\mathrm{K}$. The lifetime of P^* state is about (7.6 ps) at 285 K and (10 ps) at 77 K in the D mutant [113]. From these data a value of ε_3 can be estimated to be about $200 - 500\,\mathrm{cm}^{-1}$ above P^* and this case was analyzed in the work [91] for 5-sites kinetic model of RC. The other possibility that we have to investigate is that ε_3 can be $200 - 500\,\mathrm{cm}^{-1}$ below P^*. In this case the increase of the lifetime of the D mutant, in comparison to the wild type, should be also caused by changes in the electronic couplings on the subunit L. This possibility leads to, assuming the changes in comparison to wild type of RC in parameters, ε_3=$-200\,\mathrm{cm}^{-1}$, V_{13}=$16\,\mathrm{cm}^{-1}$ and in addition for DH, KDH mutants V_{35}=$6\,\mathrm{cm}^{-1}$. Consequently, to elucidate the observed QY's in D, DH, KDH mutants, we established a 6-sites kinetic model with a contribution of the superexchange mechanism of ET. We have also included in the model a possibility of repopulation of accessory bacteriochlorophyll BChl_L from the bacteriopheophytin BPh_L molecule on the branch L because of the smaller energy difference between the states $P^+\mathrm{BChl}_L^-$ and $P^+\mathrm{BPh}_L^-$ compared to WT of RC.

Next, we obtain the QY's and rate constants for D, DH, KDH mutants which are in good agreement with experimental data. Moreover, we have predicted the change of QY's and rate constant depending on temperature in the case of high temperature regime. At lower temperatures we get the QY's through the branch L which are increasing together with decreasing of temperatures (it is depending on whether energy level ε_3 is below or above P^*). Up to now no experimental evidence is observed for temperature dependence of D, DH, KDH mutants to give more credible information about their behaviour and tell us which results are nearest to the reality.

From our analysis it follows that the superexchange mechanism operating in parallel with the sequential process can be used to get a reliable QY's. From Tables 4.2, 4.3 we can see that the superexchange mechanism contributes a very small value and therefore does not change the final quantum-yield visibly. In an approximation a parameter K, which characterizes the asymmetry of ET, can be expressed for the coherent sequential model by $K \approx (\varepsilon_2 - \varepsilon_1)^2/(\varepsilon_3 - \varepsilon_1)^2$ and for the incoherent sequential model by $K \approx$

$\exp\{(E_3 - E_2)/k_BT\}$, where the activation energy E_i is given by $E_i = (\varepsilon_i - \varepsilon_1 - \lambda)^2/4\lambda$, $i = 2, 3$. λ is the medium reorganization energy. These two approximate expressions of the parameter K for the coherent and the incoherent models are identical to the corresponding formulas of a superexchange and sequential (two-step) model, respectively [84]. But the parameter K expressed for our coherent and incoherent models before approximation, is more complex with 6-ET kinetic sites.

The change of the free energy of the states $P^+\mathrm{BChl}_L^-$, $P^+\mathrm{BChl}_M^-$ significantly influences the QY. The free-energy arrangement can be verified by the determination of the temperature dependence of QY. For the 6-sites kinetic model, concretely for mutant $F(L121)D$ (where the energy level ε_5 is increased but it is below the energy level ε_3), we obtain the results which are in good agreement with the observed data at high-temperature regime and could elucidate the observed data also in the low temperature regime (77 K). An experimental measurement observed in $L(M212)H$ mutant the small reduction of Φ_L from the state $P^+\mathrm{BPh}_L^-$ to the state $P^+Q_L^-$ by a low temperature at the same time with the increase deactivation of $P^+\mathrm{BPh}_L^-$ to the ground state. In our model we have not considered deactivation from $P^+\mathrm{BPh}_L^-$ to the ground state and this might be the reason that Φ_L increased by the low temperature in this mutant. However, the quantum yields Φ_L and Φ_M are more sensitive to the first step of ET and so small changes in the second step of ET have no strong influence on the QY. The result is that our model predicts the similar QY's in these two mutants. The essential difference between $F(L121)D$, $L(M212)H$ and other mutants of RC is the fact that they have very small energy difference between states $P^+\mathrm{BCh}_L^-$ and $P^+\mathrm{BPh}_L^-$ on the branch L, and therefore the repopulation of BCh_L is possible.

In order to obtain numerical results at a low-temperature regime we have to use the formula for k_{ij} where the low-frequency mode is described quantum-mechanically and consequently compare the calculated results with the observed quantum yields.

Chapter 5

Conclusions: the main results of doctoral thesis

The aim of this dissertation is to get a deeper understanding and description of asymmetric electron transfer in the photosynthetic bacterial reaction centers. This is the first step to a better understanding of the process of electron transfer and thus the transport of energy in photosynthetic organisms. Consequently, it could open a way for using the solar energy more effectively. In the following I summarize achievements and the main results of my doctoral thesis.

- Stochastic and nonstochastic models of asymmetric electron transfer in photosynthetic bacteria have been suggested. For both the approaches generalized master equations for a system of N molecules for population probability were established. The expressions which characterize the asymmetry of electron transfer depending on parameters included in the models were derived. Also analytical expressions for the rate constants were found in the models.
- Analytical expressions for the ratios of quantum yields of electron escape via the branch L, M or deactivation of the system to the ground state were defined. In all the models from indicated analytical expressions numerical values of quantum yields and the rate constants for WT and also some mutations of RC were computed. As well the temperature dependence of the quantum yields and rate constants for several mutations of RC were found out. The computed results are in a good accordance with the experimental data.
- In the stochastic models it was shown that there are two ways how to explain the unidirectionality of electron transfer in RC. The first one is a large difference of the noise on L and M side of RC's. The second one is a large difference in energy levels of the accessory bacteriochlorophylls on the M and L branches of RC's. The results demonstrate that an individual amino acid residue can, through its influence on the free energy of the charge-separated states, effectively dictate the balance between the ET to the L and M-side chromophores of the RC's. Despite the crucial role of energy levels of accessory bacteriochlorophyll molecules for the unidirectionality the overall reaction required certain relation among the parameters describing the whole systems. In some cases all asymmetries of the system contribute to the unidirectionality of the ET. It means that the asymmetries of the hopping terms, energy levels and also the imaginary part of the energy levels of molecules contribute to the unidirectionality.

- Using the models we have derived the generalized master equations (*GME*), which describe the primary charge transfer in the photosynthetic reaction centers. Usually these integrodifferential equations (*GME*) are changed to differential equations (master equations) without a verification of the correctness of this step. To justify this change it has to be shown that the memory kernels $W_{ij}(t)$ fulfill certain conditions. Specifically, if the memory kernel is damped very quickly in comparison to the relaxation of the system to the steady state, the ET has an incoherent character. When these conditions are not fulfilled, ET has a coherent or partially coherent (damped with oscillations) character and the (*GME*) must be used to describe the relaxation of the system to the steady state.
- The asymmetry of electron transfer in photosynthetic reaction centers can be explained in several ways. One approach [37, 39, 40] which is presented in Chapter 2,3 assumes that the stochastic fluctuation does not depend on the localization of the electron in the branch. In other words the transfer of electrons has a hot character. The second possible explanation, presented in Chapter 3,4, is based on the model where we suggest that in the RC the vibrational modes with a fast enough relaxation are present and the system can partially relax to thermal equilibrium after each ET step. We think that both the approaches give qualitatively the same ET asymmetry dependence on the free energy and electronic coupling parameters. This means that using slightly different parameters which characterize the models we can get the same quantum yields at high temperature and also similar rate constants. The difference in the parameters and also the interplay between the forward and backward kinetics, which depends on the temperature in incoherent sequential model and does not depend on the temperature in the hot electron transfer case, predicts a different dependence of ET asymmetry on the temperature in the incoherent sequential model in comparison to the model where the electron transfer has a hot or coherent character.
- Due to the presence of an imaginary part of energy levels in our models we get the effect, which was named "fear of death". With this effect, for strong enough sink parameters the electron has a tendency to avoid the place with greater sink.
- From the outcome of our models it was found out that superexchange mechanism of ET has only a very small effect on the final quantum yields. There is also a possibility that with decreasing temperature the reorganization energy is also decreasing so that at low temperature the incoherent sequential ET is changed to the coherent sequential and it can have a similar contribution to QY as the superexchange mechanism. Moreover, the application of incoherent sequential model to ET in some mutants of RC can not describe the directionality of ET and it can also indicate that ET in RC can have coherent or hot character at the first stage.
- From the indicated results it is evident that these models provide an estimation of energetic and kinetic parameters of the systems, the knowledge of which is very important for understanding the origin of asymmetric electron transfer in the primary process during photosynthesis. The photosynthetic reaction centers are complex systems in which one step is correlated with the following one to achieve the best efficiency of their activity.
- To give a more credible information about the free energy arrangement and possible asymmetry in the electronic coupling terms we have to compare the theoretical prediction with observed quantum yields also at the low temperature regime. Still a little is known about the parameters which we have included into our theoretical models

especially at low temperatures. Therefore, we have to wait for new experimental measurements that can shed more light into this problem.

- It is possible that the primary charge separations in photosynthesis can have a nonlinear character. Therefore, we will need a nonlinear model of the electron transfer to obtain a precise description of the charge-separation processes. In such a nonlinear model we can use a gauge-field-theory approach [117, 118] to solve the problem of unidirectionality of ET in reaction centers.
- I tried to offer in my thesis a complete analysis of unidirectionality of ET in RC's and addressed all relevant issues which arose during my research work. The results from this doctoral thesis was already published and it has met with a positive feedback.

The highly asymmetric electron transfer in photosynthetic reaction centers is a promising and interesting field of research in biophysics. In my thesis I offer solutions to several problems because the better understanding of this mechanism could help us to solve the puzzle of the conversion of solar energy into chemical usable energy of photosynthetic organisms. It would be also very beneficial to obtain the M-branch electron transfer of an RC mutant with the same L-branch electron transfer rate as the wild type RC. Nevertheless, I am convinced that the ideas and calculations presented in this thesis will contribute to better understanding of photosynthesis and other related biomolecular systems.

Appendix A

Projection operators

Projection operators make us possible to separate not important information from an important one. Solving Liouville equation we get a complete information about systems, which can be very complicated for the next use. Establishing suitable projection operators allows us an effective choice of important information for us. Projection operators are called also superoperators. Projection operators must fulfill the expressions

$$D = D^2, \quad D + (1 - D) = 1. \tag{A.1}$$

The time evolution of the operators of density state is described by the Liouville equation

$$i\hbar \frac{\partial \rho(t)}{\partial t} = [H, \rho(t)]. \tag{A.2}$$

We can write Liouville operators in the form

$$L\rho(t) \equiv \frac{1}{\hbar}[H, \rho(t)]. \tag{A.3}$$

By using (A.3) we can rewrite equation (A.2) in the form

$$i\frac{\partial}{\partial t}\rho(t) = L\rho(t). \tag{A.4}$$

The quantum Liouville operator has four-index form and its elements are defined

$$(L\rho(t))_{ij} = \sum_{k,l} L_{ijkl}\rho_{kl}(t). \tag{A.5}$$

From the definition, the operator L commutes with hamiltonian H (in units $\hbar = 1$)

$$L_{ijkl} = H_{ik}\delta_{jl} - H_{lj}\delta_{ik}. \tag{A.6}$$

Using (A.1) and following applications of D and $(1 - D)$ on the equation (A.4) we get

$$i\partial_t D\rho(t) = DL(t)\rho(t) = DL(t)D\rho(t) + DL(t)(1 - D)\rho(t), \tag{A.7a}$$

$$i\partial_t(1 - D)\rho(t) = (1 - D)L(t)\rho(t) = (1 - D)L(t)(1 - D)\rho(t) + (1 - D)L(t)D\rho(t). \tag{A.7b}$$

From Eq. (A.7b) we can compute the expression $(1-D)\rho(t)$ then put it to the (A7a). In the case when it is fulfilled

$$\begin{aligned} i\partial_t[e^{i(1-D)Lt}(1-D)\rho(t)] &= e^{i(1-D)Lt}(1-D)LD\rho(t), && \text{(A.8a)} \\ ie^{i(1-D)Lt}(1-D)\rho(t) &= (1-D)LD\rho(0) \\ &\quad + \int_0^t e^{i(1-D)L\tau}(1-D)LD\rho(\tau)d\tau, && \text{(A.8b)} \\ i(1-D)\rho(t) &= e^{-i(1-D)Lt}(1-D)LD\rho(0) \\ &\quad + \int_0^t e^{-i(1-D)L(t-\tau)}(1-D)LD\rho(\tau)d\tau, && \text{(A.8c)} \end{aligned}$$

we get the Nakajima-Zwanzig identity

$$\begin{aligned} \partial_t D\rho(t) &= -iDLD\rho(t) - DL\int_0^t e^{-i(1-D)L(t-\tau)}(1-D)LD\rho(\tau)d\tau \\ &\quad -DLe^{-i(1-D)Lt}(1-D)LD\rho(0). \end{aligned} \tag{A.9}$$

By suitable choice of initial conditions, the term $DLe^{-i(1-D)Lt}(1-D)LD\rho(0)$ will be equal zero. With a simple calculation we get (Appendix E) that also the term $iDLD\rho(t) = 0$. We will work to the second order of perturbation theory. In this approximation we have

$$\partial_t D\rho(t) = -DL(t)\int_0^t L(\tau)D\rho(\tau)d\tau. \tag{A.10}$$

For illustration we show some type of projection operators [79, 114, 115]:

(1) Nakajima-Zwanzig projection operator has the form

$$\begin{aligned} D_{abcd} &= \delta_{ab}\delta_{ac}\delta_{bd}, \\ (D\rho(t))_{ab} &= \delta_{ab}\rho_{aa}(t) = \delta_{ab}P_a(t). \end{aligned} \tag{A.11}$$

(2) Peierov projection operator has the form

$$\begin{aligned} D_{abcd} &\equiv D_{m\mu,n\nu,p\pi,s\sigma} = \delta_{mn}\rho^R_{\mu\nu}\delta_{mp}\delta_{ns}\delta_{\pi\sigma} \quad , \quad \sum_\nu \rho^R_{\nu\nu} = 1 \\ (D\rho(t))_{m\mu,n\nu} &= \delta_{mn}\rho^R_{\mu\nu}\sum_\pi \rho_{m\pi,m\pi}(t) = \delta_{mn}\rho^R_{\mu\nu}\sum_\pi P_{m\pi}(t) = \delta_{mn}\rho^R_{\mu\nu}P_m(t), \end{aligned} \tag{A.12}$$

where $\rho^R_{\mu\nu}$ is an arbitrary matrix with indices, which describe the bath of investigated system. $P_m(t)$ is the probability of founding system in the state m regardless of the surrounding bath.

Appendix B

Derivation of GME for stochastic model of ET

We begin from the equations (2.15)

$$\partial_t D\rho_I(t) = -DL(t)\int_0^t L(\tau)D\rho_I(\tau)d\tau, \tag{B.1}$$

and use the projection operator (2.16) in the form

$$(DA)_{mn} = \delta_{mn}\langle A_{mm}\rangle. \tag{B.2}$$

First, we will compute the left side of equation (B.1). With using (B.2) we can write

$$\partial_t(D\rho_I(t))_{aa} = \partial_t\langle\rho_I(t)_{aa}\rangle. \tag{B.3}$$

If we assume (2.3) and (2.7) we get

$$\begin{aligned} B.3 &= \partial_t\Big\{\exp[\frac{i}{\hbar}\int_0^t(h_a(\vec{R})+\varepsilon_a-i\Gamma_a)d\tau]\rho_{aa}(t)\exp[-\frac{i}{\hbar}\int_0^t(h_a(\vec{R})+\varepsilon_a+i\Gamma_a)d\tau]\Big\} \\ &= \partial_t(\exp[\frac{2\Gamma_a t}{\hbar}]P_a(t)) = \frac{2\Gamma_a}{\hbar}P_a(t)\exp[\frac{2\Gamma_a t}{\hbar}]+\exp[\frac{2\Gamma_a t}{\hbar}]\partial_t P_a(t). \end{aligned} \tag{B.4}$$

The right side of equation (B.1), with using the prediction $P_a(t) = \langle\rho_{aa}(t)\rangle$ and (A.5), (A.6) can be computed,

$$\begin{aligned} (DL_I(t)L_I(\tau)D\rho_I(\tau))_{aa} &= \langle(L_I(t)L_I(\tau)D\rho_I(\tau))_{aa}\rangle = \langle L_I(t)_{aabc}L_I(\tau)_{bcef}(D\rho_I(\tau))_{ef}\rangle \\ &= \langle L_I(t)_{aabc}L_I(\tau)_{bcef}\delta_{ef}(\rho_I(\tau))_{ff}\rangle \\ &= \frac{1}{\hbar^2}\langle\Big(V_I(t)_{ab}\delta_{ac}-V_I^+(t)_{ca}\delta_{ab}\Big)\Big(V_I(\tau)_{be}\delta_{cf}-V_I^+(\tau)_{fc}\delta_{be}\Big)\rangle \\ &\quad\times\delta_{ef}\exp[\frac{2\Gamma_f\tau}{\hbar}]P_f(\tau), \end{aligned} \tag{B.5}$$

we get

$$\begin{aligned} (DL_I(t)L_I(\tau)D\rho_I(\tau))_{aa} &= \frac{1}{\hbar^2}\sum_b\Big\{\langle V_I(t)_{ab}V_I(\tau)_{ba}\rangle e^{\frac{2\Gamma_a\tau}{\hbar}}P_a(\tau) \\ &\quad-\langle V_I(t)_{ab}V_I^+(\tau)_{ba}\rangle e^{\frac{2\Gamma_b\tau}{\hbar}}P_b(\tau) \\ &\quad-\langle V_I^+(t)_{ba}V_I(\tau)_{ab}\rangle e^{\frac{2\Gamma_b\tau}{\hbar}}P_b(\tau) \\ &\quad+\langle V_I^+(t)_{ba}V_I^+(\tau)_{ab}\rangle e^{\frac{2\Gamma_a\tau}{\hbar}}P_a(\tau)\Big\}, \end{aligned} \tag{B.6}$$

where from equation (2.8) $V_I(t)$ can be defined as

$$V_I(t)_{ab} = V_{ab}e^{\frac{i}{\hbar}(\varepsilon_a-\varepsilon_b)t}e^{\frac{\Gamma_a-\Gamma_b}{\hbar}t}\exp[\frac{i}{\hbar}\int_0^t(h_a(\tau)-h_b(\tau))d\tau], \tag{B.7a}$$

$$V_I(t)^+_{ab} = V_{ab}e^{\frac{i}{\hbar}(\varepsilon_b-\varepsilon_a)t}e^{\frac{\Gamma_b-\Gamma_a}{\hbar}t}\exp[\frac{i}{\hbar}\int_0^t(h_b(\tau)-h_a(\tau))d\tau]. \tag{B.7b}$$

If we put (B.7a) into (B.6) we get the following equation

$$\begin{aligned} B.6 = \frac{1}{\hbar^2}\sum_b \Big\{ & V_{ab}V_{ba}e^{\frac{i(\varepsilon_a-\varepsilon_b)}{\hbar}(t-\tau)}e^{\frac{\Gamma_a-\Gamma_b}{\hbar}(t-\tau)}\langle\exp[\frac{i}{\hbar}\int_\tau^t(h_a(\tau_1)-h_b(\tau_1))d\tau_1]\rangle e^{\frac{2\Gamma_a\tau}{\hbar}}P_a(\tau) \\ & -V_{ab}V_{ba}e^{\frac{i(\varepsilon_a-\varepsilon_b)}{\hbar}(t-\tau)}e^{\frac{\Gamma_a-\Gamma_b}{\hbar}(t+\tau)}\langle\exp[\frac{i}{\hbar}\int_\tau^t(h_a(\tau_1)-h_b(\tau_1))d\tau_1]\rangle e^{\frac{2\Gamma_b\tau}{\hbar}}P_b(\tau) \\ & -V_{ab}V_{ba}e^{\frac{i(\varepsilon_b-\varepsilon_a)}{\hbar}(t-\tau)}e^{\frac{\Gamma_a-\Gamma_b}{\hbar}(t+\tau)}\langle\exp[\frac{i}{\hbar}\int_\tau^t(h_b(\tau_1)-h_a(\tau_1))d\tau_1]\rangle e^{\frac{2\Gamma_b\tau}{\hbar}}P_b(\tau) \\ & +V_{ab}V_{ba}e^{\frac{i(\varepsilon_b-\varepsilon_a)}{\hbar}(t-\tau)}e^{\frac{\Gamma_a-\Gamma_b}{\hbar}(t-\tau)}\langle\exp[\frac{i}{\hbar}\int_\tau^t(h_b(\tau_1)-h_a(\tau_1))d\tau_1]\rangle e^{\frac{2\Gamma_a\tau}{\hbar}}P_a(\tau)\Big\}. \end{aligned} \tag{B.8}$$

Now after integration (B.8) for the overdamped regime (2.25) and with using (2.5) and (2.6), we can substitute (B.4), (B.8) into (B.1) and find generalized master equations for the population probabilities

$$\begin{aligned} \frac{\partial P_i(t)}{\partial t} = & -\frac{2\Gamma_i}{\hbar}P_i(t)-\sum_{j=1}^n\frac{2\mid V_{ij}\mid^2}{\hbar^2}\int_0^t\cos[\frac{\varepsilon_i-\varepsilon_j+\Delta_{ij}}{\hbar}(t-\tau)] \\ & \times\Theta_{ij}(t-\tau)\exp[-\frac{\Gamma_i+\Gamma_j}{\hbar}(t-\tau)](P_i(\tau)-P_j(\tau))d\tau, \\ & i=1...n \quad , \quad i\neq j \end{aligned} \tag{B.9}$$

where $P_i(t)$ is the population probability $P_i(t)=\langle\rho_{ii}(t)\rangle$ and $\Theta_{ij}(t)$ for the overdamped regime (2.18), (2.25) has the form

$$\Theta_{ij}(t)=\exp\Big(-\frac{\Gamma^e_{ij}}{\hbar}\Big\{t-\tau^e_{ij}\Big[1-\exp\Big(-\frac{t}{\tau^e_{ij}}\Big)\Big]\Big\}\Big), \quad i,j=1,...,n. \tag{B.10}$$

Finally, we can solve (B.9) for two limiting cases, the fast and slow modulation limit as is shown in sections 2.3.1 and 2.3.2, respectively.

Appendix C

Derivation of rate constant in underdamped regime

We will work in the strongly underdamped limit where condition $\omega_{L(M)}\tau_{L(M)} \gg 1$ is fulfilled. We start from equations (2.46)

$$\begin{aligned} w_L(p) &= \frac{2J_L^2}{\hbar^2}\int_0^\infty \cos[\frac{\varepsilon_L}{\hbar}t]\exp[-\frac{\Gamma_1+\Gamma_3+\hbar p}{\hbar}t] \\ &\exp\left\{-\frac{\langle\xi_L^2\rangle}{\hbar^2\omega_L^2}\left[\frac{2t}{\tau_L}+1-\exp(-\frac{t}{\tau_L})\left(\cos(\omega_L t)+\frac{3}{\omega_L\tau_L}\sin(\omega_L t)\right)\right]\right\}dt. \end{aligned} \tag{C.1}$$

One can rewrite the above expression to the following form

$$\begin{aligned} w_L(p) &= \frac{2J_L^2}{\hbar^2}\int_0^\infty \cos[\frac{\varepsilon_L}{\hbar}t]\exp[-\frac{\Gamma_1+\Gamma_3+\hbar p}{\hbar}t] \\ &\exp\{-\frac{2\langle\xi_L^2\rangle}{\hbar^2\omega_L^2\tau_L}t\}\exp\{-\frac{\langle\xi_L^2\rangle}{\hbar^2\omega_L^2}\} \\ &\exp\left\{\frac{\langle\xi_L^2\rangle}{\hbar^2\omega_L^2}e^{-t/\tau_L}\cos(\omega_L t)+\frac{3\langle\xi_L^2\rangle}{\hbar^2\omega_L^3\tau_L}e^{-t/\tau_L}\sin(\omega_L t)\right\}dt. \end{aligned} \tag{C.2}$$

Now we can distribute the last term in expression (C.2) to the form

$$\begin{aligned} &\exp\left\{\frac{\langle\xi_L^2\rangle}{\hbar^2\omega_L^2}e^{-t/\tau_L}\cos(\omega_L t)+\frac{3\langle\xi_L^2\rangle}{\hbar^2\omega_L^3\tau_L}e^{-t/\tau_L}\sin(\omega_L t)\right\} = \\ &\exp\left\{\frac{\langle\xi_L^2\rangle}{\hbar^2\omega_L^2}e^{-t/\tau_L}\frac{1}{2}(e^{i\omega_L t}+e^{-i\omega_L t})+\frac{3\langle\xi_L^2\rangle}{\hbar^2\omega_L^3\tau_L}e^{-t/\tau_L}\frac{1}{2i}(e^{i\omega_L t}-e^{-i\omega_L t})\right\}. \end{aligned} \tag{C.3}$$

We will continue with modification of the last term to the final form

$$\begin{aligned} &\exp\left\{\frac{\langle\xi_L^2\rangle}{\hbar^2\omega_L^2}e^{-t/\tau_L}\frac{1}{2}(e^{i\omega_L t}+e^{-i\omega_L t})+\frac{3\langle\xi_L^2\rangle}{\hbar^2\omega_L^3\tau_L}e^{-t/\tau_L}\frac{1}{2i}(e^{i\omega_L t}-e^{-i\omega_L t})\right\} = \\ &\exp\left\{\frac{\langle\xi_L^2\rangle}{2\hbar^2\omega_L^2}e^{-t/\tau_L}e^{i\omega_L t}(1+\frac{3}{i\omega_L\tau_L})\right\}\exp\left\{\frac{\langle\xi_L^2\rangle}{2\hbar^2\omega_L^2}e^{-t/\tau_L}e^{-i\omega_L t}(1-\frac{3}{i\omega_L\tau_L})\right\}. \end{aligned} \tag{C.4}$$

Using the expansion of the exponential terms, (C.4) can be recast in the form

$$\sum_{\alpha,\beta=0}^{\infty}\frac{1}{\alpha!\beta!}\left(\frac{\langle\xi_L^2\rangle}{2\hbar^2\omega_L^2}e^{-t/\tau_L}\right)^{\alpha+\beta}\left(1+\frac{3}{i\omega_L\tau_L}\right)^{\alpha}\left(1-\frac{3}{i\omega_L\tau_L}\right)^{\beta}e^{i\omega_L(\alpha-\beta)t}. \tag{C.5}$$

With the substitution $q = \alpha - \beta$ we can rewrite expression (C.5) to

$$\sum_{q=-\infty}^{\infty}\sum_{\beta=0}^{\infty}\frac{1}{\beta!(\beta+q)!}\left(\frac{\langle\xi_L^2\rangle}{2\hbar^2\omega_L^2}e^{-t/\tau_L}\right)^{2\beta+q}\left(\sqrt{1+\frac{3}{i\omega_L\tau_L}}\right)^{2\beta+q}\left(\sqrt{1-\frac{3}{i\omega_L\tau_L}}\right)^{2\beta+q}$$
$$\times\left(\frac{\sqrt{1+\frac{3}{i\omega_L\tau_L}}}{\sqrt{1-\frac{3}{i\omega_L\tau_L}}}\right)^{q}e^{i\omega_L qt}, \tag{C.6}$$

by using the definition of Bessel function we get the expression

$$\sum_{q=-\infty}^{\infty}\left(\frac{\sqrt{1+\frac{3}{i\omega_L\tau_L}}}{\sqrt{1-\frac{3}{i\omega_L\tau_L}}}\right)^{q}I_q\left\{\frac{\langle\xi_L^2\rangle}{\hbar^2\omega_L^2}e^{-t/\tau_L}\sqrt{1+\frac{9}{(\omega_L\tau_L)^2}}\right\}e^{i\omega_L qt}. \tag{C.7}$$

Splitting of (C.7) gives the terms

$$C.7 \approx I_0\left\{\frac{\langle\xi_L^2\rangle}{\hbar^2\omega_L^2}e^{-t/\tau_L}\right\}+\sum_{q=1}^{\infty}I_q\left\{\frac{\langle\xi_L^2\rangle}{\hbar^2\omega_L^2}e^{-t/\tau_L}\right\}$$
$$\times\left[\left(\frac{1+\frac{3}{i\omega_L\tau_L}}{1-\frac{3}{i\omega_L\tau_L}}\right)^{q/2}e^{i\omega_L qt}+\left(\frac{1-\frac{3}{i\omega_L\tau_L}}{1+\frac{3}{i\omega_L\tau_L}}\right)^{q/2}e^{-i\omega_L qt}\right]. \tag{C.8}$$

By using the relations $\frac{1}{1\pm\varepsilon}\approx 1\mp\varepsilon$, $(1\pm\varepsilon)^n\approx 1\pm n\varepsilon$ for $\varepsilon\to 0$ (that is fulfilled in the strongly underdamped limit) we get

$$I_0\left\{\frac{\langle\xi_L^2\rangle}{\hbar^2\omega_L^2}e^{-t/\tau_L}\right\}+2\sum_{q=1}^{\infty}I_q\left\{\frac{\langle\xi_L^2\rangle}{\hbar^2\omega_L^2}e^{-t/\tau_L}\right\}\left\{\cos(\omega_L qt)+\frac{3q}{\omega_L\tau_L}\sin(\omega_L qt)\right\}. \tag{C.9}$$

If we put (C.9) to (C.2), we finally obtain the expression

$$\begin{aligned} w_L(p) &= \frac{2J_L^2}{\hbar^2}\exp\{-\frac{\langle\xi_L^2\rangle}{\hbar^2\omega_L^2}\}\int_0^{\infty}\left\{\cos[\frac{\varepsilon_L}{\hbar}t]\exp[-\frac{\Gamma_1+\Gamma_3+\hbar p}{\hbar}t]\exp\{-\frac{2\langle\xi_L^2\rangle}{\hbar^2\omega_L^2\tau_L}t\}\right. \\ &\left.\times\left[I_0\{\frac{\langle\xi_L^2\rangle}{\hbar^2\omega_L^2}e^{-t/\tau_L}\}+2\sum_{q=1}^{\infty}I_q[\frac{\langle\xi_L^2\rangle}{\hbar^2\omega_L^2}e^{-t/\tau_L}][\cos(\omega_L qt)+\frac{3q}{\omega_L\tau_L}\sin(\omega_L qt)]\right]\right\}dt, \end{aligned} \tag{C.10}$$

here with using the distribution $\sin(\alpha)\cos(\beta) = 1/2[\sin(\alpha+\beta)+\sin(\alpha-\beta)]$, $\cos(\alpha)\cos(\beta) = 1/2[\cos(\alpha+\beta)+\cos(\alpha-\beta)]$ and after integration we get the expression for the rate constant

$$\begin{aligned} k_L &= \frac{2J_L^2}{\hbar^2\omega_L}e^{-S_L}\left\{\sum_{k=0}^{\infty}\frac{1}{k!k!}(S_L/2)^{2k}\frac{\Omega_L+2k/\alpha_L}{(\Omega_L+2k/\alpha_L)^2+p_L^2}\right. \\ &+\sum_{k=0}^{\infty}\sum_{q=1}^{\infty}\frac{1}{k!(k+q)!}(S_L/2)^{2k+q}\left[\frac{\Omega_L+(2k+q)/\alpha_L+\frac{3q}{\alpha_L}(q-p_L)}{[\Omega_L+(2k+q)/\alpha_L]^2+[q-p_L]^2}\right. \\ &\left.\left.+\frac{\Omega_L+(2k+q)/\alpha_L+\frac{3q}{\alpha_L}(q+p_L)}{[\Omega_L+(2k+q)/\alpha_L]^2+[q+p_L]^2}\right]\right\}, \end{aligned} \tag{C.11}$$

where $S_L = \frac{\langle\xi_L^2\rangle}{\hbar^2\omega_L^2}$, $\alpha_L = \omega_L\tau_L$, $\Omega_L = \frac{\Gamma_1+\Gamma_3}{\hbar\omega_L}+\frac{2S_L}{\alpha_L}$, $p_L = \frac{\varepsilon_L}{\hbar\omega_L}$ and $k_L = w_L(p\to 0^+)$.

Appendix D

Derivation of GME for nonstochastic model of ET

We begin similarly as for the stochastic model of electron transfer from the equation

$$\partial_t D\rho_I(t) = -DL(t)\int_0^t L(\tau)D\rho_I(\tau)d\tau, \tag{D.1}$$

but we are using the projection operator in the form

$$DB = \sum_{j=1}^{N} Tr(|j\rangle\langle j|B)\rho_j|j\rangle\langle j|, \tag{D.2}$$

where ρ_j is the equilibrium medium density matrix in the state $|j\rangle$, i.e.,

$$\rho_j = \frac{\exp(-H_j/k_BT)}{Tr^Q \exp(-H_j/k_BT)}. \tag{D.3}$$

By using (D.2) on the left side of equation (D.1) and if we assume that the population on the state $|j\rangle$ at time t is given by $P_j(t) = Tr(|j\rangle\langle j|\rho(t))$, $Tr \equiv Tr^Q Tr^e$, we get

$$\begin{aligned}\partial_t\langle n|D\rho_I(t)|n\rangle &= \partial_t\Big\{\langle n|\sum_m P_m(t)\rho_m|m\rangle\langle m|n\rangle e^{\frac{2\Gamma_m}{\hbar}t}\Big\} = \rho_n\partial_t\Big\{e^{\frac{2\Gamma_n}{\hbar}t}P_n(t)\Big\} \\ &= \rho_n\Big\{\frac{2\Gamma_n}{\hbar}P_n(t)\exp[\frac{2\Gamma_n t}{\hbar}] + \exp[\frac{2\Gamma_n t}{\hbar}]\partial_t P_n(t)\Big\}. \end{aligned}\tag{D.4}$$

If we use (D.2), on the right side of equation (D.1) we can write

$$\langle n|DL(t)\int_0^t L(\tau)D\rho_I(\tau)d\tau|n\rangle = \langle\langle|n\rangle\langle n|L(t)\int_0^t L(\tau)D\rho_I(\tau)d\tau\rangle\rangle\rho_n. \tag{D.5}$$

Now we need to compute the expression bellow, by using (A.6) on (D.5) we get

$$\begin{aligned}\langle\langle|n\rangle\langle n|L(t)L(\tau)D\rho_I(\tau)\rangle\rangle &= \langle\langle|n\rangle\langle n|\Big\{\frac{1}{\hbar}[V_I(t)L(\tau)D\rho_I(\tau) - L(\tau)D\rho_I(\tau)V_I^+(t)]\Big\}\rangle\rangle \\ &= \langle\langle|n\rangle\langle n|\Big\{\frac{1}{\hbar^2}\Big[V_I(t)[V_I(\tau)D\rho_I(\tau) - D\rho_I(\tau)V_I^+(\tau)] \\ &\quad -[V_I(\tau)D\rho_I(\tau) - D\rho_I(\tau)V_I^+(\tau)]V_I^+(t)\Big]\Big\}\rangle\rangle. \end{aligned}\tag{D.6}$$

Finally we obtain for (D.6) the expression

$$(D.6) = \frac{1}{\hbar^2}\langle\langle|n\rangle\langle n|\Big\{V_I(t)V_I(\tau)D\rho_I(\tau) - V_I(t)D\rho_I(\tau)V_I^+(\tau) - V_I(\tau)D\rho_I(\tau)V_I^+(t) + D\rho_I(\tau)V_I^+(\tau)V_I^+(t)\Big\}\rangle\rangle. \quad (D.7)$$

We need to compute all terms in (D.7), beginning with the first one. Using (D.2),(3.2),(3.6) we can rewrite the first term to the form

$$\langle\langle|n\rangle\langle n|V_I(t)V_I(\tau)D\rho_I(\tau)\rangle\rangle = \sum_{m(\neq n)}\langle\langle V_I(t)_{nm}V_I(\tau)_{mn}\rho_n\rangle\rangle P_n(\tau)e^{\frac{2\Gamma_n}{\hbar}\tau}. \quad (D.8)$$

Substituting (3.8) into equation (D.8) we find

$$\langle\langle|n\rangle\langle n|V_I(t)V_I(\tau)D\rho_I(\tau)\rangle\rangle = \sum_{m(\neq n)} J_{nm}^2\langle\langle e^{\frac{i}{\hbar}H_n(t-\tau)}e^{-\frac{i}{\hbar}H_m(t-\tau)}\rho_n\rangle\rangle P_n(\tau)e^{\frac{2\Gamma_n}{\hbar}\tau}. \quad (D.9)$$

We can rewrite hamiltonian (3.2) to the form

$$\begin{aligned} H_n &= \varepsilon_n - i\Gamma_n + \sum_\alpha\left[\frac{p_\alpha^2}{2m_\alpha} + \frac{1}{2}m_\alpha\omega_\alpha^2(x_\alpha - d_{n\alpha})^2\right] \\ &= \varepsilon_n - i\Gamma_n + \sum_\alpha\left[\hbar\omega_\alpha(b_\alpha^+b_\alpha + 1/2) - m_\alpha\omega_\alpha^2 d_{n\alpha}(b_\alpha + b_\alpha^+)\sqrt{\frac{\hbar}{2m_\alpha\omega_\alpha}} + \frac{1}{2}m_\alpha\omega_\alpha^2 d_{\alpha n}^2\right] \\ &= \varepsilon_n - i\Gamma_n + E_{rn}^\alpha + \sum_\alpha\left[\hbar\omega_\alpha(b_\alpha^+b_\alpha + 1/2) - \Delta_{\alpha n}(b_\alpha + b_\alpha^+)\right], \end{aligned} \quad (D.10)$$

where $E_{rn}^\alpha = \frac{1}{2}m_\alpha\omega_\alpha^2 d_{\alpha n}^2$, $\Delta_{\alpha n} = \sqrt{\hbar E_{rn}^\alpha\omega_\alpha}$ and b_α^+, b_α are creation and annihilation operators. Now substituting (D.10) into (D.9) we get

$$(D.9) = \sum_{m(\neq n)} J_{nm}^2 e^{\frac{\Gamma_n-\Gamma_m}{\hbar}(t-\tau)}e^{\frac{i}{\hbar}\Delta_{nm}(t-\tau)}\langle\langle\rho_n\exp\left[\frac{i}{\hbar}[\hbar\omega(b^+b+1/2) - \Delta_n(b+b^+)](t-\tau)\right] \times\exp\left[-\frac{i}{\hbar}[\hbar\omega(b^+b+1/2) - \Delta_m(b+b^+)](t-\tau)\right]\rangle\rangle P_n(\tau)e^{\frac{2\Gamma_n}{\hbar}\tau}, \quad (D.11)$$

where $\Delta_{nm} = \varepsilon_n + E_{rn} - \varepsilon_m - E_{rm}$. To solve equation (D.11) we have to use the relation

$$\begin{aligned} e^{-\frac{i}{\hbar}[\hbar\omega(b^+b+1/2)-\Delta_m(b+b^+)]t} &= e^{-\frac{i}{\hbar}[\hbar\omega(b^+b+1/2)-\Delta_n(b+b^+)]t} \\ &\times\exp_{[+]}\left[-\frac{i}{h}\int_0^t ds e^{\frac{i}{\hbar}[\hbar\omega(b^+b+1/2)-\Delta_n(b+b^+)]s} \right. \\ &\left.\times\Big\{(\Delta_n - \Delta_m)(b+b^+)\Big\}e^{-\frac{i}{\hbar}[\hbar\omega(b^+b+1/2)-\Delta_n(b+b^+)]s}\right], \end{aligned} \quad (D.12)$$

and we obtain

$$(D.9) = \sum_{m(\neq n)} J_{nm}^2 e^{\frac{\Gamma_n-\Gamma_m}{\hbar}(t-\tau)}e^{\frac{i}{\hbar}\Delta_{nm}(t-\tau)}e^{-\frac{2i(\Delta_n-\Delta_m)\Delta_n}{\hbar^2\omega}(t-\tau)} \times\left\langle\left\langle\rho_n\exp_{[+]}\left[-\frac{i}{\hbar}\int_0^t ds e^{i\omega sB^+B}(\Delta_n - \Delta_m)(B+B^+)e^{-i\omega sB^+B}\right]\right\rangle\right\rangle P_n(\tau)e^{\frac{2\Gamma_n}{\hbar}\tau}, \quad (D.13)$$

where we denote $B = b - \frac{\Delta_n}{\hbar\omega}$, $B^+ = b^+ - \frac{\Delta_n}{\hbar\omega}$. By using the relations $e^{i\omega s B^+ B} B e^{-i\omega s B^+ B} = B e^{-i\omega s}$, $e^{i\omega s B^+ B} B^+ e^{-i\omega s B^+ B} = B^+ e^{i\omega s}$ [116] we gain

$$(D.9) = \sum_{m(\neq n)} J_{nm}^2 e^{\frac{\Gamma_n - \Gamma_m}{\hbar}(t-\tau)} e^{\frac{i}{\hbar}\Delta_{nm}(t-\tau)} e^{-\frac{2i(\Delta_n - \Delta_m)\Delta_n}{\hbar^2\omega}(t-\tau)} P_n(\tau) e^{\frac{2\Gamma_n}{\hbar}\tau}$$
$$\times \exp\left[-\frac{(\Delta_n - \Delta_m)^2}{\hbar^2} \int_0^t ds_1 \int_0^{s_1} ds_2 \Big\{ \langle\langle \rho_n B^+ B \rangle\rangle e^{i\omega(s_1 - s_2)} + \langle\langle \rho_n B B^+ \rangle\rangle e^{-i\omega(s_1 - s_2)} \Big\} \right]. \tag{D.14}$$

In (D.14) it was assumed that $\langle\langle \rho_n B^+ B^+ \rangle\rangle = 0$, $\langle\langle \rho_n B B \rangle\rangle = 0$. Moreover, if we denote $\langle\langle \rho_n B^+ B \rangle\rangle = \bar{n}$ and using commutation relations for the operators $bb^+ - b^+ b = 1$, we find

$$(D.9) = \sum_{m(\neq n)} J_{nm}^2 e^{\frac{\Gamma_n - \Gamma_m}{\hbar}(t-\tau)} e^{\frac{i}{\hbar}\Delta_{nm}(t-\tau)} e^{-\frac{2i(\Delta_n - \Delta_m)\Delta_n}{\hbar^2\omega}(t-\tau)} P_n(\tau) e^{\frac{2\Gamma_n}{\hbar}\tau}$$
$$\times \exp\left[-\frac{(\Delta_n - \Delta_m)^2}{\hbar^2} \int_0^t ds_1 \int_0^{s_1} ds_2 \Big\{ \bar{n} e^{i\omega(s_1 - s_2)} + (\bar{n}+1) e^{-i\omega(s_1 - s_2)} \Big\} \right]. \tag{D.15}$$

After integration (D.15) and a simple modification we finally find

$$\langle\langle |n\rangle\langle n| V_I(t) V_I(\tau) D\rho_I(\tau) \rangle\rangle = \sum_{m(\neq n)} J_{nm}^2 e^{\frac{\Gamma_n - \Gamma_m}{\hbar}(t-\tau)} e^{\frac{i}{\hbar}(\varepsilon_n - \varepsilon_m)(t-\tau)}$$
$$\times \exp\left[\frac{E_{nm}^r}{\hbar\omega} \Big\{ \bar{n} e^{i\omega(t-\tau)} + (\bar{n}+1) e^{-i\omega(t-\tau)} - (2\bar{n}+1) \Big\} \right] P_n(\tau) e^{\frac{2\Gamma_n}{\hbar}\tau}, \tag{D.16}$$

where the $E_{nm}^\alpha = \frac{1}{2} m_\alpha \omega_\alpha^2 (d_{n\alpha} - d_{m\alpha})^2$ is the reorganization energy of the αth mode when the system transfer from the state $|n\rangle$ to the state $|m\rangle$. Similarly we can compute next three terms in (D.7) and substituting (D.7), (D.4) into (D.1) we can express the general master equation in the form

$$\begin{aligned} \partial_t P_n(t) &= -\frac{2\Gamma_n}{\hbar} P_n(t) - \sum_{m=1}^{N} \int_0^t W_{nm}(t-\tau) P_n(\tau) d\tau \\ &\quad + \sum_{m=1}^{N} \int_0^t W_{mn}(t-\tau) P_m(\tau) d\tau, \quad n = 1, ..., N, \quad n \neq m, \end{aligned} \tag{D.17}$$

where

$$\begin{aligned} W_{nm}(t) &= 2\frac{|V_{nm}|^2}{\hbar^2} \mathrm{Re}\Big\{ \exp\left[-\frac{\Gamma_n + \Gamma_m}{\hbar} t \right] \exp\left[\frac{i(\varepsilon_n - \varepsilon_m)}{\hbar} t \right] \\ &\quad \times \exp\left\{ \sum_\alpha \frac{E_{nm}^\alpha}{\hbar\omega_\alpha} [(\bar{n}_\alpha + 1) e^{-i\omega_\alpha t} + \bar{n}_\alpha e^{i\omega_\alpha t} - (2\bar{n}_\alpha + 1)] \right\} \Big\}. \end{aligned} \tag{D.18}$$

Here, $\bar{n}_\alpha = [\exp(\hbar\omega_\alpha / k_B T) - 1]^{-1}$ is a thermal population of the αth mode and $V_{nm} = V_{mn} = J_{nm}$ is the interaction energy between n and m sites.

Appendix E

Derivation of $DL(t)D = 0$ for the models of ET

We begin with the derivation for the stochastic model of electron transfer. By using the projection operators (2.16) acting on an arbitrary operator B in the Hilbert space, the relation for $DL(t)DB$ can be expressed as

$$\begin{aligned}(DL(t)DB)_{mn} &= \delta_{mn}(L(t)DB)_{nn} = \delta_{mn}\sum_{a,b}\langle L(t)_{nnab}(DB)_{ab}\rangle \\ &= \delta_{mn}\sum_{a,b}\left\langle L(t)_{nnab}\delta_{ab}\langle(B)_{aa}\rangle\right\rangle = \delta_{mn}\sum_{a}\left\langle L(t)_{nnaa}\langle(B)_{aa}\rangle\right\rangle \\ &= \delta_{mn}\sum_{a}\langle L(t)_{nnaa}\rangle\langle(B)_{aa}\rangle. \qquad \text{(E.1)}\end{aligned}$$

Now we can compute the Liouville operator $L(t)_{nnaa}$. By using (A.6), (B.7a), we obtain

$$L(t)_{nnaa} = V_I(t)_{na}\delta_{na} - V_I^+(t)_{an}\delta_{na} = \delta_{na}(V_I(t)_{na} - V_I^+(t)_{an}) = 0, \qquad \text{(E.2)}$$

which means that for stochastic model of ET the relation $DL(t)DB = 0$ is fulfilled.

For the nonstochastic model of electron transfer by using the projection operator (3.10) the relation for $DL(t)DB$ can be rewritten as follows:

$$\begin{aligned}DL(t)DB &= \sum_n\left\langle\left\langle|n\rangle\langle n|L(t)DB\right\rangle\right\rangle\rho_n|n\rangle\langle n| = \sum_n\frac{1}{\hbar}\left\langle\left\langle\langle n|[V_I(t)DB\right.\right. \\ &\quad -DBV_I^+(t)]|n\rangle\left.\right\rangle\rangle\rho_n|n\rangle\langle n| = \sum_{n\neq m}\frac{1}{\hbar}\left\langle\left\langle\langle n|V_I(t)|m\rangle\langle m|DB|n\rangle\right.\right. \\ &\quad -\langle n|DB|m\rangle\langle m|V_I^+(t)|n\rangle\left.\right\rangle\rangle\rho_n|n\rangle\langle n| = \sum_{n\neq m}\frac{1}{\hbar}\left\langle\left\langle V_I(t)_{nm}(DB)_{mn}\right.\right. \\ &\quad -(DB)_{nm}V_I^+(t)_{mn}\left.\right\rangle\rangle\rho_n|n\rangle\langle n|. \qquad \text{(E.3)}\end{aligned}$$

Substituting (3.8) into (E.3) we get (E.3)=0, it means that also for the nonstochastic model of electron transfer the relation $DL(t)DB = 0$ is fulfilled.

Bibliography

[1] D.W. Reed and R.K. Clayton, Biochem. Biophys. Res. Commun. **30** (1968) 471.

[2] G. McDermott, Nature **374** (1995) 517.

[3] R. J. Cogdell *et al.*, J. Bacteriol. **181** (1999) 3869.

[4] Jennifer L. Herek *et al.*, Nature **417** (2002) 533.

[5] P. Mitchell, Science **206** (1979) 1148.

[6] J.M. Anderson and B. Andersson, Trends Biol. Sci. **7** (1982) 288.

[7] D.A. Berthold, G.T Babcock, and C.F. Yocum, FEBS Lett. **134** (1981) 231.

[8] J. Deisenhofer *et al.*, Nature **318** (1985) 618.

[9] J.P. Allen and J.C. Willams, FEBS Lett. **438** (1998) 5.

[10] J. Amesz, J. Photochem. Photobiol. **30** (1995) 89.

[11] H. Sakurai, N. Kusumoto, and K. Inoue, Photochem. Photobiol. **64** (1996) 5.

[12] J.H. Golbeck, Proc. Natl. Acad. Sci. U.S.A. **90** (1993) 1642.

[13] W.D. Schubert *et al.*, Nat. Struct. Biol. **3** (1996) 965.

[14] W. Nitschke and A.W. Rutherford, Trends. Biol. Sci. **16** (1991) 241.

[15] J. Deisenhofer *et al.*, J. Mol. Biol. **180** (1984) 385.

[16] H. Michel *et al.*, EMBO J. **5** (1986) 2445.

[17] L. N. M. Duysens, Biochim. Biophys. Acta **19** (1956) 188.

[18] H. Michel *et al.*, EMBO J. **4** (1985) 1667.

[19] K. A. Weyer *et al.*, EMBO J. **6** (1987) 2197.

[20] J. Deinsenhofer and H. Michel, EMBO J. **8** (1989) 2149.

[21] J. L. Martin *et al.*, Physica A **83** (1986) 957.

[22] A. J. Hoff and J. Deisenhofer, Phys. Reports **287** (1997) 1.

[23] Van Brederode *et al.*, Biochemistry **36** (1997) 6855.

[24] B. A. Heller, D. Holten, and C. Kirmaier, Science **269** (1995) 940.

[25] J. Li *et al.*, Biochemistry **37** (1998) 2818.

[26] M. H. B. Stowel *et al.*, Science **276** (1997) 812.

[27] Ch. Kirmaier and D. Holten, Proc. Natl. Acad. Sci. U.S.A. **87** (1990) 3552.

[28] E. Takahashi and C. A. Wraight, Biochemistry (1992) 855.

[29] V. A. Shuvalov and L. N. M. Duysens, Proc. Natl. Acad. Sci. U.S.A. **83** (1986) 1690.

[30] J. N. Gehlen, M. Marchi, and D. Chandler, Science **263** (1994) 499.

[31] Kyong-Hi Rhee *et al.*, Nature **396** (1998) 283.

[32] F. Widdel *et al.*, Nature **362** (1993) 834.

[33] H. Miyashita *et al.*, Nature **383** (1996) 402.

[34] Don Dewault, *Quantum Mechanical Tunnelling in Biological Systems* (Cambridge University Press, 1981).

[35] E. G. Petrov, *Physics of Electron Transfer in Biosystems* (Kiev 1984).

[36] M. Pudlak and R. Pincak, *Proceedings of the Conference Small Triangle Meeting on Theoretical Physics*, October 25-26, Košice (2000) 44.

[37] R. Pincak and M. Pudlak, Physical Review E **64** (2001) 031906.

[38] M. Pudlak and R. Pincak, *Proceedings of the Conference Small Triangle Meeting on Theoretical Physics*, September 25-26, Snina (2001) 49.

[39] M. Pudlak and R. Pincak, Chemical Physics Letters. **342** (2001) 587.

[40] M. Pudlak and R. Pincak, Physical Review E **68** (2003) 0519XX.

[41] R. Pincak and M. Pudlak, *Proceedings of the Conference Small Triangle Meeting on Theoretical Physics*, October 8-10, Snina (2002) 58.

[42] R. Pincak and M. Pudlak, Contribution at the European Conference of Mathematical and Theoretical Biology, July (2002) Milano, published in *Mathematical Modelling & Computing in Biology and Medicine*, (V.Capasso Ed.), The MIRIAM Project Series, Progetto Leonardo, ESCULAPIO Pub. Co., Bologna, Italy, (2003) 434.

[43] R. Pincak and M. Pudlak, in preparation.

[44] H. Haken and P. Reineker, Z. Phys. **249** (1972) 253.

[45] P. Reineker, B. Kaiser, and A. M. Jayannavar, Phys. Rev. A **39** (1989) 1469.

[46] A. Blumen and R. Silbey, J. Chem. Phys. **69** (1978) 3589.

[47] V. Čápek and V. Szös, Phys. Status Solidi B **131** (1985) 667.

[48] D. W. Brown, K. Lindenberg, and B. J. West, J. Chem. Phys. **83** (1985) 4136.

[49] M. Pudlak, Chem. Phys. Lett. **235** (1995) 126.

[50] M. Pudlak, Chem. Phys. Lett. **221** (1994) 86.

[51] M. Pudlak, Czech. J. Phys. **48** (1998) 293.

[52] V. Čápek and V. Szös, Phys. Status Solidi B **125** (1984) K137.

[53] P. Chvosta and I. Barvik, Z. Phys. B: Condens. Matter **85** (1991) 227.

[54] V. M. Kenkre and P. Reineker, *Exciton Dynamics in Molecular Crystals and Aggregates*, Springer Tracts in Modern Physics **94** (Springer, Berlin, 1982).

[55] A. A. Ovchinnikov, S. F. Timashev, and A. A. Bely, *Kinetics of Diffusion Controlled Chemical Processes* (Nova Science, Commack, NY, 1989).

[56] V. I. Klyatskin, *Statistical Description of Dynamical Systems with Fluctuating Parameters* (Nauka, Moskva, 1975).

[57] P. Hänggi, Z. Phys. B **31** (1978) 407.

[58] M. Pudlak, J. Chem. Phys. **108** (1998) 5621.

[59] J. Jortner, S. A. Rice, and R. M. Hochstrasser, *Radiationless Transitions in Photochemistry*, Advances in Photochemistry **7** (Wiley, New Yourk, 1996) 149.

[60] S. Lin *et al.*, Biochemistry **35** (1996) 3187.

[61] A. K. W. Taguchi *et al.*, Biochemistry **35** (1996) 3175.

[62] M. E. Van Brederode *et al.*, Chem. Phys. Lett. **268** (1997) 143.

[63] Ch. Kirmaier, D. Weems and D. Holten, Biochemistry **38** (1999) 11 516.

[64] L. L. Laporte *et al.*, J. Phys. Chem. **100** (1996) 17 696.

[65] E. Katilius *et al.*, J. Phys. Chem. B **103** (1999) 7386.

[66] T. Artl and B. Dohse *et al.*, Biochemistry **35** (1996) 9235.

[67] T. Artl and M. Bibikova *et al.*, J. Phys. Chem. **100** (1996) 12 060.

[68] M. R. A. Blomberg, P. E. M. Siegbahn, and G. T. Babcock, J. Am. Chem. Soc. **120** (1998) 8812.

[69] W. W. Person, Z. T. Chu, and A. Warshel, Biochim. Biophys. Acta **1017** (1990) 251.

[70] S. Tanaka and R. A. Marcus, J. Phys. Chem. B **101** (1997) 5031.

[71] E. Sim and N. Makri, J. Phys. Chem. B **101** (1997) 5446.

[72] R. A. Marcus, Chem. Phys. Lett. **133** (1987) 471.

[73] M. Pudlak and K. V. Shaitan, J. Biol. Phys. **19** (1993) 39.

[74] I. A. Goyuchuk, E. G. Petrov, and V. May, J. Chem. Phys. **103** (1995) 4937.

[75] M. Plato *et al.*, J. Am. Chem. Soc. **110** (1988) 7279.

[76] M. Bixon, J. Jortner, and M. E. Michel-Beyerle, Biochim. Biophys. Acta **1056** (1991) 301.

[77] J. Hasegawa and H. Nakatsuji, J. Phys. Chem. B **102** (1998) 10 420.

[78] P. O. J. Scherer, C. Scharnagl, and S. F. Fischer, Chem. Phys. **197** (1995) 333.

[79] R. Zwanzig, Physica **30** (1964) 1109.

[80] N. Hashitsume, P. Shibata, and M. Shingu, J. Stat. Phys. **17** (1972) 253.

[81] M. Sparpaglione and S. Mukamel, J. Chem. Phys. **88** (1988) 3263.

[82] M. Morillo, D. Y. Yang, and R. I. Cukier, J. Chem. Phys. **90** (1989) 5711.

[83] R. Kubo, M. Toda, and N. Hashitsume,*Statistical Physics II, Nonequilibrium Statistical Mechanics* (Springer, Berlin, Heidelberg, New York, 1998).

[84] J. Jortner *et al.*, Biochim. Biophys. Acta **932** (1988) 52.

[85] P. Chvosta and I. Barvik, Z. Phys. B-Condensed Matter **85** (1991) 227.

[86] M. E. van Brederode and R. van Grondelle, FEBS Leters **455** (1999) 1.

[87] M. E. van Brederode *et al.*, Proc. Natl. Acad. Sci. U.S.A **96** (1999) 2054.

[88] W. M. Zhang, T. Meier, V.Chernyak, and S. Mukamel, J. Chem. Phys. **108** (1998) 7763.

[89] V. Szöcs, P. Banacky, and P. Reineker, Chem. Phys. **199** (1995) 1.

[90] V. Čápek and I. Barvik, Physica A **294** (2001) 388.

[91] M. Pudlak, J. Chem. Phys. **118** (2003) 1876.

[92] M. Bixon, J. Jortner, and M. E. Michel-Beyerle, Chem. Phys. **197** (1995) 389.

[93] B. A. Heller, D. Holten, and Ch. Kirmaier, Biochemistry **35** (1996) 15 418.

[94] Ch. Kirmaier, Ch. He, and D. Holten, Biochemistry **40** (2001) 12 132.

[95] M. Marchi *et al.*, J. Am. Chem. Soc. **115** (1993) 4178.

[96] Ch. Kirmaier *et al.*, J. Phys. Chem. B **106** (2002) 1799.

[97] H. Sumi, Phys. Rev. Lett. **50** (1983) 1709.

[98] V. Čápek and V. Szöcs, Czech. J. Phys. **36** (1986) 1182.

[99] H. Dekker, Physica A **175** (1991) 485.

[100] M. Pudlak, Czech. J. Phys. **44** (1994) 153.

[101] R. H. Dogonadze *et al.*, J. Electroanal. Chem. **75** (1977) 315.

[102] J. Jortner, J. Chem. Phys. **64** (1976) 4860.

[103] Y. Hu and S. Mukamel, J. Chem. Phys. **91** (1989) 6973.

[104] J. S. Joseph and W. Bialek, J. Phys. Chem. **97** (1993) 3245.

[105] R. Islampour and S. H. Lin, J. Phys. Chem. **95** (1991) 10 261.

[106] M. Bixon and J. Jortner, J. Chem. Phys. **107** (1997) 5154.

[107] L. D. Zusman and D. N. Beratan, J. Chem. Phys. **110** (1999) 10 468.

[108] H. Sumi, J. Electroanal. Chem. **438** (1997) 11.

[109] A. Kimura and T. Kakitani, Chem. Phys. Lett. **298** (1998) 241.

[110] R. Egger, C. H. Mak, and U. Weis, Phys. Rev. E **50** (1994) R655.

[111] N. Ivashin *et al.*, J. Phys. Chem. B **102** (1998) 5017.

[112] D. Kolbasov and A. Scherz, J. Phys. Chem. B **104** (2000) 1802.

[113] K. Czarnecki *et al.*, J. Phys. Chem. A **103** (1999) 2235.

[114] W. Peier, Physica **57** (1972) 565.

[115] H. Grabert, *Projection Operator Techniques in Nonequilibrium Statistical Mechanics* (Springer, Berlin, Heidelberg, New York, 1982).

[116] H. Haken, *Quantum Field Theory of Condense Matter* (Alfa, Bratislava, 1987).

[117] V. A. Osipov, E. A. Kochetov, and M. Pudlak, JETP **96** (2003) 140.

[118] R. Pincak and V. A. Osipov, Physics Letters A **314** (2003) 315.

List of publications

- **R. Pincak** and M. Pudlak
Noise breaking the twofold symmetry of photosynthetic reaction centers: Electron transfer, Physical Review E **64** (2001) 031906.
- M. Pudlak and **R. Pincak**
The role of accessory bacteriochlorophylls in the primary charge transfer in the photosynthetic reaction centers, Chemical Physics Letters **342** (2001) 587.
- M. Pudlak and **R. Pincak**
Modeling charge transfer in the photosynthetic reaction center, Physical Review E **68** (2003) 0519XX (in press).
- **R. Pincak** and M. Pudlak
Electron Transfer and Quantum Yields in Photosynthetic reaction centers, Contribution at the European Conference of Mathematical and Theoretical Biology, July (2002) Milano, published in *Mathematical Modelling & Computing in Biology and Medicine*, (V.Capasso Ed.), The MIRIAM Project Series, Progetto Leonardo, ESCULAPIO Pub. Co., Bologna, Italy, (2003) 434.
- M. Pudlak and **R. Pincak**
Transport of Electrons in Reaction Centers, Proceedings of the Conference Small Triangle Meeting on Theoretical Physics, October, Košice (2000) 44.
- M. Pudlak and **R. Pincak**
Charge separation in photosynthesis, Proceedings of the Conference Small Triangle Meeting on Theoretical Physics , September, Snina (2001) 49.
- **R. Pincak** and M. Pudlak
Kinetic model of electron transfer in bacterial photosynthetic reaction center, Proceedings of the Conference Small Triangle Meeting on Theoretical Physics, October, Snina (2002) 58.

Additional publication

- **R. Pincak** and V. A. Osipov
Localized electron states near pentagons in variously shaped carbon nanoparticles, Physics Letters A **314** (2003) 315.